Lene Therese Backus Erichsen

# Aging and Second Life Performance of Lithium-Ion Batteries

## Effects of Temperature and Cycling Conditions

Master's thesis in Energy and Environment
Supervisor: Odne Stokke Burheim and Preben Vie
Co-supervisor: Markus Solberg Wahl
June 2023

Master's thesis

NTNU
Norwegian University of Science and Technology
Faculty of Engineering
Department of Energy and Process Engineering

NTNU
Norwegian University of
Science and Technology

Lene Therese Backus Erichsen

# Aging and Second Life Performance of Lithium-Ion Batteries

## Effects of Temperature and Cycling Conditions

Master's thesis in Energy and Environment
Supervisor: Odne Stokke Burheim and Preben Vie
Co-supervisor: Markus Solberg Wahl
June 2023

Norwegian University of Science and Technology
Faculty of Engineering
Department of Energy and Process Engineering

NTNU
Norwegian University of
Science and Technology

NTNU | Faculty of Engineering
Department of Energy and Process Engineering

| | |
|---|---|
| **Report title:**<br>Aging and Second Life Performance of Lithium-Ion Batteries: Effects of Temperature and Cycling Conditions<br><br>**Submission deadline:** 11.06.23 | **Report title Norwegian:**<br>Effekt av aldring på second life ytelse til litium-ion batterier: Påvirkning av temperatur of syklingsbetingelser |
| **Project participant:**<br>Lene Therese Backus Erichsen<br>Lene.erichsen@gmail.com | **Internal supervisors:**<br>Odne Stokke Burheim<br>Professor, NTNU<br>odne.s.burheim@ntnu.no<br><br>Markus Solberg Wahl<br>Postdoctoral Fellow<br>markus.s.wahl@ntnu.no |
| **Field of study:**<br>Energy and the Environment | **Project Number:**<br>TEP4906 |
| **External company contact:**<br>IFE | **External supervisor:**<br>Preben J. S. Vie<br>Senior Scientist<br>preben.vie@ife.no / preben.j.s.vie@ntnu.no |

# Preface

This master thesis is a continuation of the project report "Ageing performance of second-life batteries" by Lene T.B. Erichsen[1] in the subject TEP4506. It is the final assessment in the master's program Energy and the Environment at NTNU Trondheim.

This thesis evaluates the effects of different first life conditions that affect a battery's ability for second life cycling. It has been very inspiring working with batteries the last year. Exploring the science behind battery technology and understanding its limitations have given me invaluable experience and knowledge.

I want to thank my supervisor Professor Odne Stokke Burheim for guidance and support throughout this year. I would also like to thank Postdoctoral Fellow Markus Solberg Wahl for help in the lab, and many good discussions about my work. In addition, my external supervisor Preben Vie for batteries, lots of data, and always having good answers to my questions.

The Research Council of Norway is acknowledged for the support to the Norwegian Micro- and Nano-Fabrication Facility, NorFab. A big thanks to Torleif Lian for allowing me to do ARC measurements at FFI and doing further tests on my cells for me. Lastly, I would like to thank my father, Leif Erichsen, for helping me proofread and discuss my work throughout my entire education.

Since this is a continuation of a project report, some parts of the theory are equal or based on the project report. This is shown with citations. Any figures without citation are made by the author.

Lene T.B. Erichsen

Trondheim, 11.06.2023

## Abstract

This master thesis addresses the aging and second life of lithium-ion batteries. The main objective is to understand how first life conditions affect a cell's ability for a safe and long second life. This is done using XALT 31 Ah cells from XALT Energy. Three cells were aged at IFE in 2015/2016 at 25 and 45°C, while five others were stored. Experimentally all cells were aged further at NTNU. The aged cells were cycled at a C-rate of C/4 at 25°C. While the uncycled cells were cycled at 5, 25, and 45°C at 1C. Data from the cells were analyzed using increment capacity analysis and resistance measurements. State of Health measurements was used to understand what influences aging. In addition, material ARC was used to evaluate thermal runaway temperature. SEM images were also taken to visually evaluate the effects of cycling.

Results from the cycling indicated that temperature has a large effect on the capacity decrease of the XALT cells. High temperature leads to the largest increase in resistance as a result of SEI layer growth.

At 5°C the cycling performance is very limited. Only 14 cycles were performed before the cell's capacity reached 65% of the initial capacity. Increased resistance, $dQdV$ curves, and material ARC all point towards the presence of plated lithium on the anode surface. SEM images show some mossy texture which is normally found to be lithium metal. In addition, a bubbly texture that has not previously been seen on anode surfaces was also found. Based on these results, the cells a 5°C can completely be ruled out as second life cells due to both safety and performance.

In regards to second life cycling, the cells cycled at 25°C for first life showed the least capacity decrease for second life. At the end of the project, the cells have been cycled for about 500 second life cycles with practically no decrease in capacity. In addition, there are no differences in the $dQdV$ plots during the 500 cycles. Cells cycled at 45°C for first life degrade faster during second life than the cells at 25°C. With a decrease in capacity of about 2.5% over 500 cycles.

Increment capacity analysis is a non-invasive analysis method that works very well differentiating XALT cells cycled at different temperatures. Based on this, it is possible to find the cells that will work best for second life with regards to safety and performance. Based on the results of the experiments in this thesis, XALT cells cycled at room temperature of 25°C will have the best second life performance. Cells cycled at 45°C can also work. However, the capacity decreases faster, and this can also affect safety. Cells cycled at low temperatures should be avoided for second life due to lithium plating, which decreases capacity fast and negatively affects safety.

Further work includes further cycling second life cells to increase the probability of the current results. In addition, cycling more cells creates a better foundation to draw conclusions about the trends commented on in this thesis. All second life cycling is done at the same temperature and C-rate, further work could therefore involve testing a wider range of both C-rates and temperatures.

# Abstract in Norwegian (Sammendrag)

Denne masteroppgaven tar for seg aldring og second life for litium-ion-batterier. Hovedmålet er å forstå hvordan forholdene i first life påvirker cellens evne til en trygg og lang second life. Dette gjøres ved å bruke XALT 31 Ah-celler fra XALT Energy. Tre celler ble eldet hos IFE i 2015/2016 på 25 og 45°C, mens fem andre ble kun lagret. Alle cellene ble ytterligere eldet ved NTNU. De gamle cellene ble syklet med en C-rate på C/4 ved 25°C, mens de usyklede cellene ble syklet på 5, 25 og 45°C med 1C. Dataene fra cellene ble analysert ved hjelp av $dQdV$ kurver og motstandsmålinger. SoH målinger ble brukt for å forstå hva som påvirker aldring. I tillegg ble material-ARC brukt for å lithium plating. SEM-bilder ble også tatt for å visuelt evaluere effektene av sykling.

Resultatene fra syklingen indikerer at temperatur har stor påvirkning på kapasitetsreduksjonen til XALT-cellene. Høy temperatur fører til den største økningen i motstand som et resultat av vekst av SEI-laget.

Ved 5 °C er syklingsytelsen begrenset. Etter kun 14 sykluser var kapasiteten redusert til 65% av opprinnelig verdi. Økt motstand, $dQdV$ kurver og material-ARC peker alle mot tilstedeværelsen av lithium plating på anodeoverflaten. SEM-bilder viser en moseaktig tekstur som vanligvis er forbundet med funn av litiummetall på overflaten. I tillegg ble det også funnet en boblete tekstur som ikke tidligere har blitt funnet på anodeoverflater. Basert på disse resultatene kan cellene syklet på 5°C helt utelukkes som second life celler på grunn av både sikkerhet og ytelse.

Når det gjelder second life sykling viste cellene som ble syklet på 25°C i first life minst kapasitetsreduksjon ved second life. Ved prosjektets slutt har cellene syklet omtrent 500 sykluser i second life med tilnærmet ingen reduksjon i kapasitet. I tillegg er det svært små forskjeller i $dQdV$ plottene i løpet av de 500 syklusene. Cellene som ble syklet på 45°C i first life mister kapasitet mye raskere i second life enn cellene som ble syklet på 25°C, med en kapasitetsreduksjon på omtrent 2,5%

$dQdV$kurver er en ikke-inngripende analysemetode som fungerer svært godt til å skille XALT-celler som er syklet ved ulike temperaturer. Basert på dette er det mulig å finne de cellene som vil fungere best for second life med hensyn til sikkerhet og ytelse. Resultatene fra eksperimentene i denne oppgaven viser at XALT-celler som er syklet ved romtemperatur på 25°C vil ha den beste ytelsen i second life. Cellene som er syklet ved 45°C kan også fungere, men kapasiteten reduseres raskere og dette kan også påvirke sikkerheten. Celler som er syklet ved lave temperaturer bør unngås for second life på grunn av lithium plating, som reduserer kapasiteten raskt og påvirker sikkerheten negativt.

Videre arbeid inkluderer ytterligere sykling av celler i second life for å øke kvaliteten av nåværende resultater. I tillegg gir sykling av flere celler et bedre grunnlag for å trekke konklusjoner om de trendene som er kommentert i denne oppgaven. All sykling i second life gjøres ved samme temperatur og C-rate, så videre arbeid kan involvere testing av et bredere spekter av både C-rater og temperaturer.

# List of Figures

# Table of Contents

# Chapter 1

# Introduction

To ensure a safe planet for all people and creatures, society needs to undergo a green transition. The UN has developed 17 sustainable development goals to transform the world. The goals call for action from all countries regardless of income and living conditions. One of the major goals is described in the Paris agreement, stating that the average temperature should not increase more than 2°C, preferably no more than 1.5°C to avoid catastrophic consequences. At this point, the world is not on track to reach this goal. Renewable energy only accounts for 17% of total energy consumption today, and cities account for 75% of all emissions. In 2030 660 million people will still not have access to electricity.[2]


**Figure 1.1:** Relevant UN sustainable development goals for the project.[2]

How can batteries aid in the transition toward a greener world and reaching sustainable development goals? Batteries can work as long-term storage for both electric machines and vehicles, as well as grid energy storage applications. In addition as an energy source for an increasing amount of household items. The first battery was invented by Alessandro Volta in 1800, made with cobber and zinc electrodes. Lead acid batteries were invented in 1859 and are still the most used battery technology in internal combustion vehicles. Today lithium-ion batteries have become an important technology due to their high electrochemical potential and light weight. Lithium has more energy per unit weight than other metals, which makes it an ideal element to use for energy storage. Compared to lead acid batteries, with an energy density of 40 Wh/kg, lithium-ion batteries have an energy density of about 80 Wh/kg.[3]

According to SSB, in Norway in 2021, 65% of new cars were electric vehicles, and 16% of all cars in Norway were electric[4]. Though the energy density of batteries is much lower than that of diesel and gasoline, electric vehicles have become an important part of the transport sector. This can be accounted for by both social sanctions and the low carbon footprint of EVs. As the battery technology is improved, EVs have become a real competitor of combustion engine vehicles. This also includes buses, vehicles on construction sites, and ferries.

The growth in battery production approximately doubles every five years[5]. With the rise in electric machines and applications, the number of used or "dead" batteries also accumulates quickly. The rate of production surpasses the rate of recycling greatly. In addition, the current recycling process mainly focuses on components with high economic value, such as Al, Fe, Co, and Ce, and not on general circular economy considerations.[6] While some recycling procedures exist, the capacity is still very low. It is, therefore, important to look at other options for end-of-life.

Considering batteries that are removed due to safety reasons, there can still be a considerable amount of capacity left in the cells when they are removed. For EVs, batteries are usually removed after losing 20% of the initial capacity. Recycling these cells might not be the most appropriate solution in a circular economy and abundance of materials. Reuse is preferable because it prolongs the material cycle life. second life applications usually have less strict technical requirements than first life with regards to cycle and rate performance. Some examples of second life applications are small- and large-scale energy storage systems, stabilize power output for renewable energy, and peak shaving for the electricity grid.[7]

The thought of second life applications is not new, but the number of projects has increased rapidly in the last five years. The slow growth is generally due to the battery industry's immaturity and relatively small scale. As the industry grows and matures, the demand increases. Today almost all major automotive companies have second life applications in the company pipeline. For many companies, the most crucial aspect is the price compared to using new batteries. In addition, other types of batteries, such as flow batteries, might provide more competitive prices and better performance in the coming years.[7]

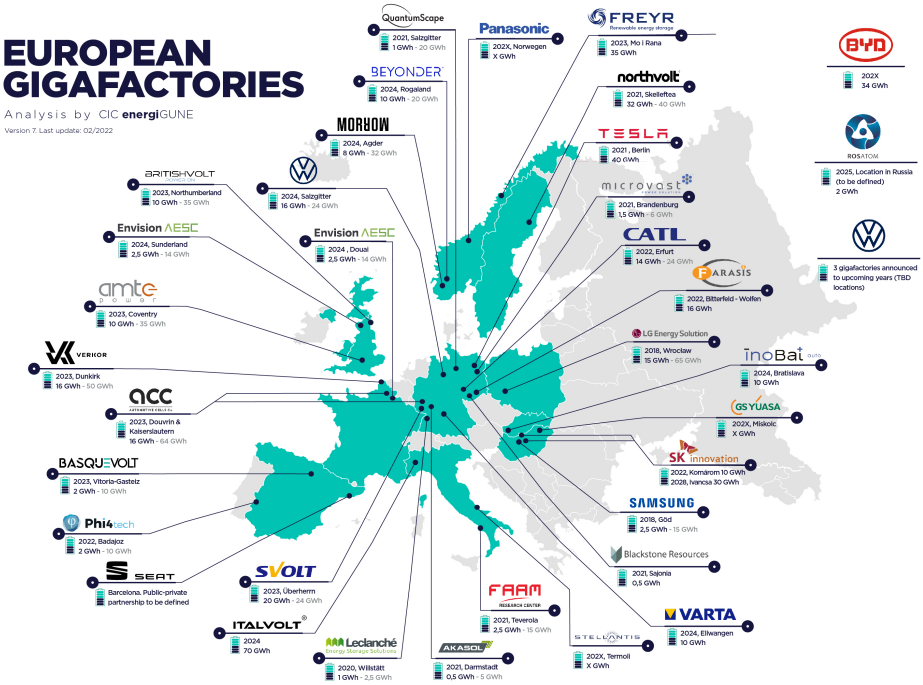


**Figure 1.2:** Battery gigafactory plans in Europe[8]

The global supply of second life batteries is expected to grow as a result of the increase in battery production, as seen by the growth of giga battery factory plans in the world[8]. The second life supply is assumed to be 1 GWh in 2020, with an increase to 15 GWh in 2025, and between 112 – 227 GWh in 2030[7]. This is a large amount of energy that should be taken advantage of. Else this will lead to huge waste if not disposed of or used correctly.

An important question to ask for second life batteries is how long they will last. Degradation depends on materials, manufacturing, and use. In addition, aging studies take a long time, so data can be limited. Battery cells are complicated systems where all processes are not yet fully elucidated. In general, many studies focus on the aging effects in battery cells, but second life studies are scarce. The most important factor for second life use is a relatively long life without compromising safety. This is currently not an easy task as the use in first life, which is not always known, affects second life safety greatly. [9]

It is important to understand both aging and second life performance to utilize second life cells as optimally as possible. This thesis focuses on understanding how different first life conditions affect batteries' ability to function as second life batteries. The focus throughout is safe cycling to simulate real-life conditions for second life cells. The case framework was developed in collaboration with IFE.

This thesis is a continuation of a project report in the subject TEP4521 and is part of the second life project, which is a collaboration between NTNU, IFE, FFI, UiA, Department of Chemical Engineering at UC London, and The Solar Energy Cluster.

The work in this thesis involves experimentally analyzing cells based on cycling conditions. The data is then compared to see which conditions result in the best second life cycling. In addition, cells are analyzed using SEM, material ARC, and $dQdV$ plots. A conclusion is then made based on the findings, and further work on the subject is presented.

# Chapter 2

# Theory

## 2.1 Electrochemistry

Electrochemistry is the description of the conversion between chemical and electrical energy. Batteries use a chemical reaction to generate electricity. It is, therefore, important to understand the electrochemical relations to understand the functions of a battery cell. An electrochemical cell converts chemical energy to electrical energy. The amount of energy depends on the cell potential and the number of electrons transported during the reaction.[10]

It is not possible to measure the potential of an electrode, but it is possible to measure the difference in potential between two electrodes. This can be done using any electrode, but the standard hydrogen electrode is often used as a reference electrode. As shown in equation 2.1, this is given as the standard potential of 0 V.[11]

$$2H_{aq}^{+} + 2e^{-} \rightleftharpoons H_{2(g)} \tag{2.1}$$

When measuring these potentials at each half-cell, it is possible to find the overall potential of a cell. The cell potential is defined as the difference between the reduction potential of two half-cells, and this is given in equation 2.2.[12]

$$E_{cell}^{\circ} = E_{cathode}^{\circ} - E_{anode}^{\circ} \tag{2.2}$$

A system's reaction energy, called enthalpy, is based on equation 2.3, where $\Delta G$ is the reversible work known as Gibbs free energy and reversible heat as a product of entropy change and temperature. All symbols are denoted with lowercase letters and macrons when related to molar properties.[12]

$$\Delta H = \Delta G + T\Delta S \tag{2.3}$$

For electrochemical processes, it is interesting to investigate the reversible work. Reversible work related to molar properties is given in equation 2.4, where z is moles of charge, F is Faradays constant, and $E_{cell}$ is the cell potential in volt.

$$\Delta \bar{g} = \Delta \bar{h} - T\Delta \bar{s} = -zFE_{cell} \tag{2.4}$$

Reversible work only occurs at equilibrium. Once a process moves away from equilibrium, irreversible losses occur, and the entropy rises. For an electrochemical cell, this is when a current passes through the system. These irreversibilities are generally accounted for as ohmic potential drop, charge transfer overpotential, and concentration polarisation overpotential. These are described further in chapter 2.1.2. The reversible work is a sum of reversible potential and the three irreversible losses given in equation 2.5, where $rj$ is the ohmic potential drop and $\eta$ accounts for the other losses.[13]

$$E^{rev} = E^{cell}_{spont} + rj + \eta \tag{2.5}$$

When there is no drawn current, at an open circuit, reversible cell potential $E^{rev}$ can be measured. When a current is drawn, the potential is lower and can be measured as $E^{cell}_{spont}$. The energy efficiency of a cell can be found based on these two potentials. This is given in equation 2.6, which also shows how this relates to overpotentials.[13]

$$\varepsilon_{spont} = \frac{E^{cell}_{spont}}{E^{rev}} = \frac{E^{rev} - rj - \eta}{E^{rev}} \tag{2.6}$$

### 2.1.1 Galvanic and Electrolytic Cells

Galvanic cells, also called voltaic cells, are electrochemical cells where spontaneous oxidation and reduction reactions occur and produce electrical energy. The cells take advantage of the difference in standard electrode potential of two solutions called half-cells. The electrode where the oxidation occurs is called the anode, and the reduction occurs at the cathode. Together this is called a redox reaction. In principle, any galvanic cell can be used as a battery. Electrolytic cells work the opposite way of galvanic cells. An external power source drives a non-spontaneous reaction. A galvanic cell can also be used as an electrolytic cell in reverse.[1, 10, 14]

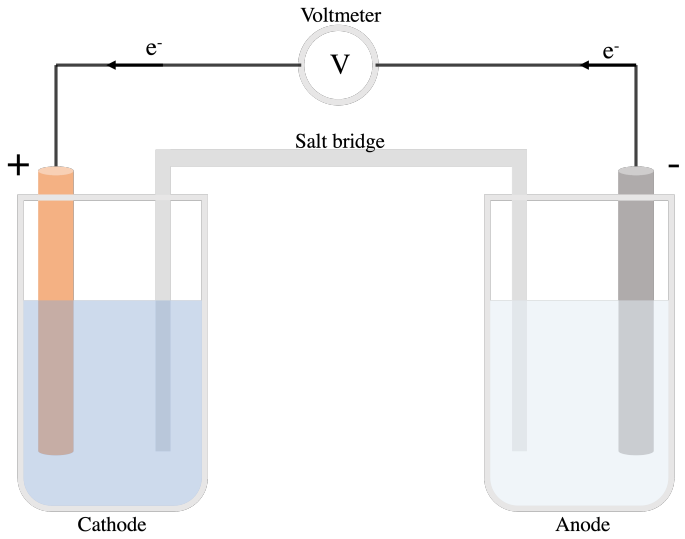


**Figure 2.1:** Galvanic cell with a cathode, anode, salt bridge, and voltmeter.

### 2.1.2 Irreversible Losses

For a spontaneous cell, the efficiency lowers due to irreversible losses. This can also be called overpotentials. It is the difference between the theoretical and actual voltage during operation. The instant resistance measured after the current is turned off is the ohmic resistance for batteries. While between 0 - 100 ms accounts for the charge transfer resistance, and after this, concentration overpotential accounts for the rest. This can be seen in Figure 2.2.[15]

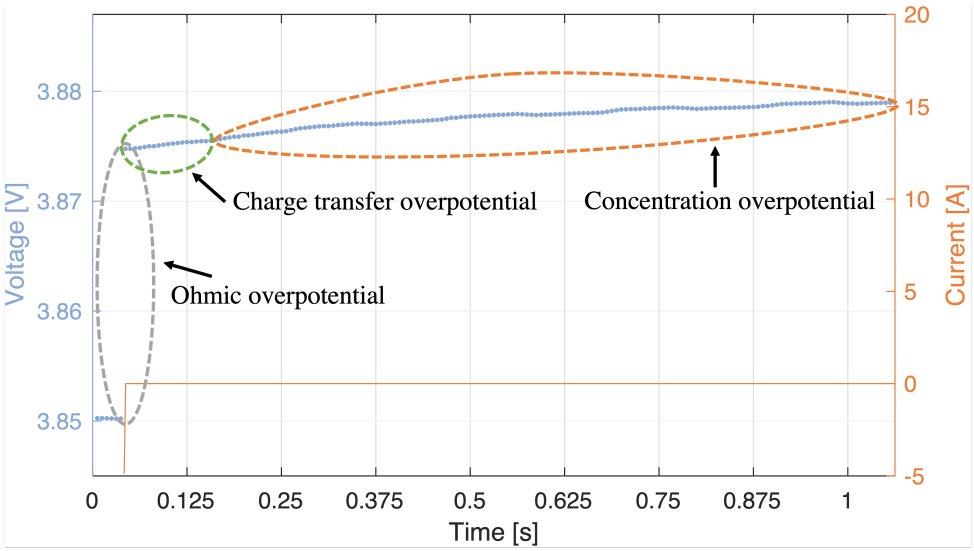


**Figure 2.2:** Overpotential for a battery after the current is turned off, inspired by Schweiger at al.[15]

#### Ohmic Overpotential

Ohmic overpotential is defined using ohms law in equation 2.7, where R is resistance, and I is the current. This implies that the ohmic potential drop varies linearly with the current. Ohmic overpotential is based on the internal resistance of a cell. Ideally, the internal resistance should be as low as possible, as this leads to a higher current. Internal resistance is a combination of the resistance in the electrodes, electrolyte, separator, and current collectors.[13]

$$\eta_{ohmic} = RI \tag{2.7}$$

#### Charge Transfer Overpotential

When a reaction moves away from equilibrium, one current will be larger than the other. This leads to potential change caused by friction from the exchange of electrons faster than at equilibrium. This is called charge transfer reaction overpotential. The Butler-Volmer equation shown in equation 2.8 expresses the electrode equilibrium currents as a function of $j_0$ as exchange current density, $\alpha$ is the symmetry coefficient and $\eta_r$ is overpotential values.[13]

The advantage of using Butler-Volmer is the high precision at low current densities. Because of the two iterative terms, the equation is not very practical for engineering calculations.[13]

$$j = j_0(exp[\frac{(1-\alpha)zF}{RT}\eta_r] - exp[\frac{\alpha zF}{RT}]\eta_r) \tag{2.8}$$

In many problems, the current density and overpotentials are so large that the back reaction can be neglected. The Bulter-Volmer equation can then be arranged as the Tafel equation shown in equation 2.9, which is much easier to work with. a and b are tabulated values.[13]

$$\eta_r = a + blogj \tag{2.9}$$

**Concentration Overpotential**

Concentration overpotential is due to concentration gradients in the bulk electrolyte or electrode surface. This happens due to the speed of the mass transport as a cell undergoes a reaction. Larger concentration overpotentials occur when the cell reaction is faster than the mass transport. This can lead to an accumulation of products or depletion of reactants on the electrode surface.[13]

## 2.2 Structure of Lithium-ion Cell

A Li-ion battery cell in Figure 2.3 consists of two current collectors, anode, cathode, electrolyte, and separator. The anode and cathode contain the active material and are called electrodes. The anode is connected to a current collector made of cobber, and the cathode to a current collector of aluminum. Between the electrodes is an electrolyte-filled separator. The electrolyte prevents short-circuiting and contains Li-ions used during cycling. All these parts are put in a casing, such as a cylinder or a pouch, with external tabs sticking outside. [1]

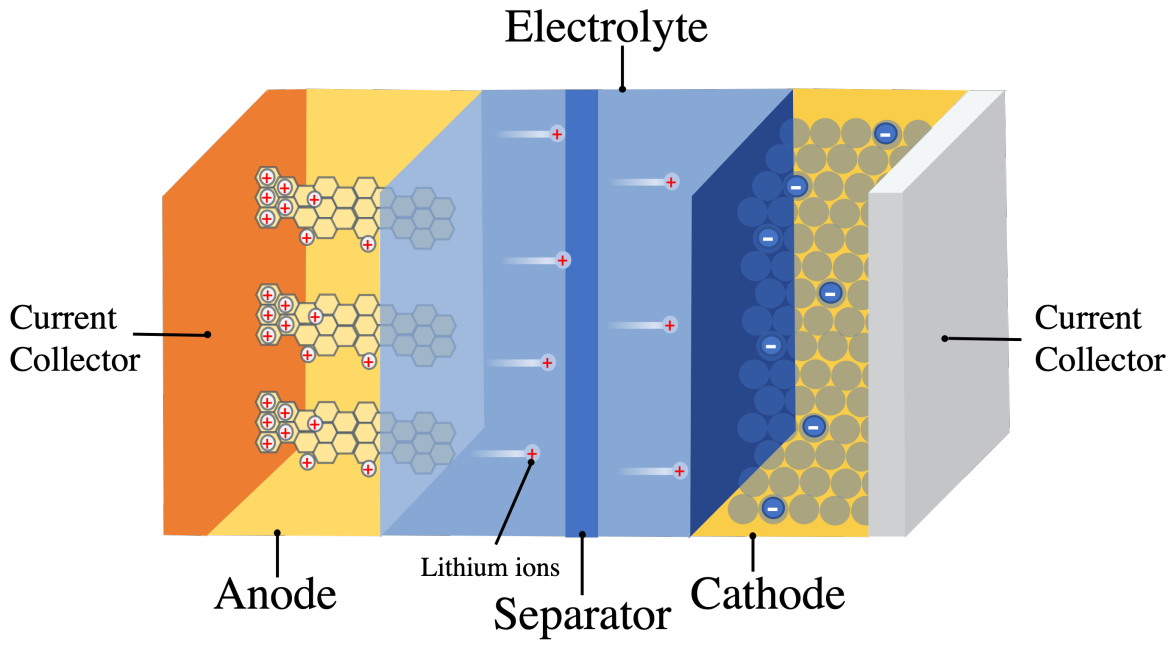


**Figure 2.3:** Lithium ion cell structure. Made by author, inspired by [16]

While the cell charges, Li-ions from the cathode dissolve in the electrolyte solution through an oxidation reaction. The Li-ions travel through the electrolyte and separator to the anode, where they intercalate into the anode structure. At the same time, the electrons move through the outer circuit. During discharge, the flow of electrons and Li-ions move the opposite way. [1]

Figure 2.4 shows a typical weight distribution in percentage for a LiB cell. The electrodes account for the highest proportion, almost 40%. The current collectors are the second highest at 15%, followed by electrolyte at 11%. The separator has the lowest weight percentage at 4%.[17]

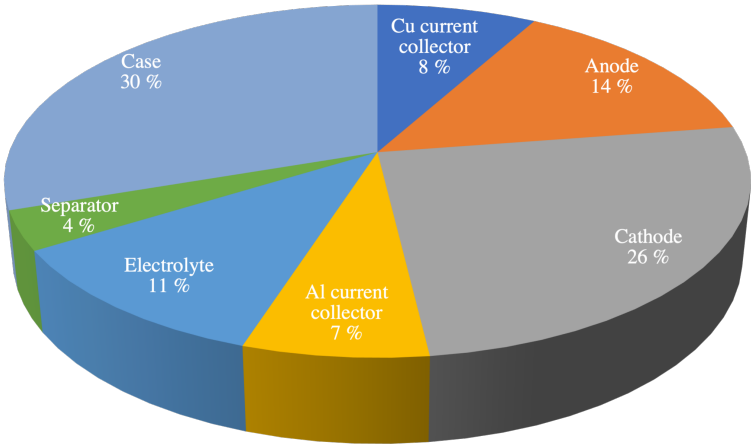


**Figure 2.4:** Weight distribution in the percentage of a typical LiB cell. Values from He et al. [17]

### 2.2.1 Anode

The anode is the negative side of the cell and consists of active material, binder, and current collectors. As of 2015, 98% of all anodes on the market were carbon-based. Materials such as silicon, lithium metal, and tin have been researched in recent years. The anode has a large effect on the performance of the whole cell. Graphite is the most used anode material in commercial cells due to its low costs and stable charge and discharge performance. The graphite structure allows Li-ions to intercalate and de-intercalate from the space between layers. Using graphite prevents anode size, structure, and shape changes during cycling. A carbon coating on the surface of the anode has been reported to improve the charge and discharge performance. In addition to graphite, hard carbon can be used. Compared to graphite, hard carbon has a higher capacity but lower density and larger irreversible capacity loss.[18–20]

Other anode materials with higher battery capacity than graphite are alloy anodes such as aluminum, magnesium, and silver. Alloy anodes have between two and ten times higher specific capacity than carbon-based anodes. In addition, Conversion Type Anode Materials, CTAM, have become promising anode materials due to their high specific capacity. Drawbacks include poor conductivity for both electrons and ions and large volume expansion. Silicon is also sometimes used as an anode material for Li-ion batteries. Si has the highest gravimetric and volumetric capacity. It is also relatively abundant on Earth. Challenges with silicon include large volume variations.[18, 19]

### 2.2.2 Cathode

The cathode is the positive electrode, and cathode materials vary much more than anode materials. The materials must be able to store lithium in a crystal lattice reversibly. All cathodes consists of the current collector, a conductive binder, and the active material. The most used active material chemistries are LCO, NMC, NCA, LMO, and LFP. A comparison of some important properties of the different types is found in Figure 2.5. To be a suitable cathode material, some properties that are favored are:[21, 22]

1. High free energy reaction with lithium. This leads to high voltage.
2. Needs to be able to incorporate many Li-ions reversibly. This leads to high energy density and rechargeability.
3. Must be able to incorporate Li-ions without causing structural changes. This is vital to be able to ensure long cycle life.
4. Need to be able to intercalate Li-ions fast. This leads to high power capability.
5. The material needs to be a good electrical conductor while not reacting with the electrolyte.
6. Optimally has low cost and is commercially available.

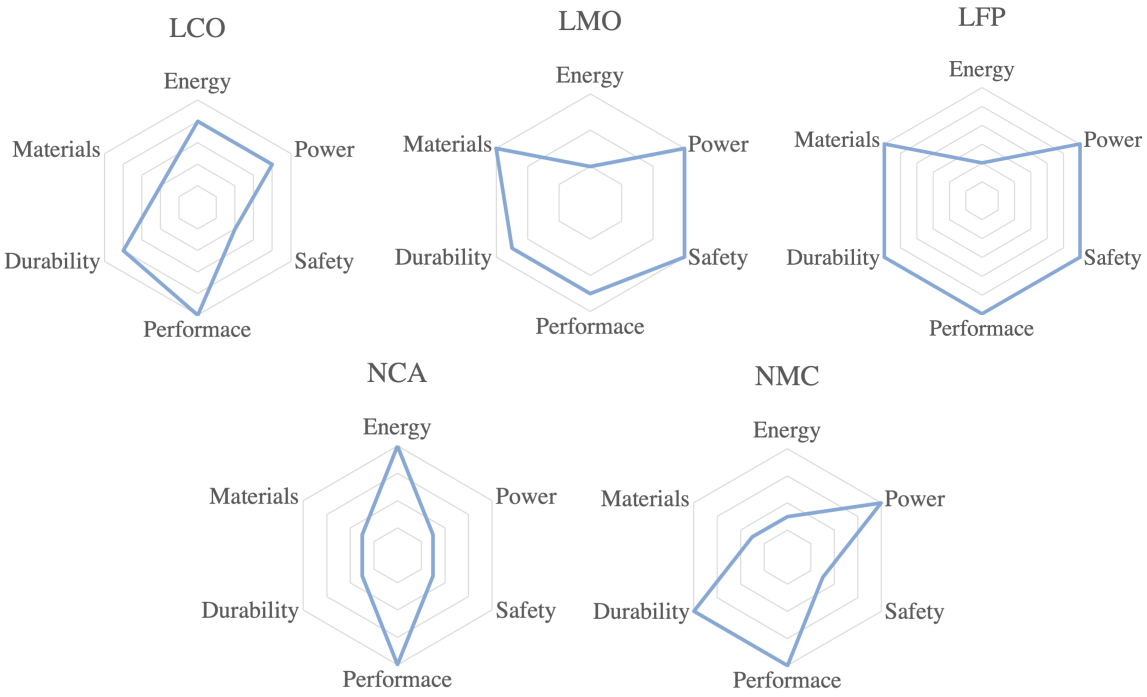


**Figure 2.5:** Comparison of cathode chemistries. Figure from Zubi et al.[21]

Depending on the material, the cathode can be arranged in a layered, spinel, or olivine crystal structure. The layered structure is the simplest, used in LCO and NMC cathodes. Li-ions are intercalated between the layers of cathode material. In the spinel structure, the cathode material is in a lattice framework, and the Li-ions are inserted in tunnels formed as the material crystallizes. In the very complex olivine structure, Li-ions are intercalated between crystallized molecules.[22, 23]

Today most of the cathode materials are transition metals in groups 3 - 12 in the periodic table. These elements have incomplete electron shells, which is optimal for creating positively charged ions as the electrons are removed. In addition, they are good conductors of both heat and electricity. LCO was the first chemistry to become commercially available in 1991. LCO has high specific energy, but CO has low stability. This results in a thermal runaway (Chapter 2.5.6) at only 150°C.[21, 22, 24]

Following LCO, LMO was commercialized in 1996. LMO has a low internal resistance, leading to a high specific power but lower energy density. In addition, the safety is better due to MO having higher thermal stability than CO. Shorty after, in 1999, LFP was available. LFP was promising due to its durability, safety, and eco-friendly materials. However, the specific energy is relatively low, which was a setback for this technology regarding EVs and other larger mobile applications. NCA was also introduced in 1999. NCA cells have a much lower share of cobalt than LCO, which is essential for stability. With high specific energy and longer cycle life, NCA has been used in EVs.[21]

Five years later, NMC was available. NMC has lower energy density than NCA but longer cycle life. LFP, LCO, and NMC account for 80% of all Li-ion cells made today. NMC chemistry is becoming a leading choice in the industry due to its high energy density, low cost, and high voltage. NMC's balanced composition offers excellent energy and power density across a wide temperature range, making it flexible to cater to different application needs. It has a long cycle life, with some cases exhibiting up to 6000 full depth of discharge cycles, making it ideal for long-lasting applications. The discharge depth must be reduced to achieve the best performance when combined with a graphite anode. In some cases, this leads to only 80% of the capacity being used.[21, 25]

High nickel content leads to high specific energy, while high manganese content increases specific power. However, nickel-rich combinations have structural degradation issues, manganese-rich combinations have reduced capacity, and cobalt-rich combinations have high cost and safety concerns. The traditional material combination is a 1:1:1 ratio of nickel, manganese, and cobalt. This can be written as $LiNi_{1/3}Co_{1/3}Mn_{1/3}O_2$.[22, 26]

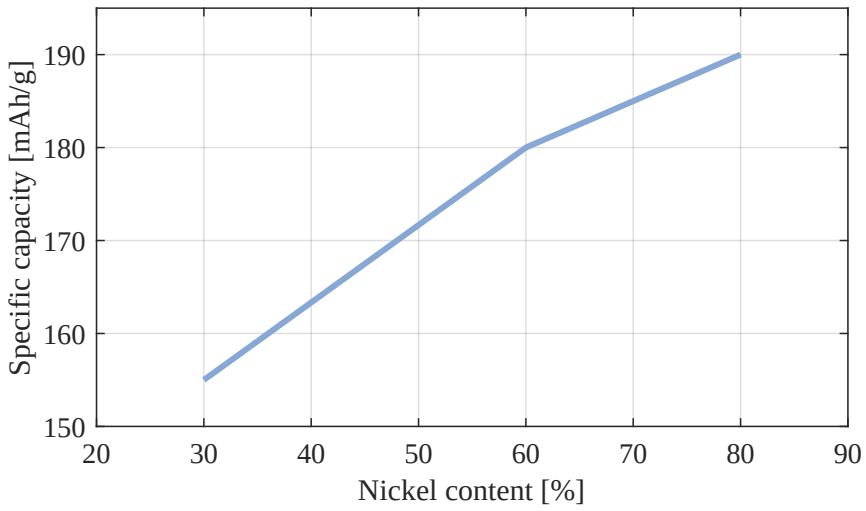


**Figure 2.6:** Nickel content and energy density of NMC cells [22]

Development is done on combinations with more nickel, which means less cobalt, reduced costs, and increased energy density. Figure 2.6 shows the relation between the nickel content of a cell and the energy density of the cell. The goal is to find a combination where the positive sides of high nickel content are optimized while trying to avoid structural degradation issues.[22, 26]

Research is also done on cathodes consisting of blends of different chemistries. The objective of a blend is to take advantage of the best properties of each chemistry used to achieve better performance than each chemistry would have individually.[27]

### 2.2.3 Current Collectors

The current collectors are connected to the electrodes and connect the cell with the external circuit. They need to allow the flow of electrons but not ions. They are usually made of cobber for the anode and aluminum at the cathode. These metals are favored due to their high conductivity. The current collectors are different materials because of the metals' electrochemical stability windows. Cobber has a stability window from 0 to 3.2 V. Above this, the Li-ions will react and oxidize. The stability window is higher for aluminum, but it will react with lithium below 0.6 V.[22, 28]

The thickness has decreased from 18 to 15% in the last two decades. This leads to increased energy density. The current collectors are vital for the electrical conductivity of the cell. A too-thin current collector reduces electrical conductivity and heat transfer, which leads to a lower power density. There is, therefore, a trade-off between energy and power when deciding current collector thickness. Other materials than Al and Cu can be reviewed to increase the performance further, as well as different structures and treatments such as etching and coatings.[28]

### 2.2.4 Electrolyte

The electrolyte between the electrodes and separator consists of lithium salts and organic solvents. The organic solvents are essential for performance because they increase the mobility of the Li-ions moving between the electrodes. The electrolyte is usually a liquid but is also sometimes a polymer gel, and some of the most used compounds are organic solvents like dimethyl carbonate, propylene carbonate, and ethylene carbonate, and salts such as $LiBF_4$ and $LiPF_6$.[22, 29]

A characteristic of the electrolyte is the ability to keep the electron count unchanged for the ions moving through. This is done by limiting the forces between the ions. Anions connect with the Li-ions while it is transported through the electrolyte without changing the electron count. When the ion reaches the electrode, the bond with the anions breaks, and the ion can become part of the oxidation or reduction process.[22, 30]

Using different additives and ratios of materials in the electrolyte promotes different characteristics. In the electrolyte, additives account for about 5%. The additives are important for the cell's safety, performance, and lifetime and usually target specific performance improvements. These include protecting the cathode, improving SEI formation, stabilizing the Li-salts, and inhibiting corrosion. However, some parameters might have to be sacrificed to achieve others. For example, an additive improving performance during low temperatures can decrease power capability. In this way, battery manufacturers can tailor additives based on the intended use of the battery.[22, 31]

Some characteristics of good electrolytes are: [22, 32, 33]

1. Stable when exposed to both positive and negative components and does not break down when in contact with the other components of the cell. Stay stable across the complete voltage window.
2. Have good ionic conductivity while exposed to as many conditions as possible, i.e., high and low temperatures and high and low voltages.
3. Have low viscosity to make the ionic movement as easy as possible.
4. Unpermable to electrons, to make sure the electron moves through the current collectors and outer circuit.
5. Not contain reactive components. This ensures that the electrolyte does not consume the Li-ions.
6. Low freezing point and high boiling point.
7. Low cost
8. Not be toxic or flammable

### 2.2.5 Separator

Separators are very important for the safety and longevity of cells. Even though it is essential, it is the least discussed component. Today, most separators are made of polyolefin plastic films. The separator is a porous membrane that physically separates the two electrodes and keeps them electrically separated. This separation prevents short-circuiting of the cell. Like the electrolyte, it needs to be ionically conducting and electrically insulating to secure that Li-ions can move through while the electrons can not. It must also have big enough pores for the Li-ions to move through, about 1 $\mu m$.[22]

The separator is 20 to 25 $\mu m$ thick, with research and development working on thinner separators of 10 to 15 $\mu m$. In regards to energy density, a thin separator is optimal. The separator must withstand puncturing or penetration from dendrites and the winding process that occurs during battery production. Both of these are harder when the separator is very thin. More research is needed to achieve optimal separator thickness.[22, 34]

Research is also done on various coatings to improve characteristics. A ceramic coating improves safety due to an increased melting point. The ceramic coating leaves the pores open while creating a protective film.[22]

## 2.3 General Terminology

This chapter explains and describes important terminology used regarding batteries. This chapter aims to give the reader an understanding of how this terminology is used in the thesis.

### 2.3.1 C-rate

The C-rate describes the rate of charge added or removed from a cell. A full discharge or charge in one hour is denoted 1C. Equation 2.10 shows how the C-rate can be calculated based on current and capacity. [1]

$$C - rate = \frac{Current[A]}{Capacity[Ah]} \tag{2.10}$$

### 2.3.2 State of Charge

The state of charge of a cell is the amount of charge in the cell compared to the amount of charge when fully charged. This can be seen in equation 2.11. As the cell age, the amount of charge when fully charged will decrease. It is important to use the current amount of charge to achieve an accurate value of the state of charge. State of charge is usually abbreviated as SoC. When a cell is not cycled from 0 – 100% SoC, the term SoC window can be used to describe the pattern. [1]

$$SoC = \frac{Amount\ of\ charge}{Amount\ of\ charge\ when\ fully\ charged} \cdot 100 \tag{2.11}$$

### 2.3.3 State of Health

The state of health, abbreviated SoH, of a cell describes the capacity of the cell compared to the capacity when the battery is new. As the name indicates, this is a measure of the health of the cell. To achieve accurate measurements and be able to compare the values, the measurements have to be done at the same C-rate and temperature. The equation for this is shown in 2.12.[1]

$$SoH = \frac{Capacity\ when\ fully\ charged}{Capacity\ when\ fully\ charged\ when\ new} \cdot 100 \tag{2.12}$$

### 2.3.4 Open Circuit Voltage and Terminal Voltage

Open circuit voltage and terminal voltage are both measured in volts. Terminal voltage is measured across the terminals. When there is no load open circuit voltage, abbreviated OCV, can be measured. OCV shows the difference in electrical potential between electrodes after a relaxation of the kinetic process. The relationship between SoC and OCV in a cell is direct but non-linear, varying for each battery. This relationship is essential for accurate battery modeling.[1, 35, 36]

### 2.3.5 Constant Current – Constant Voltage

Constant current constant voltage, CCCV, is the most widely used charging method for Li-ion batteries. The battery is first charged with a constant current at a given rate. When a decided voltage is reached, i.e., high voltage limit, the charging method switches to constant voltage. The voltage phase limits voltage increase and is positive for energy efficiency. The CV step leads to the terminal voltage moving towards OCV, defined as a fully charged cell. It also ensures that the voltage does not exceed the voltage limit, which can cause irreparable damage.[1, 37]

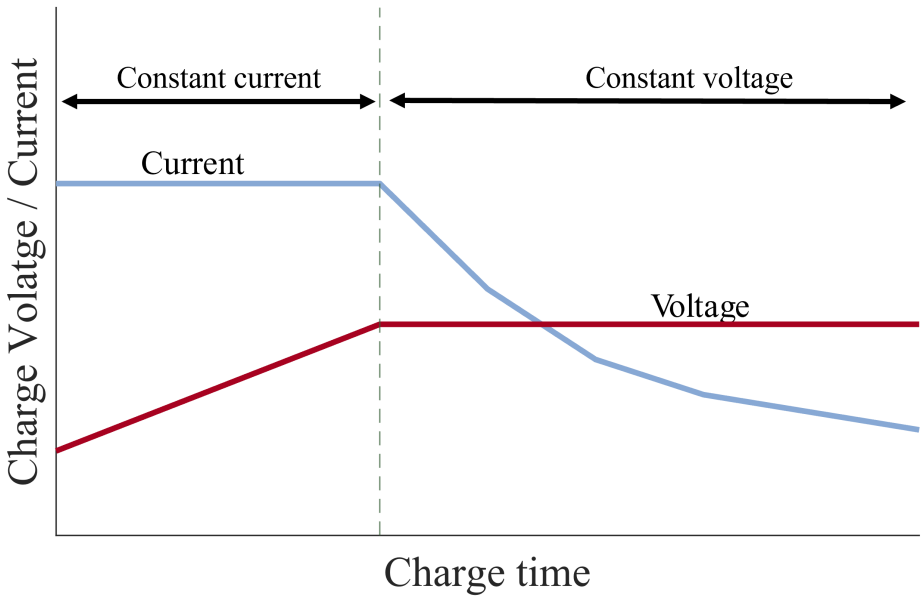


**Figure 2.7:** Constant current constant voltage charge

## 2.4 Battery Manufacturing

The manufacturing process starts with combining binder, active material, conductive additives, and solvent into a slurry. The active material can be NMC, LCO, or NCA for the cathode and graphite for the anode. The conductive additive is usually carbon black, and the solvent is NMP. The slurry is thoroughly mixed before it is coated onto a current collector, which is normally aluminum for the cathode and graphite for the anode.[38]

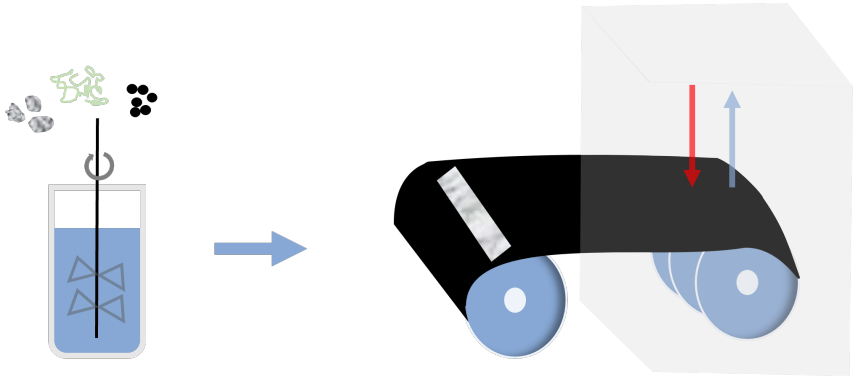

**Figure 2.8:** Slurry mixing and drying. Inspired by Bryntesen et al. [38]

The current collector sheet with slurry is dried, which leads to the evaporation of the solvent. The dry layer is then compressed or calendared down to a specified thickness or density. The sheets can then be cut or punched into desired shapes and assembled with a separator between the anode and cathode. Lastly, an electrolyte is filled, and the battery is closed.[38]

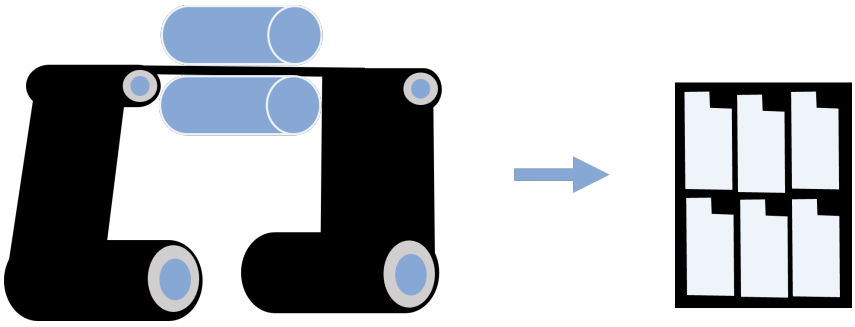

**Figure 2.9:** Calendaring and cutting. Inspired by Bryntesen et al.[38]

Formation cycles are done before the battery can be sold to a customer. The process takes a few days, and the goal is to create a stable SEI layer. This layer is described in more detail in Chapter 2.5.2. There are many different standards used for formation cycles, where in general all consist of one or more cycles at low c-rates to slowly build up the SEI layer. In addition, it is important that both electrodes and separator have become fully saturated by the electrolyte. If this is not achieved, the cell has low ionic transport. Leading to high internal resistance in the cell. [39, 40]

## 2.5 Degradation Mechanisms

After a battery is made, chemical processes occur, which leads to degradation. This happens both during cycling and when the battery is stored. Calendar aging is aging during storage, and the rate varies based on storage conditions. To measure aging, characterization tests are performed to measure capacity and resistance.[41] The predominant factor for calendar aging is the growth of the SEI layer. As the layer grows, lithium in the electrolyte is consumed. This leads to capacity fade.[1, 42]

Degradation of a battery can be divided into four main parts; loss of lithium inventory, loss of active material of the anode, loss of active material of the cathode, and increased impedance. The first three can lead to capacity fade, and loss of active material can lead to power fade. A battery cell deteriorates over time because of changes in the active material and unwanted side reactions. Aging mechanisms are generally irreversible and can lead to cell failure. All aging processes are usually accelerated by increased operating temperature. This can all be seen in Figure 2.10, which shows degradation mechanisms on both anode and cathode, what they lead to, and what causes them. The figure also includes loss of electrolyte, this is many places placed in the loss of lithium inventory category. Figure 2.10 shows many degradation mechanisms, where all do not represent an equal part of the degradation of a cell. The most prominent mechanisms are presented later in this chapter.[1, 43–46]

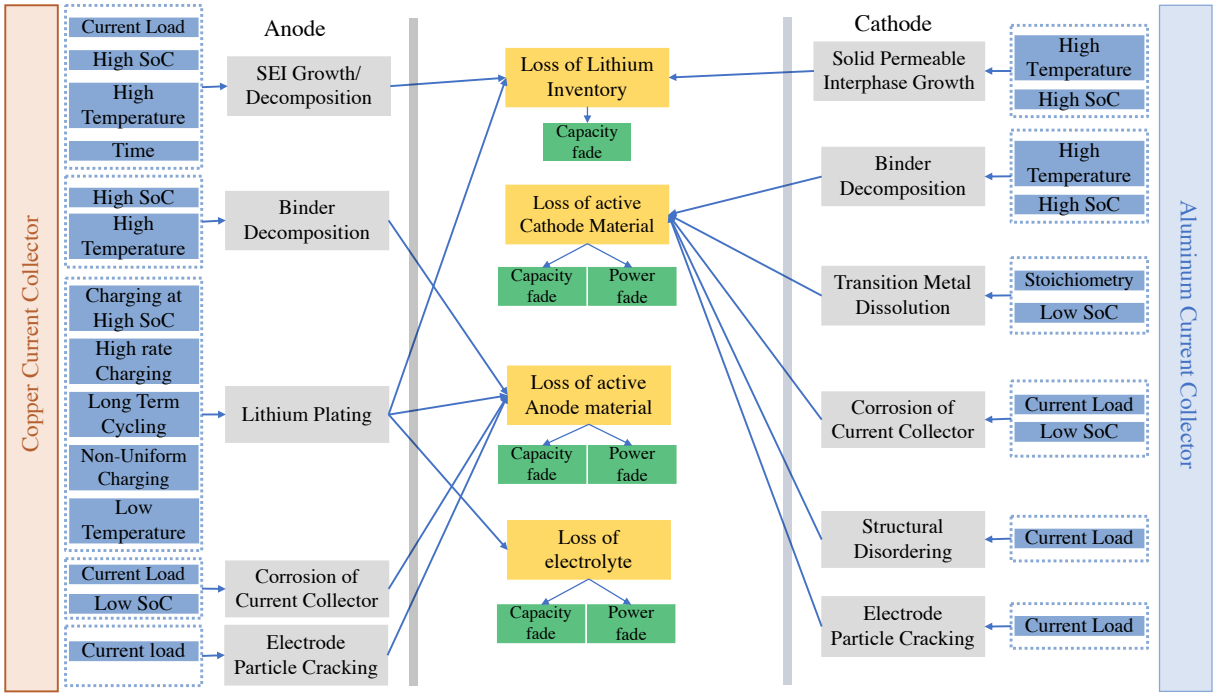


**Figure 2.10:** Figure describing the correlation between aging mechanisms and the consequences of them at the cathode and anode in a LiB cell[47]

### 2.5.1 Capacity Fade

Capacity fade is a cell's capacity loss and can be reversible and irreversible. Reversible capacity loss, called self-discharge, is only temporary and can be retrieved by charging the cell. Irreversible loss is due to the degradation of the cell and can not be recovered. Figure 2.11 shows how the capacity decreases throughout cycling. Initially, the capacity decreases fast to point A. This is followed by region B where the decrease is slowed down and again slows down further in region C. Lastly, the capacity fades very quickly in region D. The cycle number for the different regions depends on the depth of discharge, DoD, temperature, and chemistry. End of life usually is in regions C or D.[1, 48]

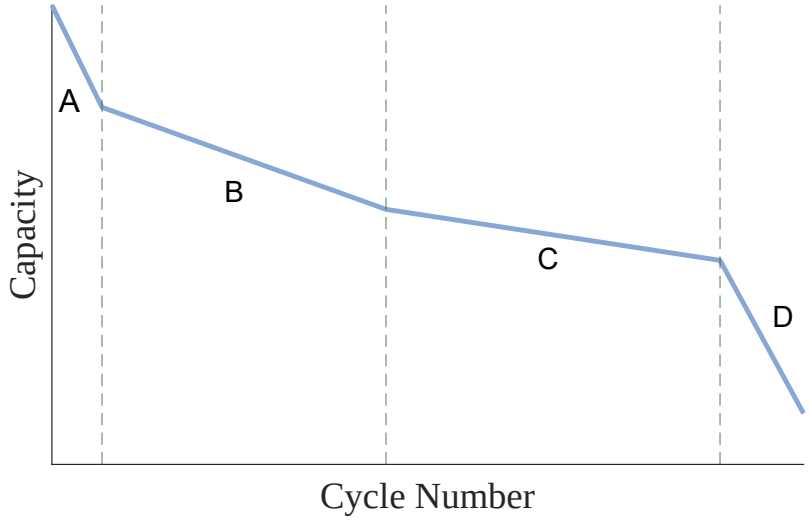


**Figure 2.11:** Typical capacity fade during cycling[48]

A capacity increase is sometimes observed at the early stages of cycling. Multiple studies have reported an initial capacity increase during cycling, but the understanding of the mechanisms is limited. Gyenes et al. [49] suggest an overhang at the anode. Li-ions are intercalated to the overhang at high SoCs in the initial cycles. This increases the amount of lithium inventory and capacity. While Severson et al. [50] suggest that negative electrode material loss leads to a higher potential difference in the cell. This results in a rise in the voltage plateau and an increased capacity. Tests done by Guo et al. [51] on an NMC/graphite cell showed an increase of 1% from the initial capacity for a battery cycled at 100% DoD and 45°C. In addition, it was shown that high temperatures and large DoDs accelerate the capacity increase and that the increased capacity originated from the graphite anode.[1]

### 2.5.2 SEI Formation and Growth

The solid electrolyte interphase, SEI, is formed as the anode comes in contact with the electrolyte. It is an electrochemical process that creates a coating on the anode surface. Li-ions form bonds with the anode molecules, which leads to some initial loss of capacity for the cell. The layer is formed during the first charge and grows slowly during cycling and storage. It pacifies the anode surface and limits the further reaction with the electrolyte, which is very positive for the stability of the cell. The layer is electrically insulating and provides ionic conductivity for the Li-ions. It protects the cell and secures safe operation, but it also increases the resistance of the cell. If the layer gets too thick, the cell's internal resistance may increase to an unacceptable value. SEI growth is one of the key aging mechanisms leading to capacity fade in a battery cell.[1, 22, 52]

The advantages of a good SEI layer are low battery resistance, less polarization, and a high discharge plateau. The SEI layer can be exposed to three different failure mechanisms; thermal failure, chemical failure, and mechanical failure. During high temperatures, some of the components of the SEI layer decompose, leading to an inhomogeneous layer where dissolution leads to the increased thickness of SEI. At 1C ohmic heat is the dominant heat source. The SEI is chemically unstable and evolves as the cell is cycled. These changes can include an increase in inorganic components and a decrease in organic components. When a chemical failure occurs, these reactions negatively damage the SEI layer and destabilize the interphase. Cycling of the cell also leads to compressive and tensile strains, which can trigger breakage and cracks in the SEI layer called mechanical failure. Mechanical failure causes consumption of more electrolyte and active Li-ions. This leads to reformation of SEI and loss of lithium inventory. As the layer increase in thickness, the resistance and heat increase. During storage, both the SEI growth rate and solvent diffusion rate are reduced. This leads to slowing the SEI growth and, thus, capacity loss.[1, 53–55]

### 2.5.3 Lithium Plating

Lithium plating is a deposition of metallic lithium on the anode surface and is a very complex process that has yet to be fully elucidated. It can occur during normal operating conditions as the cell ages but mostly happens during fast charging and charging at low temperatures and is the limiting factor for faster charging. The intercalation process on the anode is diffusion limited, meaning that only a certain amount of ions can be embedded in the structure at a specific temperature. As the charging cycles continue, the graphite vacancy sites decrease. This leads to less intercalating and more lithium plating, which reduces battery life and limits fast charging capabilities. Lithium plating promotes further degradation and has a negative impact on safety and thermal stability. In the worst case, lithium plating can lead to lithium dendrites, and lithium plating is regarded as a major reason for easier thermal runaway.[1, 47, 56]

Lithium plating can be both reversible and irreversible. Reversible plating is deposited lithium that still has electrical contact with the anode surface. The reversible plating undergoes a charge transfer reaction into the electrolyte and intercalates back into the anode. This part is called lithium stripping. Irreversible plating leads to two conditions: second SEI layer growth and dead lithium. A side reaction between plated lithium and electrolyte generates a new secondary SEI layer. This layer consumes more lithium. Dead lithium is a film of high-impedance lithium that is electrically insulating against graphite. Dead lithium can create tortuous pathways for Li-transport, reducing the active area for intercalating. This increases the internal resistance and reduces energy density. Both the second SEI layer and dead lithium reduces the battery capacity.[1, 47]

As mentioned, lithium plating can in the worst case lead to dendrites. Dendrites form on the electrode's surface, and can grow over time through the separator to the other electrode. This leads to an increased cell self-discharge rate. In the worst case to short circuit and rapid heating of the cell.[1, 47]

### 2.5.4 Cathode Electrolyte Interphase

The cathode electrolyte interphase, CEI, is a layer on the cathode surface. Unlike the SEI layer, the CEI layer still needs to be thoroughly investigated and understood. It is formed by the decomposition of the electrolyte on the cathode surface during oxidation. It is a heterogeneous film, and there are still controversies about its properties.[57] Zhang et al. [58] could not visually find any CEI layer during normal operating conditions on NMC532 cells. However, a layer could be found after shorting the cells for about 20 seconds. This lowers the cathode's stability beyond the electrolyte's stability window. Leading to electrolyte decomposition, which reacts with the cathode and creates a more visible CEI layer.

A robust and dense layer improves the thermal stability of the cathode. But an uneven and thick CEI significantly impacts the local levels of delithiation and lithiation over extended periods of cycling. This leads to irregular contraction and expansion of the lattice, eventually resulting in the formation of cracks. When the CEI breaks down, the electrolyte comes into contact with the transition metal, causing the metal to dissolve and exothermic reactions.[59]

### 2.5.5 Transition Metal Dissolution

Transition metal ions, like Manganese, are part of the cathode structure. After cycling, some transition metal ions have been noticed in the electrolyte and on the anode, especially at higher temperatures. This results from the transition metals dissolving from the cathode structure and mitigating through the electrolyte and deposit on the anode. The process leads to capacity fade and alters the surface structure of the cathode.[1, 60]

### 2.5.6 Temperature

Li-ion batteries perform best at a constant temperature of around 25°C and are very sensitive to temperatures above this. The temperature has the largest impact on both capacity fade and resistance increase aging mechanisms for all chemistries during cycling and storage. Higher temperature improves the performance by enhancing reaction kinetics, but all side reactions are also accelerated, resulting in increased degradation speed.[1, 61]

For the anode, during high temperatures, the dominating aging factor is SEI layer degradation. This can be seen as structural changes in the layer, as well as dissolution and decomposition. The organic components in the electrolyte are converted to more stable inorganic components. This increases the SEI layer resistance. Jalkanen et al. [46] showed that there was minimal lithium plating for NMC cells at 25°C. For the cathode, transition metal dissolution and surface film formation are increased. In the electrolyte, the binder can be weakened, which leads to the degradation of the composite electrode.[1, 46]

At low temperatures, the conductivity is lowered in the electrolyte. This makes it more difficult for the ions to move between the electrodes, increasing the internal resistance. This leads to less intercalating and more lithium plating.[22]

If the heat generation in a cell is higher than the dissipation of heat, the heat can lead to exothermic reactions. These reaction increase the temperature further, which again leads to more deleterious reactions. When the heat exceeds the cells heat endurance, fire and explosions can occur. The onset temperature that triggers thermal runaway vary with chemistry, SoC and abuse of the cell. At high temperatures inside a cells operating temperature, this happens as well, but much slower. This decreases the cycle life. Calendar-aged cells show an increased temperature for triggering thermal runaway and decreased exothermal rate. Cells cycled at low temperatures show a decreased thermal runaway triggering temperature and thermal stability. Regardless of aging mechanism, a larger volume of combustible gas is released when thermal runaway is triggered for aged cells. Today the main cause of battery accidents is related to thermal runaway of cells.[56, 62]

### 2.5.7 Resistance Increase

As the cell cycles, the resistance will increase. The increased resistance makes it harder for the Li-ions to move through the cell. Ohmic resistance increase leads to the moving of the discharge curve to lower voltages and the charge curve to higher voltages. This results in less energy in the cell when charging is completed. This can be due to the growth of the SEI layer over time, both during cycling and storage. In some cases, as much as 100%. Higher resistance causes a drop in voltage due to the cell consuming some energy in the form of heat.[46]

Loss of electrical contact occurs between active material particles, between the particles and the conductive additives, or between particles and current collectors. Contact losses increase internal resistance and promote aging. Volume variations, surface film formation, decomposition of the binder material, and corrosion of current collectors can result in electrical contact loss.[46] High or very low SoC leads to increased resistance. This trend is even more distinct for aged cells. Because of this, it is better for cycle life to use a smaller charge window for aged cells. Regarding temperature, higher temperature leads to lower resistance due to reaction kinetics.[63]

During early cycling, resistance can sometimes decrease. This has been explained as a geometric overhang of anode material compared to cathode material. This leads to some of the anode not having a cathode counterpart. Resulting in a slow flow of active lithium moving between the passive and active parts of the anode and a reversible resistance decrease.[1, 63]

## 2.6 Analysis Methods

In the following chapter, two analysis methods are explained and described. Incremental Capacity Analysis is a non-invasive method while Accelerating Rate Calorimetry requires opening of the cell.

### 2.6.1 Incremental Capacity Analysis

Increment capacity analysis is used to understand aging and changes in the electrodes in a non-invasive way. The method makes it possible to see gradual changes in the electrochemical behavior while only using sensors that are commonly used in battery systems, which is the reason the method is gaining popularity. It is, however, important to note that analysis is chemistry dependent. This is done by differentiating battery capacity over voltage for a full cycle. This creates $dQ/dV$ curves plotted with voltage on the x-axis, where the plateaus and peaks yield thermodynamic information about the cell's internal state. To fully understand the results, it is beneficial to first create degradation maps for the cells. The are synthetically generated curves that individually represent voltage variations for the degradation modes. These maps help understand which part of the total curve is most sensitive to each degradation mode.[64]

Cell changes are seen as shifts and changes in the peaks of the $dQ/dV$ curves. This method can detect changes in the cell before any capacity is lost. If the peak shifts to higher voltages without changing shape, it indicates an increase in ohmic resistance, while if the peak is lowered and broadened, it indicates an increase in charge transfer resistance.[64]

If a peak decreases height and shifts towards higher or lower voltages, this indicates a loss of lithium inventory, LLI. LLI can, among others, be caused by lithium plating, SEI growth, or electrolyte oxidation. If a peak is lowered at the same voltage while the total volume stays the same, it can indicate a loss of active material, LAM. LAM can be caused by transition metal dissolution, the formation of Li grains, or crystal structure disordering.[64]

### 2.6.2 Accelerating Rate Calorimetry

Accelerating rate calorimetry, ARC, is a characterization method used to investigate the thermal stability and self-heat rate of a material. The ARC does not measure any endothermic reactions but captures the impact of self-heating and thermal runaway. The device measures time, temperature, and pressure while controlling the temperature of the surroundings. This ensures that the reactions occur at adiabatic or close to adiabatic conditions. Any exothermic reaction with heating over a specific limit can be detected. The onset of exothermic reactions is usually set to $0.2°C/min$, and thermal runaway at $10°C/min$. The test can be done both on cells and specific materials.[65, 66]

Most ARC systems use the heat-wait-seek method. The method is based on the sample being heated to a set temperature. The system then waits for a period of time to establish equilibrium. After this the system enters seek mode, where it seeks for exothermic activity larger than the onset of $0.2°C/min$. If there is no activity, the temperature is increased, and the cycle is repeated until there is exothermic activity. The system will then enter exothermic mode, where the sample is just being tracked.[65, 66]

**$\phi$ factor**

Due to the adiabatic conditions simulated during the ARC test, the sample and sample holder absorbs most of the heat. It is, therefore, important to know the physical properties of the sample holder. The $\phi$ factor is used to describe the heat lost to the sample holder. It relates the heat capacity of the sample to the total heat capacity of the sample holder, called the bomb, and the clip attaching the temperature sensor to the bomb. Equation 2.13 shows this correlation, where b denotes bomb, and s denotes sample. Any additional parts that could absorb heat should be added numerator. m is the mass and cp is the heat capacity.[65]

$$\phi = 1 + \frac{m_B Cp_B + m_{Clip} Cp_{Clip}}{m_s Cp_s} \tag{2.13}$$

## 2.7 Safety Considerations

Battery cells can short-circuit due to several reasons, and this includes both internal and external short circuits. During an internal short circuit, all current in the cell moves through the short circuit site instead of the intended outer circuit. This leads to a rapid release of energy, which causes the cell to generate heat. If the amount of heat generated is larger than the amount that can be removed, the cell will begin to heat up. The cell will then continue to heat until it reaches the thermal runaway onset temperature, which is explained in chapter 2.5.6. A cell with a high SoC will have a larger amount of energy than a cell with lower SoC. A short circuit during high SoC will have larger heat generation and possibly larger consequences than a cell with lower SoC.[67, 68]

If a cell experiences high temperature it can negatively affect the cell. At about 90°C the pores in the separator begin to close, and at 120 – 130°C the separator begins to melt. The melting leads to shrinkage in the separator material, allowing the electrodes to come in contact with each other. This creates an internal short circuit of the cell.[22]

Lithium dendrites can also cause short-circuiting. If the dendrite grows through the separator and reaches the cathode, this creates a short circuit. All current is then forced through a very small point, which will generate large amounts of heat. Internal short circuits can also be caused by debris getting into the cell during manufacturing or due to failures in the manufacturing process. External short circuits are caused by a conducting material being in contact with both negative and positive terminals simultaneously. External short circuits generally have the same consequences as internal short circuits.[22]

# Chapter 3

# System and Approach

Some experiments were set up to evaluate and understand aging mechanisms in Li-ion batteries. The batteries used were received from IFE. The batteries were bought in 2015, and 3 were cycled for about a year, while the rest have been stored in a cold room. The already cycled batteries are referred to by the lot number used while cycling, respectively 194, 231, and 364. Cell 194 was cycled at 45°C, while the two others were cycled at 25°C. Cell 231 was cycled in a vertical slot, and 194 and 364 in horizontal slots.

## 3.1 Batteries

The batteries used in this project are XALT 31Ah high-energy lithium polymer cells with NMC433 cathodes. Table 3.1 shows relevant information about the cells from the datasheet. Earlier studies done by IFE on these cells indicate an overly dense anode[69].

**Table 3.1:** Values from the datasheet from the supplier of the batteries

| | |
|---|---|
| Capacity | 31 Ah |
| Nominal voltage | 3.7 V |
| Lower limit voltage | 2.7 V |
| Upper limit voltage | 4.2 V |
| Internal impedance | 1.1 m Ω |
| Weight | 0.69 kg |
| Gravimetric energy density | 160 Wh/kg |
| Volumetric energy density | 339 Wh/L |
| Charge temperature range | 0°C – 45°C |

## 3.2 Approach

The approach for the experimental work is cycling cells to be able to evaluate aging mechanisms. To compare the data from the cycling of the already cycled cells to the uncycled cells it was decided to age the cell the same way as at IFE. This includes both characterization and aging. To simulate real-life conditions the cells were cycled at three different temperatures; 5, 25, and 45°C.

Before cycling, the OCV was measured, and holes were punched to fit the cables. Next, cables and screws were attached, and the tabs were taped to avoid heat and short-circuiting. Finally, the batteries were placed in a cabinet with the desired temperature, and cables were connected to the tester system. The system used is Arbin Instruments LBT21084 with Mits Pro testing software.

### 3.2.1 Characterization

The characterization is done to gain information that aging cycling can not provide. Due to unwanted aging, characterization tests should be minimized[70]. Therefore characterizations are done every 100 cycles or after the SoH has decreased by 5%, whatever comes first. Figure 3.1 shows the schedule for characterizing the cells. Between the discharge and charge, there are 30 minutes pause. The charge capacity during C/20 is used when evaluating the cell's capacity.

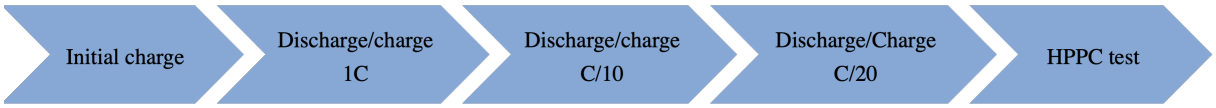


**Figure 3.1:** Schedule used to characterize cells

### 3.2.2 Hybride Pulse Power Test

The Hybride Pulse Power Test, HPPC, is used to measure the resistance of the cells. The schedule used can be found in appendix A. The test applies positive and negative pulses at different SoCs and measures the voltage during the pulse and the pause after. The difference in voltage and current is found during the test, as shown in Figure 3.2. The short pulses last 5 seconds with a one-second pause after, while the long pulses last ten seconds with three minutes pause.

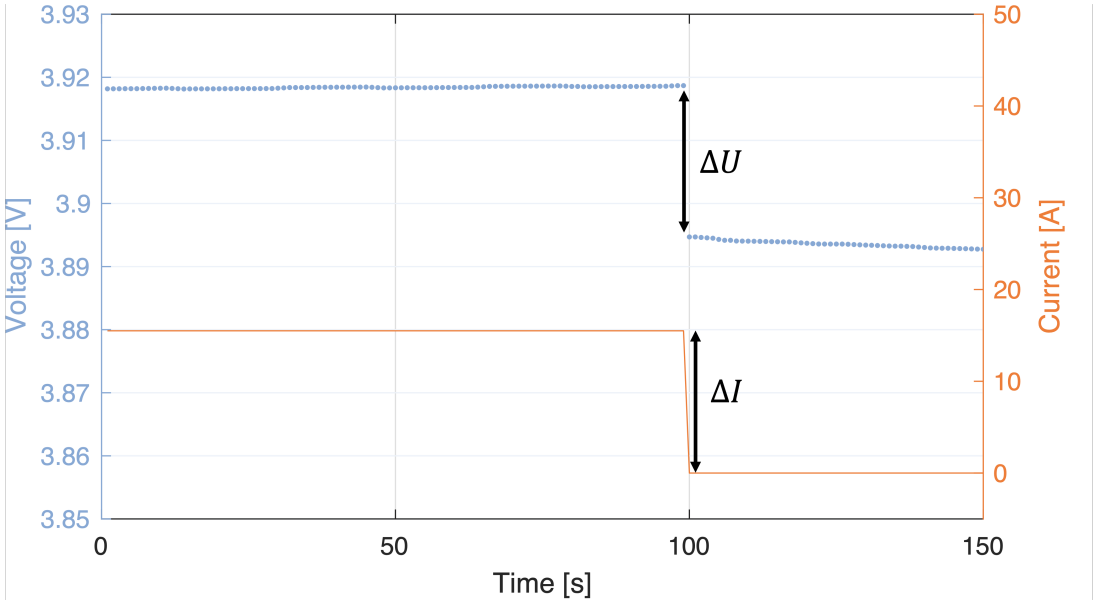


**Figure 3.2:** HPPC test showing the drop in potential as the current is turned off

The internal resistance can be calculated using Ohms law shown in equation 3.1 for the current and voltage difference between the pulse's last step and the rest period's start. For a positive pulse, the immediate decrease in voltage is due to the pure ohmic resistance of the cell[15].

$$R = \frac{\Delta U}{\Delta I} \tag{3.1}$$

### 3.2.3 Aging

For first life cycling, the cells are cycled at a C-rate of 1C. At IFE, cells 231 and 364 were cycled at 1.5C. This was not possible at NTNU due to limitations in the tester, as the maximum current of the tester is 30 A, so cycling conditions between these cells and the new cells will not be completely equal. Cells are cycled in a complete voltage window of 0 - 100% SoC. When the cells reach the end of their first life, the SoC window is reduced to 10 – 70%, and the C-rate is reduced to C/4. This is done when the slope of capacity decrease approaches vertical.

As the cells age, the heat generation increases. To ensure close to identical conditions at the start of each cycle the temperature of the cell can maximum be +1°C compared to the chamber temperature for a charge or discharge cycle to start. If this is not fulfilled, the system will wait until the temperature has decreased to start the cycle. Figure 3.3 shows the schedule used. The CCCV step has a cut-off voltage of 1.55A.

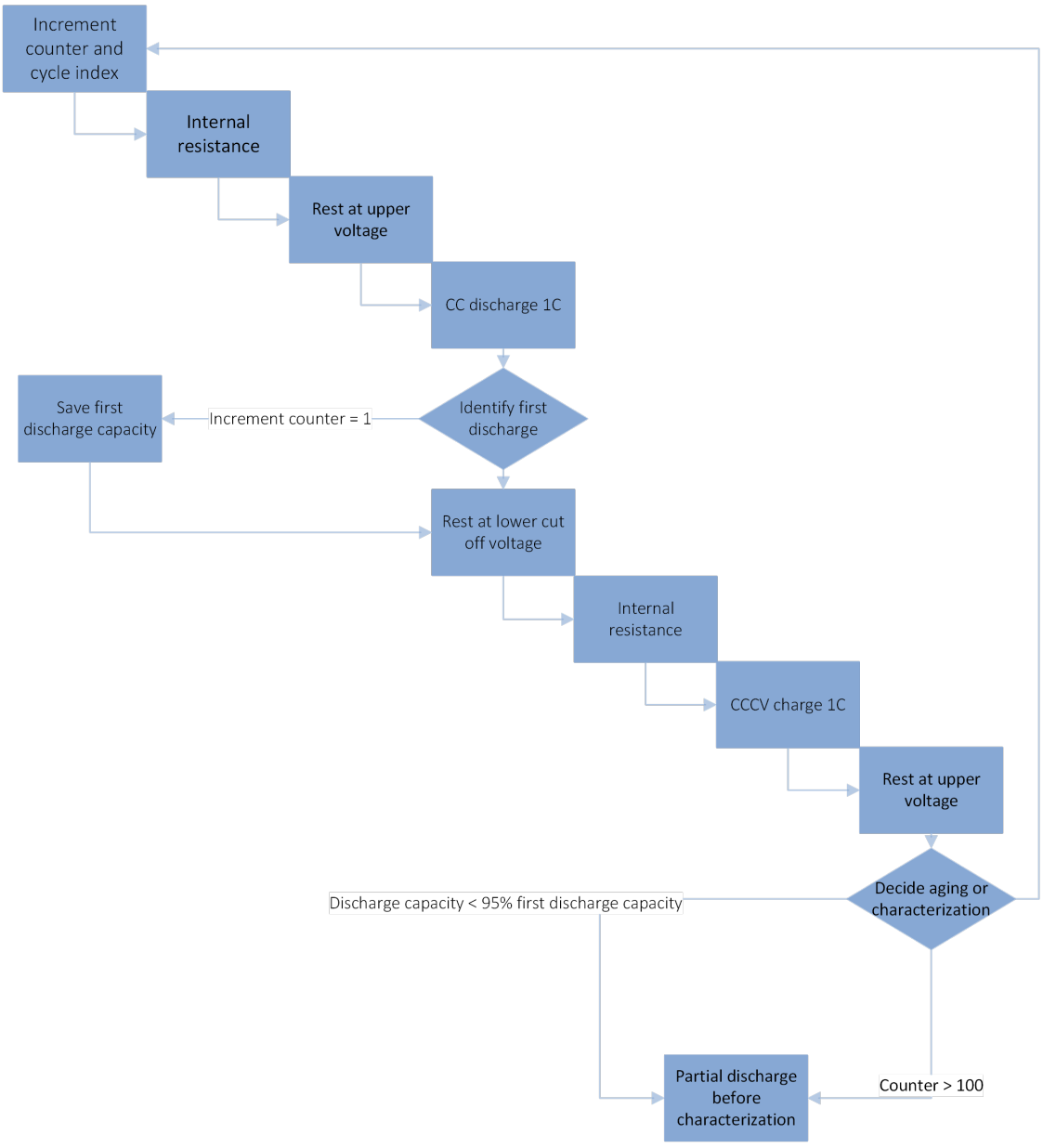


**Figure 3.3:** Aging schedule for new cells

## 3.3 Opening Cells

Opening cells make it possible to look at visual changes and take SEM images of the anodes, cathodes, and separators. In addition, parts are used to create half-cells and conduct material ARC tests. The cell is discharged to the lower voltage limit of 2.7 V and left overnight at rest. After measuring OCV, external tabs are cut off, and any remaining parts are covered with electrical tape. The cell is then put in the glove box.

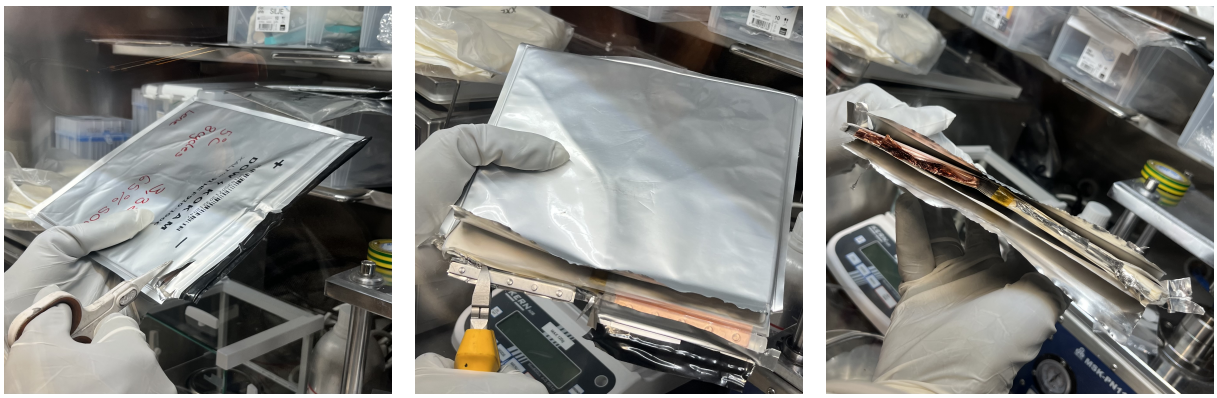

**(a)** Cutting into pouch **(b)** Cutting off tabs **(c)** Inside of pouch revealed

**Figure 3.4:** Pictures from opening a cell in the glove box

Once inside the glove box, ceramic scissors are used to open the pouch and expose the internal tabs. These are cut off using pliers. The pouch can then be entirely removed. Ceramic tools are electrically insulating and therefore used for this work. Figure 3.4 shows pictures from this process. When tabs are removed, the cell can be disassembled and divided into cathode-, anode- and separator sheets. Visual changes can be noted.

## 3.4 Increment Capacity Analysis

When analyzing the data from the $dQdV$-curves, the results from Spitthoff et al. [71] are used as a supplement as this article utilized the same cell as is used in this thesis. In addition, Spitthoff et al.[71] assume a set of degradation maps created for a 64 Ah cell can be used for the XALT cell due to the similar chemistry. These degradation maps are found in Appendix B. In addition, it was suggested to focus on peaks 1 and 2 in the charge curve when analyzing the movement of peaks. The curves were created by differentiating voltage and capacity during C/20 charge and discharge. The differentiated capacity is then divided by the derivative with respect to voltage to create $dQdV$-curves. To compare the curves to other cells, the $dQdV$-values are normalized by dividing by the cell's capacity.

### 3.4.1 Creating Half-Cells

An attempt was made to create half-cells from the XALT cell to establish degradation maps for the cell. An uncycled cell is used to make the half-cells for the degradation maps. The cell is opened, and one anode and one cathode sheet is needed. After being removed from the cell, the sheets are soaked in DMC. For the XALT cells, the outer sheets are cathode material. These can be used directly because the active material is only on one side of the sheet. On the other hand, the anode sheets have active material on both sides, and the material has to be removed from one of the sides to be used. This is because the active material on the unused side leads to doubled theoretical capacity. It is, however, uncertain how much of the material on the back side is part of the electrochemical reactions. The graphite, therefore, has to be removed from one side. This was done using NMP and gently removing the material.

A hole puncher with a diameter of 15 mm was then used to create electrodes of appropriate size for the half-cells. The half-cells are assembled in the glove box as shown in Figure 3.5. The negative electrode is Li-metal, and NMC or graphite is used as the positive electrode material. $40\mu m$ 1 M $LiPF_6$ in EC/EMC= 50/50 was used as electrolyte. When all parts are assembled, the cell is crimped and ready to use.

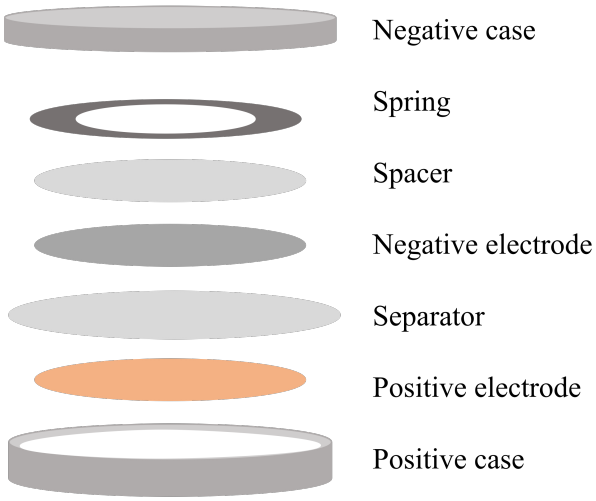


**Figure 3.5:** Composition of half-cells

### 3.4.2 Degradation Maps

To help the understanding of the dQ/dV curves in the incremental capacity analysis, degradation maps can be created using the Alawa toolbox [72]. This requires input data from both anode and cathode half-cells. The cycling done is shown in Table 3.2 and is based on cycling done by Spitthofff et al.[71]. The total area and capacity of the whole cell are used to find the initial capacity of the half-cells. This gives a capacity of $12.02 Ah/m^2$, which was then multiplied by the area of the half-cell electrode, giving a starting point for the capacity of $2.12 mAh$. After the first C/20 charge and discharge, each cell's capacity could be adapted.

**Table 3.2:** Number of cycles and C-rate for degradation maps

| Number of cycles | C-rate |
|---|---|
| 3 | C/20 |
| 3 | C/10 |
| 3 | C/5 |
| 1 | C/2 |
| 3 | 1C |
| 3 | 2C |

## 3.5 Material Accelerating Rate Calorimetry

EsARC from Thermal Hazard Technologies was used to conduct the material ARC test. Figure 3.6 shows a sketch of the test setup used at FFI.

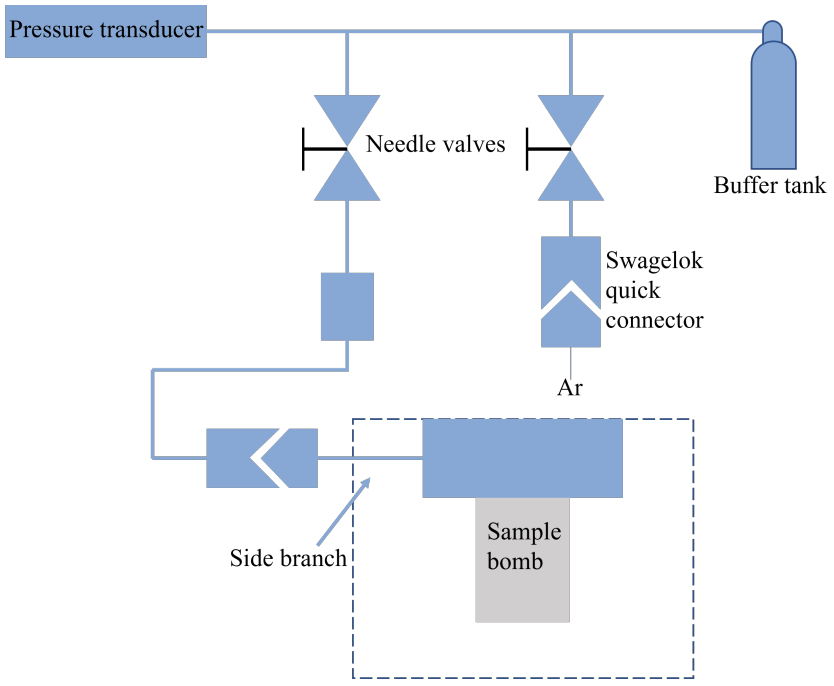


**Figure 3.6:** Material ARC test setup. Figure inspired by Troøyen et al.[65]

The background for this test is based on an article from Li et al. [56], where cells were tested at conditions where lithium plating is assumed. Half-cells were then made to see where the onset of the exothermic reactions occurred. It was shown that there was a decrease in the onset temperature for thermal runaway and self-heating for the anode half-cell. A Differential Scanning Calorimetry test measuring the heat flow out of a sample as a function of the temperature the sample is exposed to showed two heat flow peaks for uncycled graphite anodes. The first peak was the reaction between graphite and electrolyte, and the second between anode and binder. For cells with lithium plating, the anode-electrolyte reaction occurs at a much lower temperature, and the reaction is much stronger.[56]

Using ARC measurements, the goal is to indicate the presence of lithium plating by testing both anode material from an uncycled cell and a cell cycled at 5°C. Following the indications from Li et al. [56], the aged cell will experience thermal runaway at a much lower temperature than the reference anode material.

The bomb used for the tests was an ARC-ES-1750, 5.5 cm long with 0.15 mm wall thickness, and one side welded shut. Table 3.3 shows the weight of all single-use parts of the setup.

**Table 3.3**

| | |
|---|---|
| Bomb | 1.39 g |
| Nut | 9.53g |
| Washer large | 0.780 g |
| Washer small | 0.343 g |

The following settings were used for the test:

**Table 3.4**

| | |
|---|---|
| Start temperature | 40°C |
| Cut off temperature | 280°C |
| Step | 5°C |
| Temp. rate sensitivity | 0.02°C |
| Wait time | 25 min |
| Radiant heat mode | 10% |

### $\phi$ factor

A $\phi$ factor of 3 was decided, explained in Chapter 2.6.2. Using equation 2.13 and the values in Table 3.5, the amount of anode material used in the bomb was calculated to be 0.699 g.

**Table 3.5**

| | |
|---|---|
| $M_B$ | 1.39 g |
| $Cp_B$ | 0.5 J/gK |
| $M_{Clip}$ | 0.332 g |
| $Cp_{Clip}$ | 0.91 J/gK |
| $Cp_s$ | 0.72 J/gK |
| $\phi$ | 3 |

### Sample preparation for ARC

The approach used at FFI has only been used on cathode materials earlier. There was, therefore, some uncertainty about the success of the method. The sample used in the bomb for the first test was scraped off anode material from a cell cycled at 5°C. For the second and third tests, uncycled anode material was used. The cells were first discharged to the lower voltage limit of 2.7 V, 0% SoC, and left to rest. Next, the uncycled cell was opened at NTNU, and anode sheets were sent to FFI. The cycled cell was opened in the glove box at FFI, and the electrodes were separated. Since the goal was to look for plated lithium on the surface of the anode, it was decided not to soak the electrode material in DMC, as is the usual procedure. The top layer of the anode was then gently scraped off using a scalpel. The amount was decided based on the $\phi$ factor. The material was then left overnight to dry off any additional electrolyte. Figure 3.7 shows how the material looked after being scraped off.

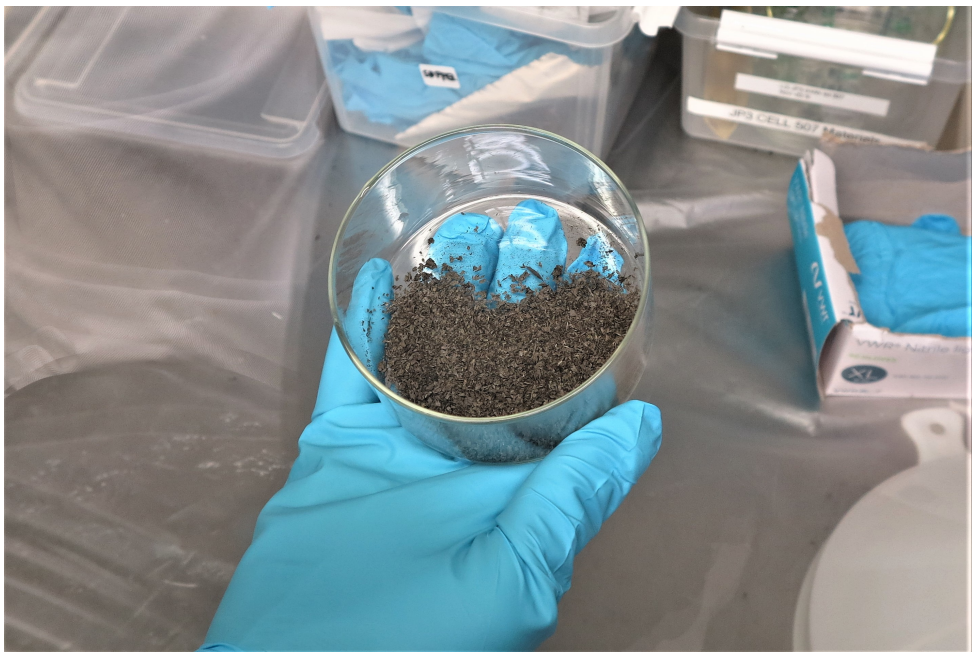

**Figure 3.7:** Scraped off anode material ready to dry overnight inside the glove box

The material was then added to the bomb using a funnel. The bomb was on top of a weight to ensure the right amount of material was put in. Since the particle size was large, a long thin mixing stick was used to push the material down. The material was tough to work with due to the reactivity, and it was therefore not possible to ensure that all material in the funnel was transferred to the bomb. 0.27 mL 1.0 M $LiPF_6$ in EC/DMC was added afterwards. A piston was then pressed down the top of the bomb with a force of 1.25 kg three times.

Usually, a piece of wool is put on the top of the bomb, but this was not done for this test. The bomb could then be fastened to the side branch with a Swagelok nut. This was first tightened by hand, followed by a full rotation with spanners. The advantage of doing the entire process inside the glove box is that the tube system and sample are never in contact with air, which could lead to an unwanted oxidation reaction.

The side branch and bomb were then moved to the ARC. Thermal paste was applied to the interface between the side branch and the lid to ensure proper heat flow. The temperature sensor was fastened to the bomb using an Al-clip. The complete setup is shown in Figure 3.8. The dent below the locking nut is the top of the sample.

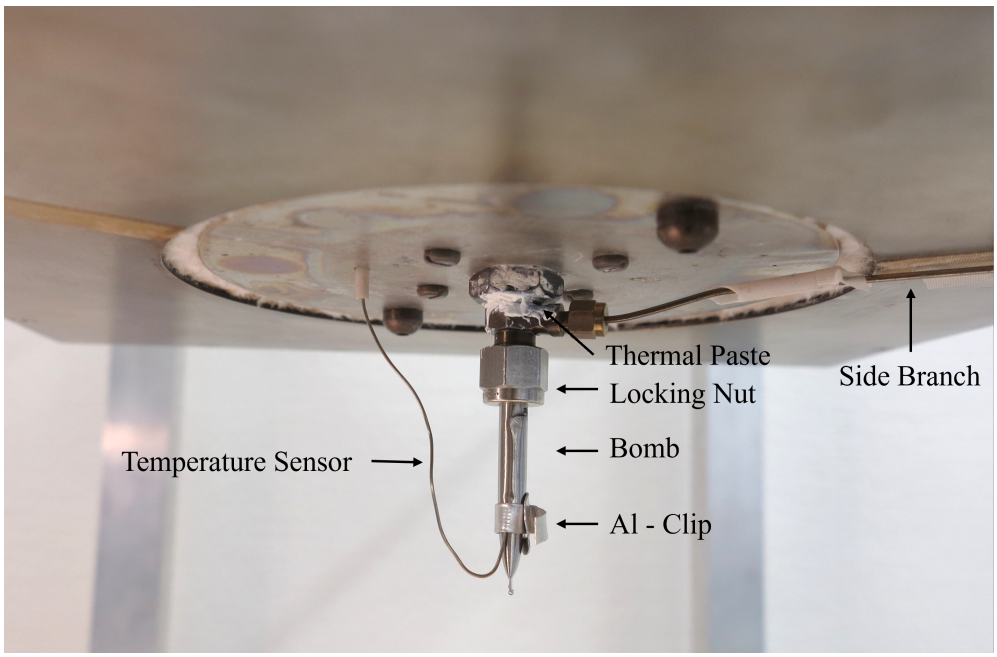


**Figure 3.8:** The bomb and side branch mounted in the lid of the ARC

## 3.6 Scanning Electron Microscope

A scanning electron microscope, SEM, was used to take images of the surface of both anode and cathode materials. FEI Apreo with EDX was used at NTNU's Nanolab facilities. SEM works by scanning the surface of a sample with a focused beam of electrons. Both cycled and uncycled cells were analyzed with SEM using the settings shown in Table 3.6

During the SEM scan, an energy-dispersive X-ray, EDX, scan is performed. EDX generates information about the chemical composition of the sample. This also includes concentration and distribution. When a sample is exposed to an electron beam, energy is released in the form of X-rays. This energy is unique for specific elements and can therefore be used to separate materials.[73] EDX is used to look for changes in the composition of the cells as they age, i.e., look for transition metal dissolution.

**Table 3.6:** Settings used for SEM images

| | |
|---|---|
| Working distance | $\approx 10mm$ |
| Voltage | 3.7 kV |
| Current | 0.20nA |
| Mode | ETD |

For the uncycled cell, two samples were prepared. One of each electrode was taken directly from the glove box to SEM. The second batch of samples was firstly dried in air overnight so as much of the electrolyte as possible evaporated. The samples were then washed using DMC to clean off any dust or other particles that could have accumulated on the surface. This was followed by two hours of drying to ensure no more DMC was still on the surface. The samples were then brought to the Nanolab, where samples were cut to fit the studs and placed in the SEM chamber.

For the aged cells, the main objective was to look for differences compared to the new cells. Li et al. [56] found a mossy material on the surface using SEM for cells cycled to promote lithium plating. The mossy material was tested using NMR spectra, and the result showed more lithium detected for samples with more mossy material. It was also found that the major component of the mossy material was plated lithium. Lithium metal on the anode surface in the shape of mossy material was also found by Kim et al. [74]. The samples from the aged cell were prepared in a glove box to avoid a reaction between lithium and air. The samples were then put in airtight pouches inside the glove box and transported to the SEM. The samples were quickly transferred from the pouch to the SEM chamber. The SEM chamber is filled with vacuum during use, so there is no additional risk of air exposure.

# Chapter 4

# Results and Discussion

The following chapter describes the results of the experiments and data analysis done in this thesis. At the time of delivery, the uncycled cells have been cycled for about 200 days and 1300 cycles, and the old cells for about 130 days and 600 cycles. The experiments aim to understand how the cells age and which cells are most suited for a second life.

## 4.1 Calendar Aging

Table 4.1 shows the charge capacity for C/10 charge for all cells at the beginning of life. This value was measured in 2015 and 2016 for the old cells, while for the new cells, this was measured in 2022. The table indicates an average decrease in capacity of 1.5% due to seven years of storage. Cell 6 was only characterized. It was then opened and used to create half-cells, take SEM images, and ARC measurements.

**Table 4.1**

| **Cell id** | Capacity [Ah] |
|---|---|
| 194 | 33.33 |
| 231 | 33.10 |
| 364 | 33.38 |
| 1 | 31.90 |
| 2 | 32.87 |
| 3 | 32.89 |
| 4 | 32.97 |
| 5 | 32.94 |
| 6 | 33.00 |

While there is some reduction in capacity, the basis of comparison from the old cells is low. It is not certain that the same trend would show with more than three cells. When evaluating the capacity of the new cells, the mean value is $32.76 \pm 0.85$ using two standard deviations of the mean. Cell 1 has a lower value than this, which can indicate some irregularities in this cell.

When the old cells started second life cycling, a characterization test was performed first. This gives a value that can be compared to the last characterization done the last time they were cycled. This correlation is shown in Table 4.2. The table shows a reduction in capacity for cells 194 and 364 and an increased capacity for the vertically cycled cell 231.

**Table 4.2**

| Cell id | Capacity 2016 [Ah] | Capacity 2023 [Ah] |
|---|---|---|
| 194 | 24.91 | 24.40 |
| 231 | 25.49 | 25.92 |
| 364 | 23.64 | 23.48 |

Cell 194 has the most significant reduction in capacity at 2%, which is slightly higher than for uncycled cells. This fall in capacity matches the rapid capacity fade at the end of cycling. The capacity of cell 364 was only reduced by 0.7%, matching the trends for this cell with long cycle life.

For cell 231, the capacity increased by 1.7%. This cell was cycled vertically in first life and horizontally in second life. Some of the effects that lead to the fast degradation in first life cycling might have been reversed by storing and new cycling horizontally.

## 4.2 Capacity Fade

Figure 4.1 shows the first and second life for the old batteries. The dashed lines are first life, and the solid lines are second life. Here the calendar aging described in the previous chapter is visualized. All data in this figure is based on C/10 charge capacity data and measurements. 'all second life cycling is done at a C/4 C-rate and 25°C.

During the start of cycling, the cell cycled at 45°C showed the highest capacity. But after about 600 cycles, at 90% SoH, the capacity decreases more rapidly. After about 800 cycles, the slope is getting close to vertical, and the SoH is quickly decreasing. The initial advantages of increased temperature, such as enhanced reaction kinetics, only last a short time. The speed of all other unwanted side reactions, for example, the growth of the SEI layer, leads this cell to age faster due to the high temperature.

The two cells cycled at 25°C show significantly different behavior. The cell cycled vertically rapidly decreases in capacity. It reaches the end of its first life before the cell cycled at 45°C. Indicating that cycling the cell vertically leads to unwanted reactions within the cell, which decreases the cell's lifetime. In comparison, the horizontally cycled cell at 25°C shows excellent results compared to the two other cells. Though it initially loses some capacity, the cell reaches about 1700 cycles before the slope increases at 84% SoH.

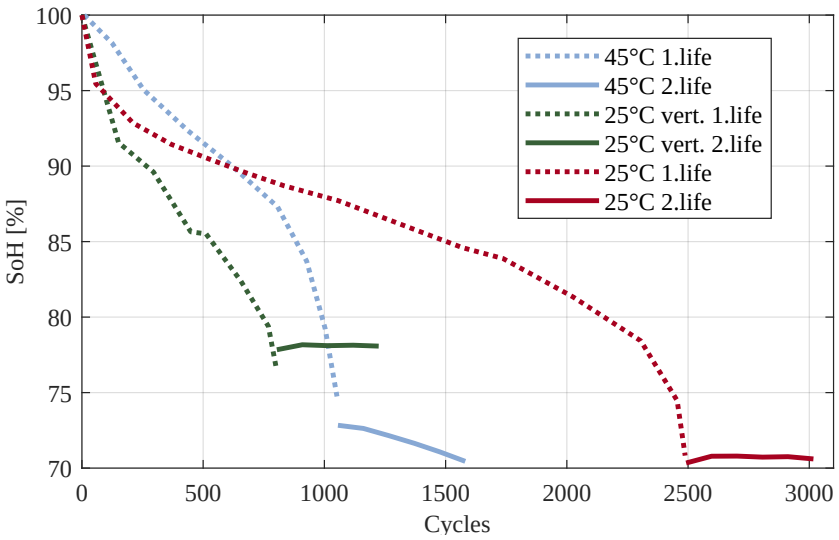


**Figure 4.1:** Capacity fade for old cells in first and second life

Regarding second life, there are two visible trends; minimal capacity decrease for the two cells at 25°C and a steeper slope for the cell at 45°C. For both cells at 25°C, the capacity increases during cycling after the first characterization during the second life cycling. After the increase in capacity, the capacity decreases very slowly at a much lower slope than at the end of the first life. It is noticeable that the cells act very similarly even though there is about a 7% difference in SoH for the cells. This indicates that the second life schedule with a reduced voltage window and C/4 C-rate is beneficial to increase the lifetime of these cells. It appears that the slower cycling during the second life can have redistributed materials that were passivated during the first life, especially since the capacity increases between the first and second characterization for the second life. It can, however, not indicate anything about the effects of the extended storage time the cells have experienced.

There is no initial increase in capacity for the 45°C cell. However, between the first and second characterization, the decrease in capacity is lower than for the rest of the cycling. The slope then increases, and this cell has the most significant decrease in capacity during second life. This can indicate that the first life cycling at high temperatures has led to irreversible degradation of the cell.

Capacity fade for the new cells is shown in Figure 4.2, where the dashed lines indicate second life cycling. These cells follow the same trends as the old cells, where the cells at 45°C initially have the highest capacity. But after about 300 cycles, the slope increases and the cells at 25°C have the lowest slope. While the cells at 25°C initially lose capacity, the slope evens out. After about 700 cycles, the capacity slope of the cells at 45°C increased. It was therefore decided to start second life at this point. As Figure 4.1 shows, the slope becomes steep beyond this point.

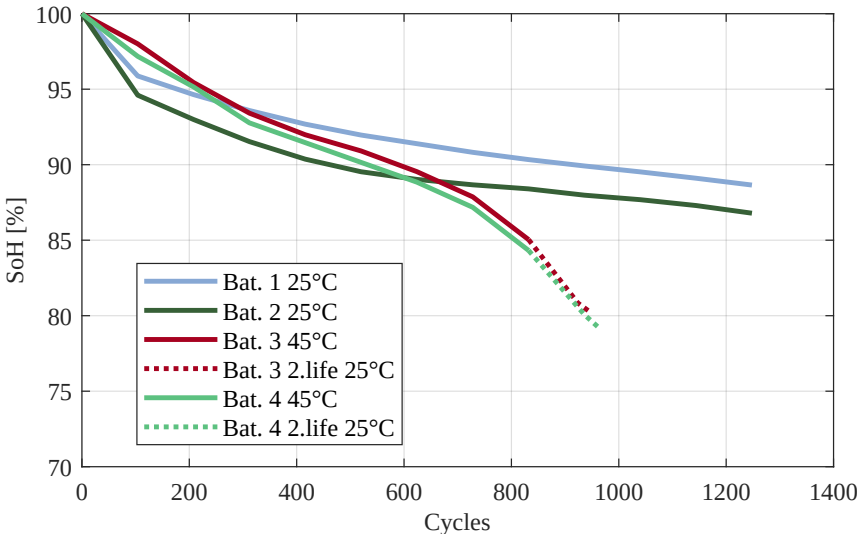


**Figure 4.2:** Capacity fade for new cells

### 4.2.1 Capacity Fade at 25°C

Figure 4.3 shows the capacity fade of all cells cycled at 25°C, making it possible to compare the capacity fade of the old and new cells. The two new cells are cycled equally as cell 364, except that cell 364 has a C-rate of 1.5 C, and the new cells have a C-rate of 1C.

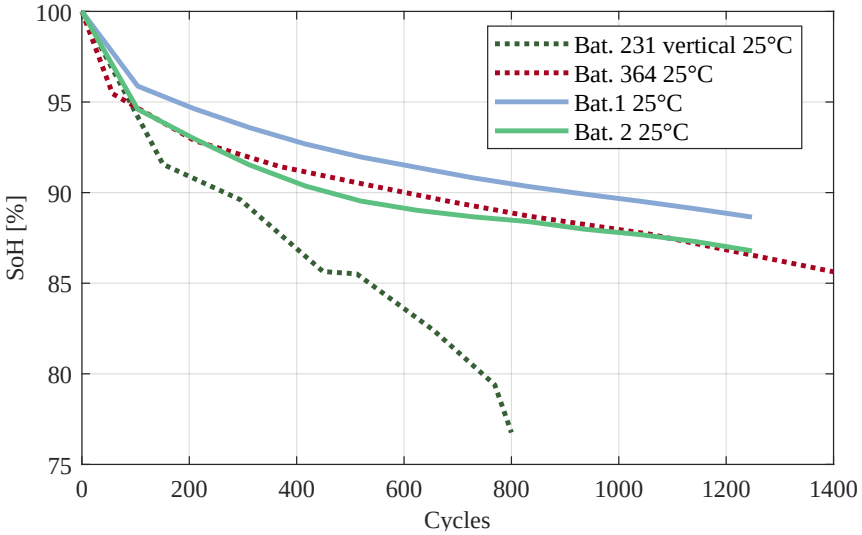


**Figure 4.3:** Capacity fade of cells cycled at 25°C

For all three horizontally cycled cells, the capacity fade is very similar. An initial drop in capacity is followed by a much lower slope over a large number of cycles. The capacity decrease can be due to a slow increase in the thickness of the SEI layer[22]. It is also noticeable that cell 1 has the highest capacity as the cells age. This cell had the lowest initial capacity, but this does not affect the cycling ability in any way. Based on the cycling so far it can be assumed that the two new cells will follow the same capacity fade trend as cell 364 for the rest of the cell lifetime.

### 4.2.2 Capacity Fade at 45°C

Figure 4.4 shows capacity loss for all cells cycled at 45°C. All three cells are cycled with the same C-rate. The only difference is the storage period for the new cells.

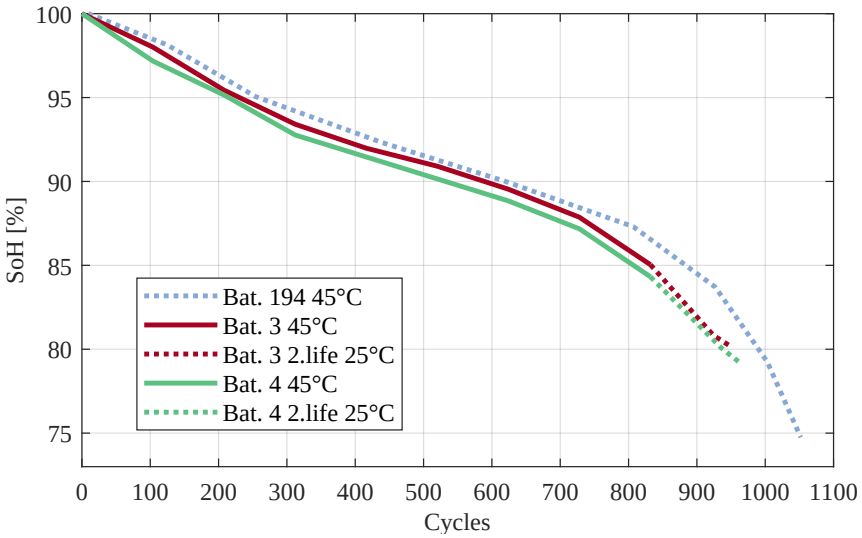


**Figure 4.4:** Capacity fade of cells cycled at 45°C

All three cells follow the same slope very closely until about 725 cycles, where the new cells start decreasing more rapidly. It was decided at this point that the cells would start second life. By starting before the slope becomes too steep, the second life is assumed to last longer. So far, the second life cycling has not resulted in a reduced slope, like for the three old cells. This can indicate that the storage period for the old cells has a positive effect on second life cycling. The last characterization has a somewhat reduced slope compared to the rest of the second life cycling, which could indicate a slowing down of the capacity fade. It is necessary to have a more extended period of second life cycling to make any finite conclusions about this.

### 4.2.3 Capacity Fade at 5°C

The cell cycled at 5°C degraded very fast. After only seven cycles, the capacity was reduced to 75%; after 13 cycles, the capacity was 65.5% SoH. This fast degradation indicates that a different aging mechanism is prominent for this cell. This rapid is most likely due to lithium plating on the anode and is further increased due to the high density of the anode[69]. Due to the dangers that come with lithium plating in regard to dendrites and short circuits, it was decided not to use this cell for second life experiments[22].

## 4.3 Internal Resistance

Internal resistance for all cells is shown in the following section. For pure ohmic resistance, the voltage difference described in chapter 3.2.2 has to be measured instantly after the current is turned off. There are, however, some limitations in the tester doing this. The fastest logging speed of the tester is 50ms, so this is used to measure resistance. This means that there most likely is some charge transfer overpotential in the resistance measurements[15]. To compare to the old cells, the resistance at 50 ms is also used for them. All resistance values in the figures are at $50 \pm 3\%$ SoC.

Figures 4.5 and 4.6 show the resistance of cells 364 and 231. Both cells start at around the same value at about 2.3 mΩ. The resistance of cell 364 decreases and reaches a minimum at about 95% SoH and increases from there. The decrease can be due to a geometric overhang on the anode. The overhang leads to a flow of active lithium between the passive and active parts of the anode, resulting in a resistance decrease[63].

For cell 364 the increase is nearly linear until about 75% SoH just before 2500 cycles. The slope then increases at the same time as the capacity loss increases. At 25°C the resistance increase is most likely due to the growth of the SEI layer[52]. For second life cycling, the resistance has decreased by about 30%. This can be due to contact resistance in the connection points at the tabs. The screws connecting the cell to power cables can come loose during cycling, increasing the measured resistance. It can also be due to passivated material becoming active aging due to the low C-rate.

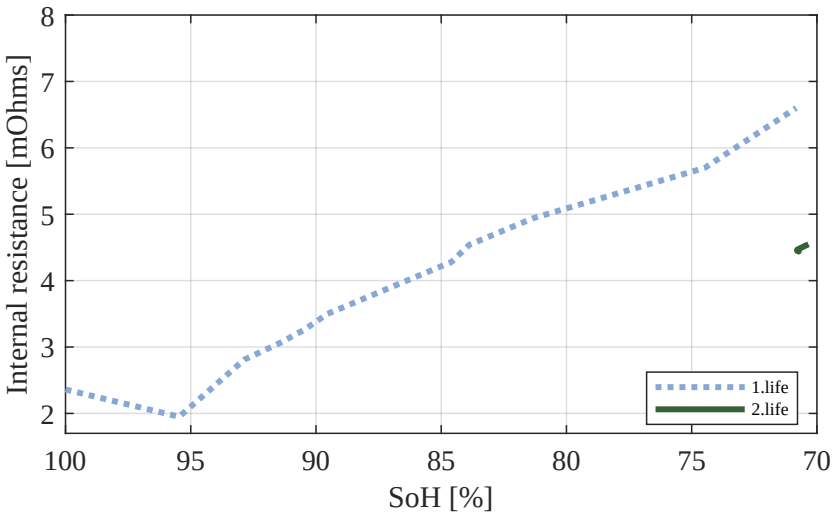


**Figure 4.5:** Resistance of cell 364 cycled at 25°C at 50% SoC

Cell 231 in Figure 4.6 does not have the initial decrease in resistance as cell 364 has. However, it has lower resistance when comparing resistance at the same SoH with cell 364. When the cell is stored vertically, gravity will affect the cell. The liquid electrolyte can accumulate in the bottom of the cell, reducing the conductivity and increasing the resistance in the top part of the cell. Gas formation due to side reactions and electrolyte decomposition can accumulate at the top of the cell, reducing conductivity and increasing resistance.

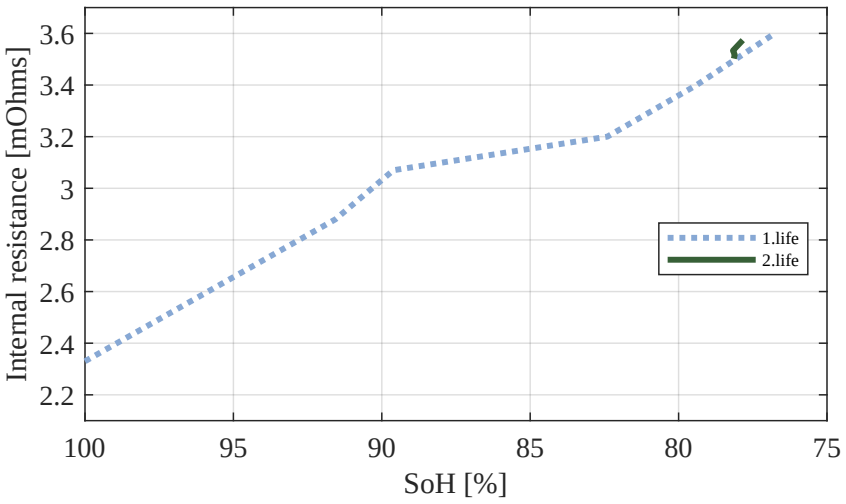


**Figure 4.6:** Resistance of cell 231 cycled at 25°C vertical for first life and horizontal for second life at 50% SoC

The resistance during second life is somewhat reduced compared to the end of first life. The slight reduction indicates that most of the resistance in the cell is due to processes that have not been removed due to the horizontal second life cycling. The low resistance compared to cell 364 might lead to better second life performance for this cell.

Figure 4.7 shows the resistance of cell 194 for first and second life. The values for this cell are very different from the rest. This cell was connected to an external tab for the first 600 cycles, which gradually increased the contact resistance of the cell.

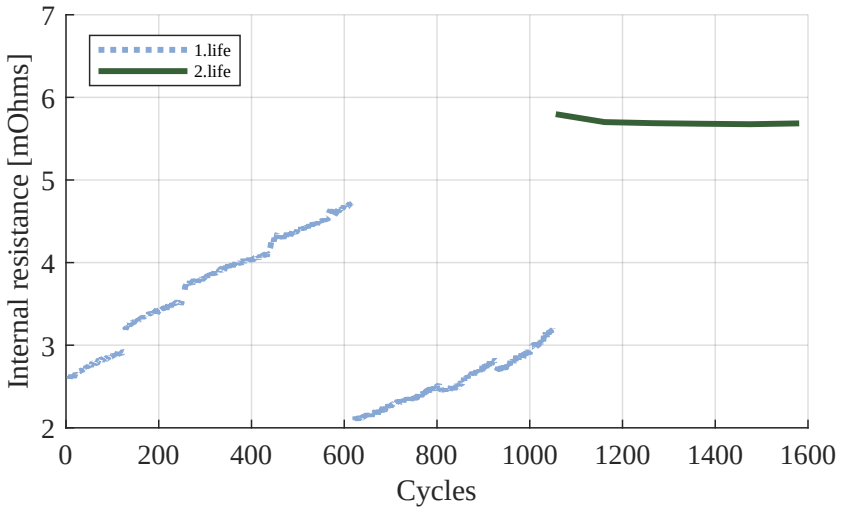


**Figure 4.7:** Resistance of cell 194 cycled at 45°C for first life and 25°C for second life at 50% SoC

At 600 cycles, the external tab was removed. After this, the actual resistance can be seen. The resistance remains relatively constant during second life even though the capacity decreases, as shown in Figure 4.1. There is a significant increase in resistance from first to second life. It is unknown why this is, but calendar aging can be one reason. During storage SEI layer increase is the primary aging mechanism, leading to increased resistance[42]. The increase could also be due to a bad connection between tabs and power cables, increasing contact resistance.

For battery 1 in Figure 4.8, cycled at 25°C, the resistance is at its maximum at 100% SoH. The cell reaches a minimum value after 100 cycles at 96% SoH. This is similar to cell 364, indicating that this decrease can be expected for the XALT cells at 25°C. The resistance at about 96% SoH lowers further for this cell compared to cell 364, which can be due to the difference in C-rate between the cells. The effects of the increased C-rate for cell 364 could lead to a thicker SEI layer for this cell.

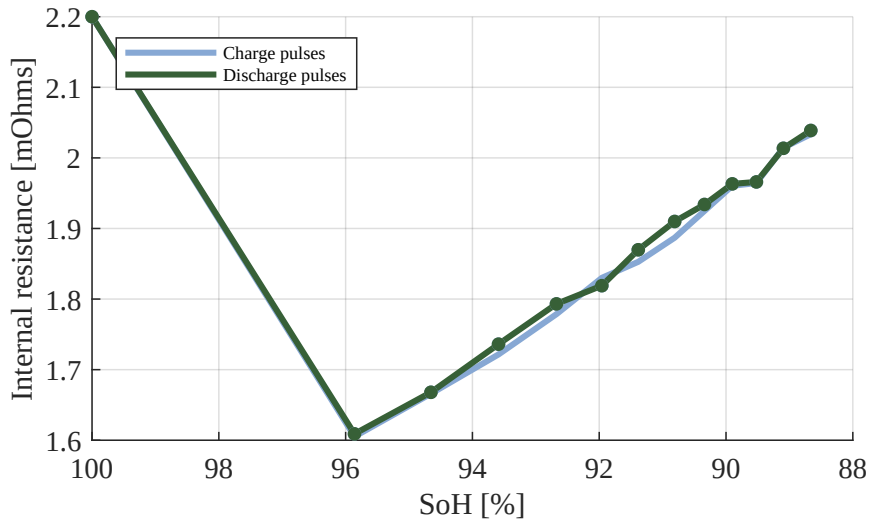


**Figure 4.8:** Internal resistance of battery 1 as a function of SoH at 50% SoC

Resistance as a function of SoH for cell 2 can be found in Figure 4.9. The resistance for cells 1 and 2 have a very similar shape when plotted as a function of SoH. There is, though, about 0.1 $m\Omega$ difference in the lowest value of the resistance. Cell 2 has the lowest decrease in resistance and has the lowest capacity as well, as seen in the capacity fade figures 4.2 and 4.3 where cell 2 has about 2.5% lower capacity than cell 1 as the cells age.

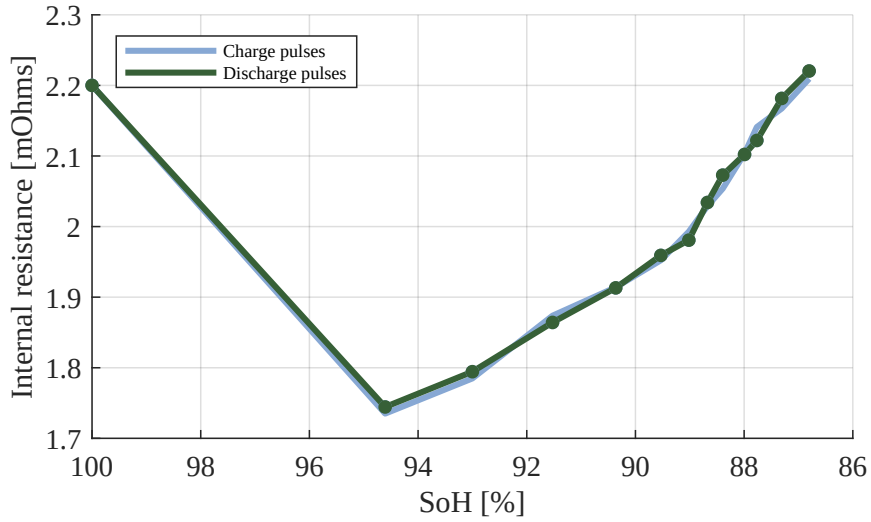


**Figure 4.9:** Internal resistance of battery 2 as a function of SoH at 50% SoC

When comparing the internal resistance values for all three cells cycled at 25°C, it is noticeable that the two cells stored for some time before cycling have a lower overall resistance. It is not certain why this happens, but it is assumed to be due to the contact resistance of the testers used at IFE[69]. Compared to other XALT cells cycled at IFE, the resistance measurements are not unusual for the cell at 25°C. However, the minimum point for the two new cells is lower than for other cells[69].

During storage, the movement of lithium ions is reduced. This allows the SEI layer to grow thicker very slowly in an even layer, and any initial cracks can fill slowly. This process could lead to a more robust, uniform SEI layer with less resistance. While for the cell that was cycled straight away, the SEI layer might have grown faster, leading to more irregularities and uneven thickness, which could lead to higher resistance. A long storage period would also lead to the electrolyte having time to thoroughly saturate and wet all layers of electrode materials, which could lead to more active surface area.

The resistance of cell 3 cycled at 45°C for first life and 25°C for second life is found in Figure 4.10. The resistance increases slowly until about 95%, when the cells at 45°C show the best performance compared to those at 25°C in Figure 4.2. The resistance increases faster until about 85% SoH when second life starts. Beyond 85% SoH, the resistance increases at a much lower rate. Even though the change to second life cycling was not visible when evaluating SoH vs. cycles, it is visible in the resistance increase rate.

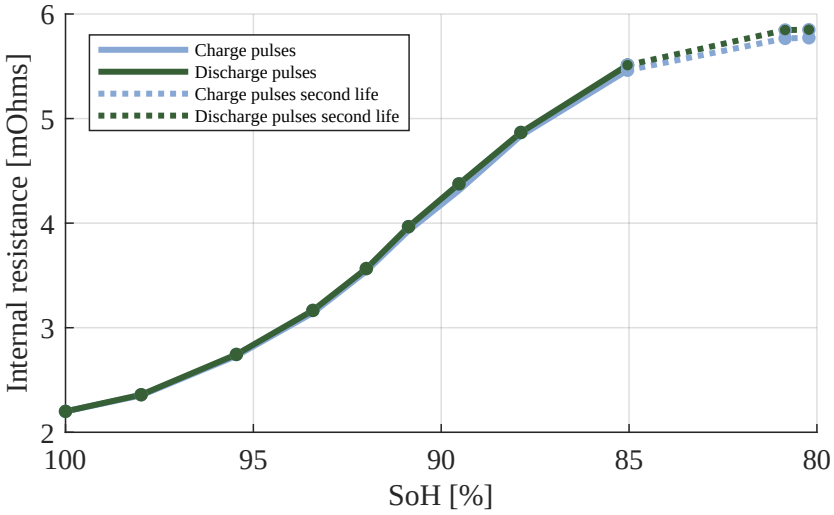


**Figure 4.10:** Internal resistance of battery 3 as a function of SoH at 50% SoC

The resistance of cell 4 in Figure 4.11 follows the same trends as cell 3. The resistance increase is very low until about 95%, when the resistance increases faster until second life starts at about 85% SoH.

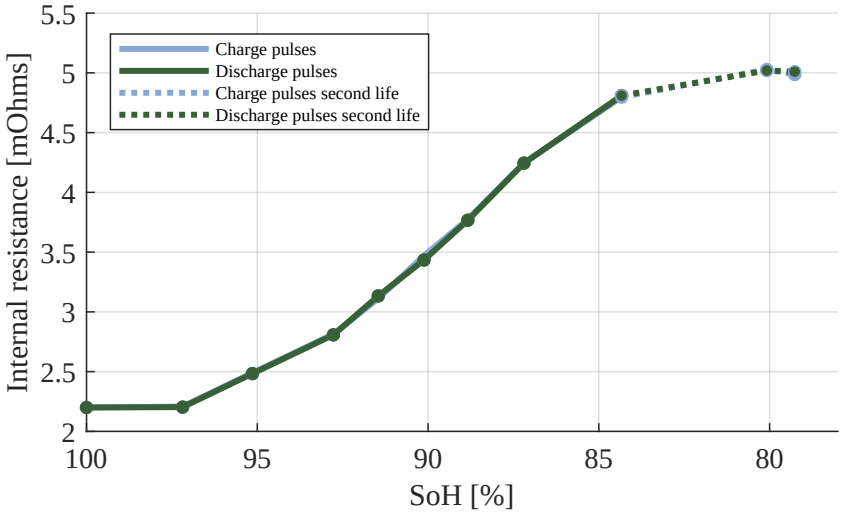


**Figure 4.11:** Internal resistance of battery 4 as a function of SoH at 50% SoC

Cells 3 and 4 cycled at 45°C do not show the initial decrease in resistance seen for the cells at 25°C. The growth of the SEI layer increases with increasing temperature[61]. In addition, increased cycling temperature can lead to decomposition of the binder material[46]. This most likely leads to a large increase in resistance, so the initial decrease is not visible. This can be why the resistance increases slower initially, where the resistance decreases for the other cells.

Figure 4.12 shows the resistance of cell 5 cycled at 5°C. The resistance grows slowly to the first characterization at 75%. After that, the resistance increases much faster to $2.9m\Omega$ at 65% SoH. With only 14 cycles the SEI layer has little time to grow. Most of the resistance increase is due to lithium plating and loss of anode material at 5°C [47]. As the lithium is plated on the surface of the anode, the concentration of active materials change, which affects the conductivity of the electrolyte.

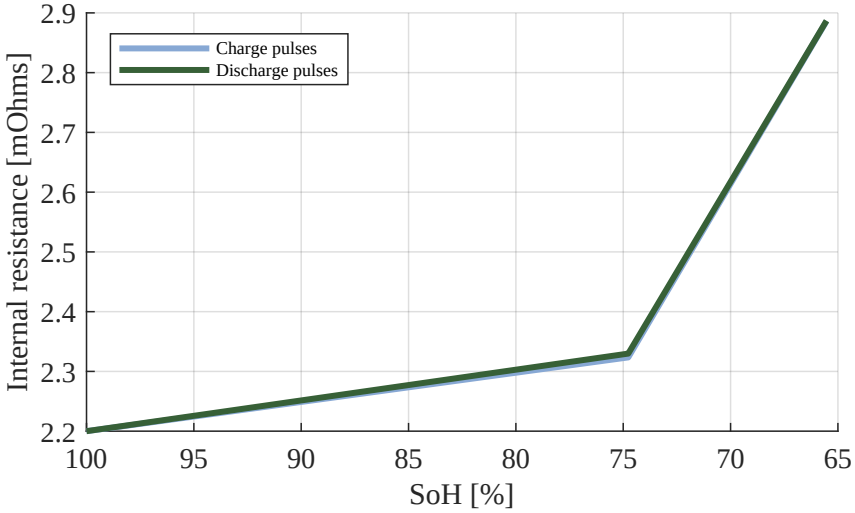


**Figure 4.12:** Internal resistance of battery 5 as a function of SoH at 50% SoC

Some of the increase in resistance for all cells can be due to contact resistance between current collector tabs and the power cables. All cells are connected with screws that over time can come loose. Depending on how tight these were screwed during assembly, this can lead to some variation in this effect on resistance.

## 4.4 Half-cells and Degradation Maps

The half-cells of both anode and cathode material were successfully assembled in the glove box. During cycling, the capacity was adjusted after the first C/20 charge and discharge cycle. The cathode half-cell worked as expected.

The anode half-cell did not work as expected. At C-rates higher than 0.2 C, the cell does not work. Even with a high log rate, there is minimal data, and each charge and discharge lasts less than 1 second. This is not expected behavior and could indicate high contact resistance. It was therefore tested to polish the cells with sandpaper, but this did not help. Therefore there is no data from the anode half-cell at higher C-rates. Because of this, it was decided to use the degradation maps from Spitthofff et al. [71] to compare to the $dQdV$-curves in the following chapter.

The limited function of the anode half-cells at high C-rates could be connected to the high density of the anode material[69]. A dense anode leads to more limited lithium intercalation. This is because there is less room for the lithium to intercalate. At high C-rates, this can hinder the lithium from becoming part of the structure, which results in increased resistance.

## 4.5 Increment Capacity Analysis

Figure 4.13 shows the $dQdV$ curve for the first C/20 done on one of the cells. In the specialization project[1], it was shown that the first C/20 $dQdV$ plot is practically identical for all XALT cells. Figure 4.13 is used as a baseline for all cells to analyze how peaks shift during cycling. The focus is on the movement of peaks 1 and 2 in the figure. This was chosen based on the findings of Spitthofff et al.[71].

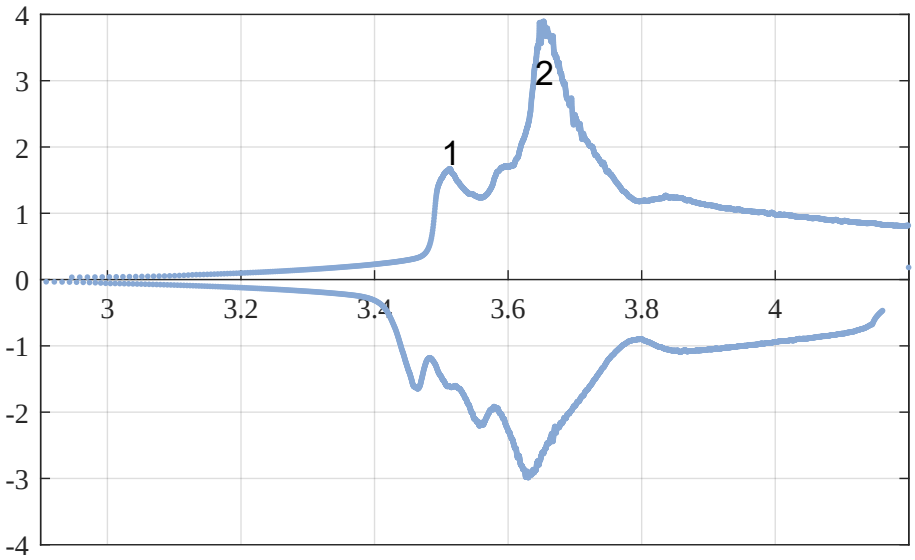


**Figure 4.13:** Baseline for increment capacity analysis

Figure 4.14 shows $dQdV$-curves for cell 1 cycled at 25°C. There are minor changes to both peaks. Some reduction at the same voltage for peak 1, indicating LAM which can be due to corrosion of the current collector or electrode particle cracking[47]. For peak two, the peak also shifts, indicating LLI[64]. LLI is most likely due to the growth of the SEI layer[22], which was also seen in Figure 4.3. LLI can also be due to lithium plating, but it is not expected to be any lithium plating at 25°C[46].

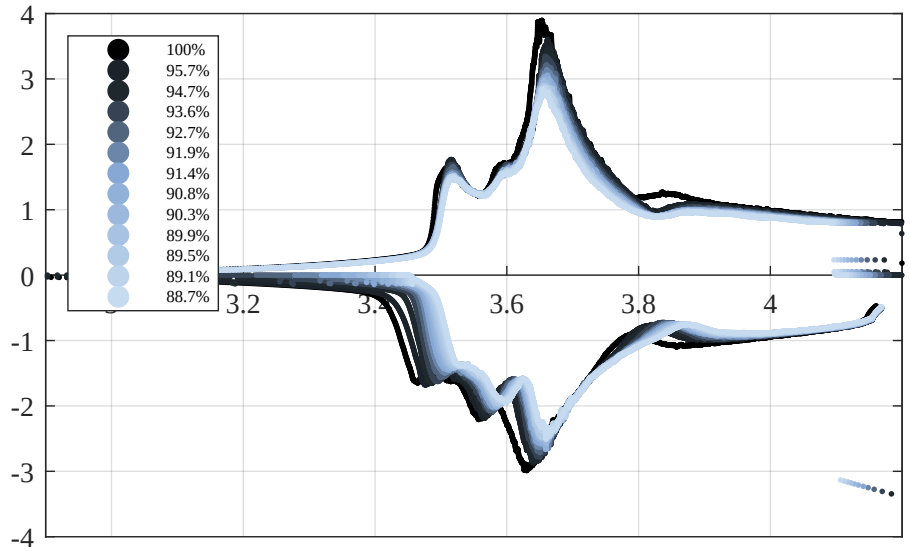


**Figure 4.14:** Increment capacity analysis of cell 1 cycled at 25°C

Figure 4.15 shows $dQdV$-curves for cell 2 cycled at 25°C. The curves for cell 2 are very similar to cell 1, as they have identical cycling conditions. The disturbances at about 3.85 V are due to a power shutoff during cycling and can be disregarded. There is slightly more reduction in the peaks for this cell. The cell has also lost more capacity than cell 1, as seen in Figure 4.3, so this is as expected. The decrease at approximately the same voltage for the first peak can indicate LAM[64]. The reduction and shift in peak 2 indicate LLI[64], and can, for this cell, likely be due to the growth of the SEI layer.

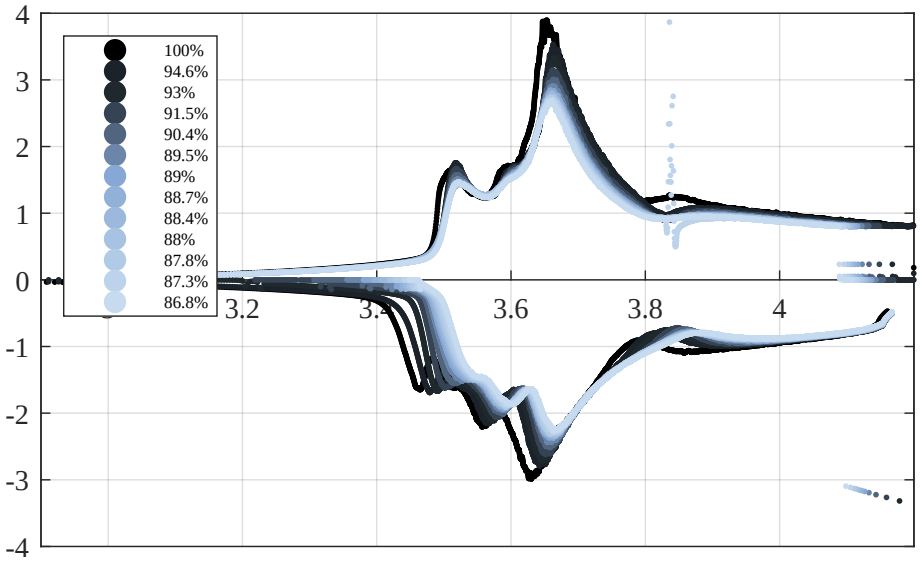


**Figure 4.15:** Increment capacity analysis of cell 2 cycled at 25°C

The $dQdV$-curves of cell 3 cycled at 45°C for first life and 25°C for second life is shown in Figure 4.16. This cell has larger changes in the curves compared to the cells at 25°C. Peak 1 is almost completely flattened, which can be due to LAM caused by binder decomposition. Peak 2 is also reduced, and the peak is shifted to a lower voltage, indicating LLI from SEI layer growth.[47, 64] It is also noticeable that the discharging ends gradually earlier as the cell ages. During second life, peak 2 continues to decrease and shift. While peak 1 seems to have stopped decreasing.

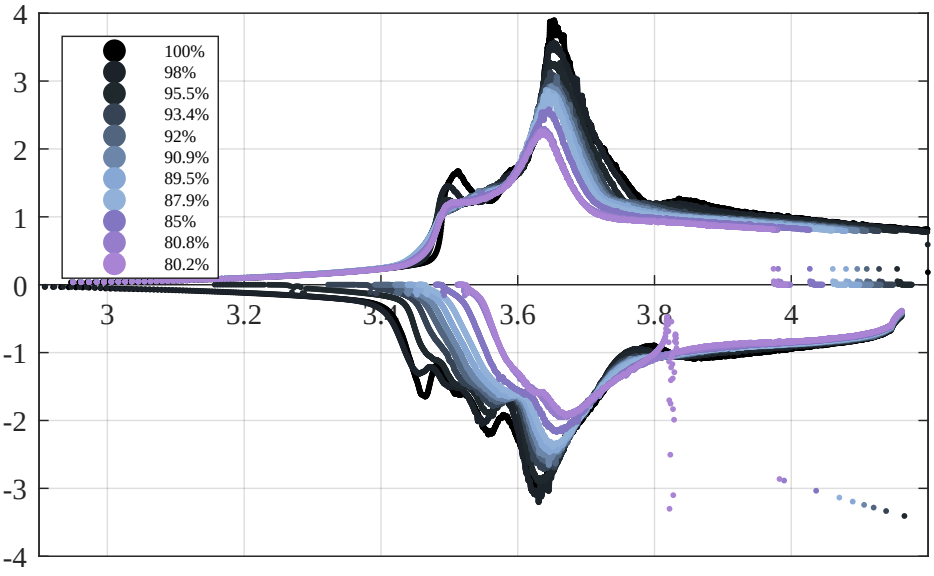


**Figure 4.16:** Increment capacity analysis of cell 3 cycled at 45°C

Cell 4 cycled at 45°C for first life and 25°C for second life is shown in Figure 4.17. It follows the same trends as cell 3. The first peak is almost completely flattened, and the second peak is shifted and reduced, which indicates LAM and LLI respectively[64]. The cell also has gradually earlier termination of discharging. The disturbances in data in this cell are also due to problems with the power supply for this cell. The first peak remains constant for second life, while the second peak continues to decrease.

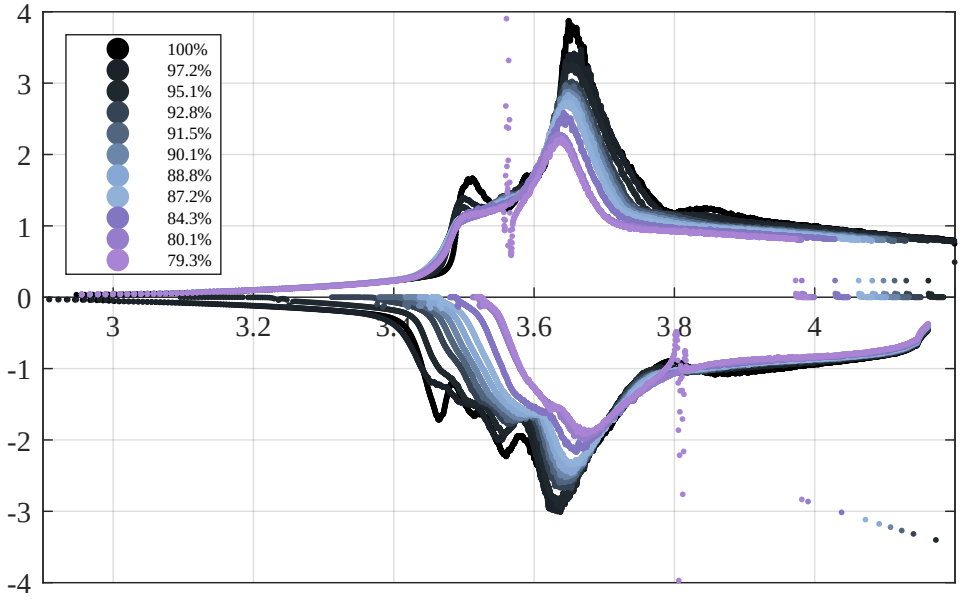


**Figure 4.17:** Increment capacity analysis of cell 4 cycled at 45°C

The minimal changes in the *dQdV* curves for second life for the 45°C cells indicate that the decrease in temperature and C-rate has not yet affected aging processes in the cells significantly. However, the resistance increase has slowed, as seen in Figures 4.10 and 4.11. This was also seen for cell 194 in Figure 4.7, where the resistance has not increased during second life. This can be indicated by the minimal changes in peak 1 compared to peak 2 for cells 3 and 4.

Cell 5 in figure 4.18 only has two characterizations during cycling. However, the trends are evident. At 75% SoH, the first peak moves to the right without reducing height, indicating resistance increase, as shown in Figure 4.12. However, from 75 to 66% SoH the peak does not shift, while the resistance increase is large. This can indicate the uncertainty in using $dQdV$ as an analysis method alone. It should be used together with other methods if the goal is to analyze degradation. It can also be used if it is only used to see that changes have occurred in the cell. Between the second and third characterization, the shift can be due to a shift of the half-cell potential[75].

Peak 2 has also shifted to the right and reduced more in height than cells cycled at 25 and 45°C, indicating LLI[64]. In this case, the LLI is most likely due to lithium plating at a low cycling temperature[47]. Unlike the cells at 45°C, charging starts, and discharge ends at a higher voltage. This happens when capacity is reduced.

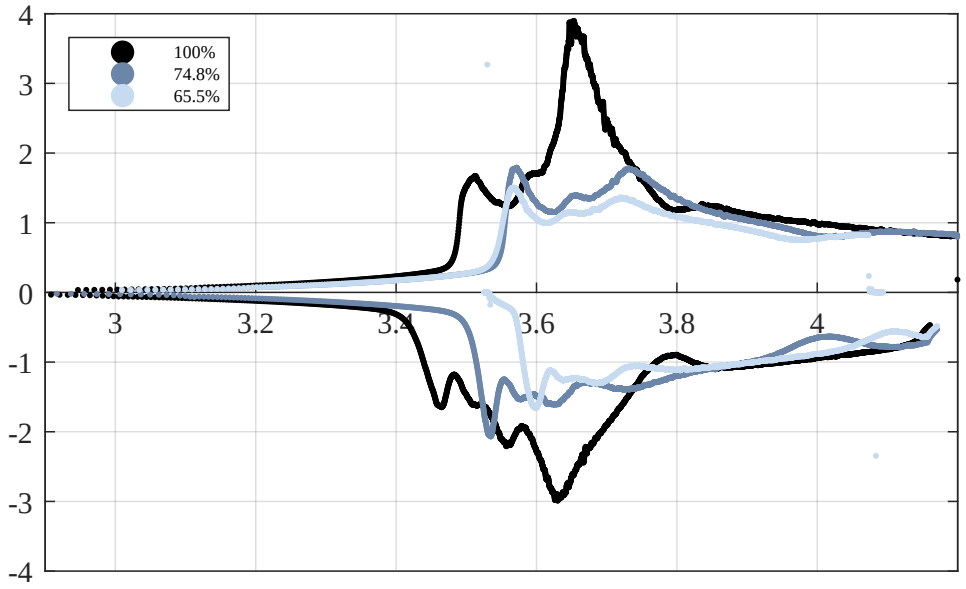


**Figure 4.18:** Increment capacity analysis of cell 5 cycled at 5°C

Figure 4.19 shows $dQdV$ curves for cell 194, which was cycled at 45°C at first life and 25°C for second life. Unlike the last figures, the values in this figure are based on C/10 charge and discharge data. IFE used C/10 data, which was therefore used for the second life cycling $dQdV$-data as well. One disadvantage of using C/10 instead of C/20 is less detailed curves. For instance, the end of discharge and the start of charge points cannot be evaluated using C/10[69].

The blue values are first life data from IFE, while the data in pink is second life cycling at NTNU. The trends from first life continue to second life, with a reduced first peak with shifts as the cell age and a reduction and shift in the second peak. Both these changes indicate LLI as the primary aging factor[64]. At high cycling temperatures, this is most likely due to the growth of the SEI layer and binder decomposition[47].

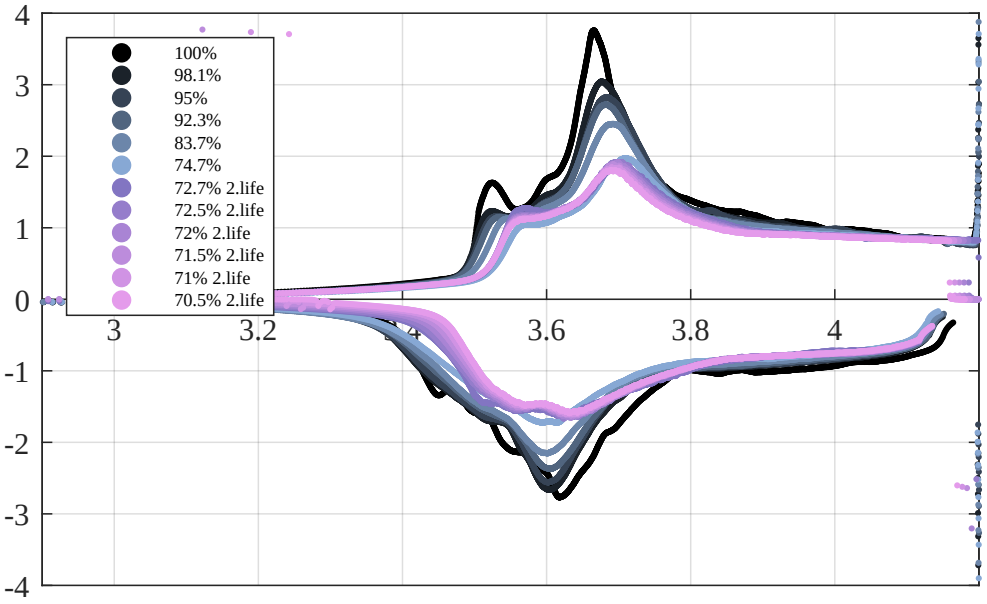


**Figure 4.19:** Increment capacity analysis of cell 194 cycled at 45°C for first life and 25°C for second life

Figure 4.20 shows the *dQdV* curves for cell 231, cycled 25°C vertically for first life and horizontally for second life. Comparing the last curve in first life and the first curve in second life, there is some improvement in the curves. Both peaks increase and move to the left, indicating a reduction in LLI[64]. This was also seen earlier in the results as capacity increased, Figure 4.1, and resistance decreased, Figure 4.6.

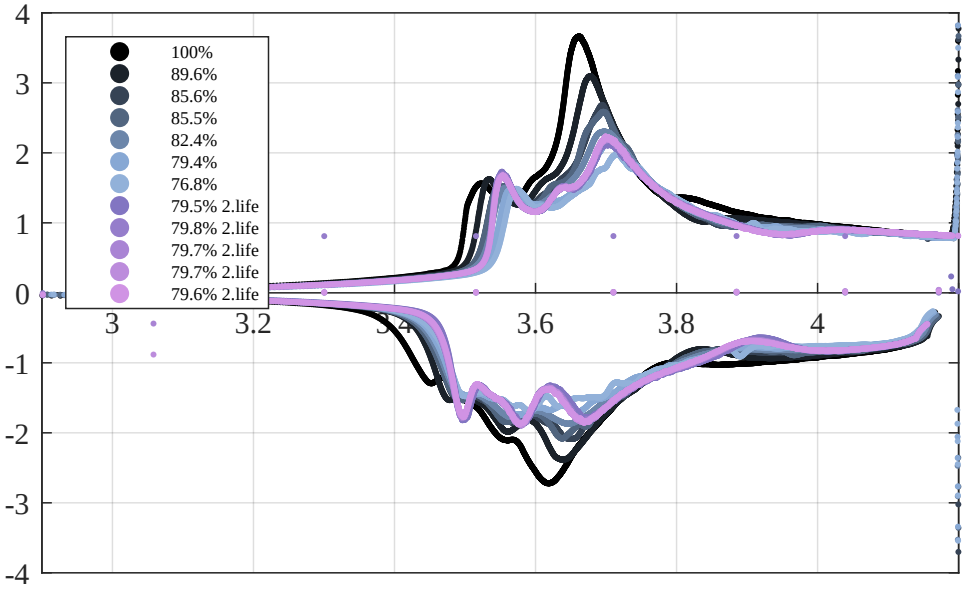


**Figure 4.20:** Increment capacity analysis of cell 231 cycled at 25°C vertically for first life and 25°C horizontally for second life

The *dQdV* curves for cell 364 are found in Figure 4.21. Also, for this cell, second life cycling has somewhat improved characteristics. The first peak has moved to the left, indicating a decrease in resistance. The second peak has increased and moved to the right, which indicates decreased LLI, resulting in increased capacity. [64] Both these trends were found in the capacity plot, Figure 4.1 and the resistance plot, Figure 4.5.

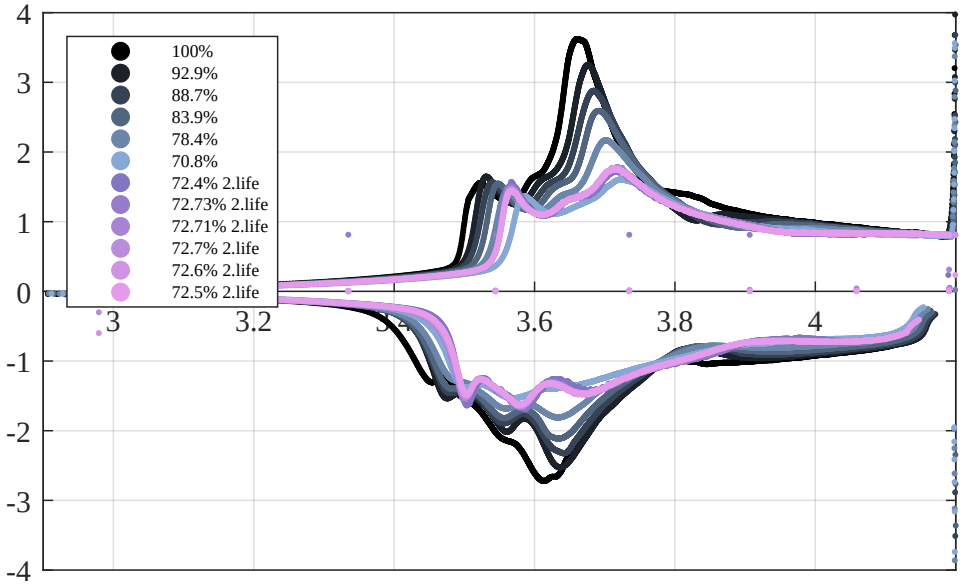


**Figure 4.21:** Increment capacity analysis of cell 364 cycled at 25°C for both first and second life

Figure 4.22 is a comparison of $dQdV$-curves for all cells in this thesis at 90% SoH, including data from the cells received from IFE. The cell at 5°C is at 75% SoH, as this was the closest data available. Comparing the three temperatures at 90% SoH it is visually possible to separate them. All cells at the same temperature show the same curve placement. Peak 1 separates the cells at 45°C from the other temperatures. Peak 2 separates the cell at 5°C from the other temperatures due to the substantial shift and reduction of the peak.

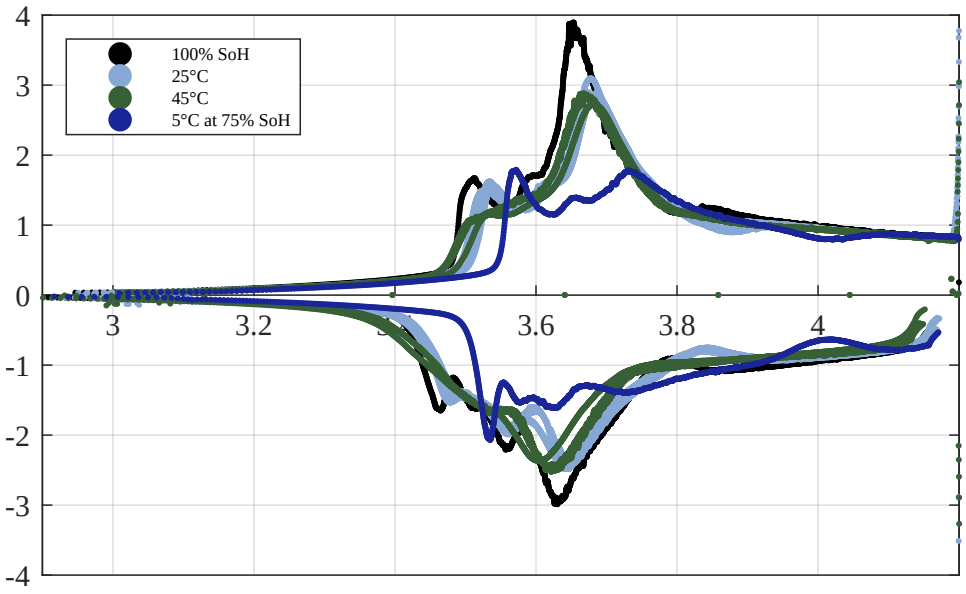


**Figure 4.22:** Increment capacity analysis of all cells at 90% SoH, 5°C cell at 75% SoH

An advantage of the temperatures being so different in the $dQdV$-plot is the ability to separate the cells only based on this for the XALT cells. This was also found for a 64 Ah NMC532 cell by Spitthofff et al. [71]. If this trend is the same for all lithium cells, this can be used to quickly understand the cycling temperature of cells in, i.e., electric vehicles. This can be utilized to find the most suitable cells for second life applications.

## 4.6 ARC

Figure 4.23 shows the ARC test setup after the test for the aged cell. The bomb was completely destroyed due to high internal pressure. This is not normal for this test and had never been experienced at FFI before. The bottom test container was filled with black powder from the bomb. Figure 4.24 shows the side branch after the test. Here the bomb can be seen in three separate parts. These visual results indicate a very energetic reaction as the anode material and electrolyte was heated during the test. This reaction is more extreme than other cells experience during thermal runaway. The fast release of energy causes pressure waves and projectiles, and following Sandia National Laboratories' [76] standard can be classified as the most dangerous type of thermal runaway. This is called energetic failure.

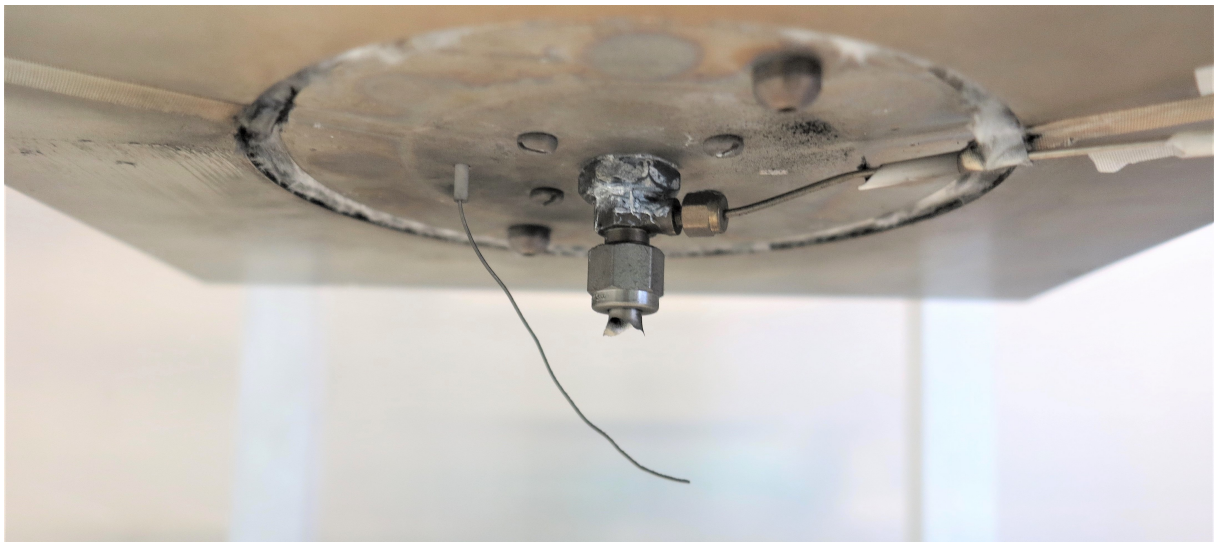

**Figure 4.23:** Setup after ARC test on cell cycled at 5°C

**Figure 4.24:** Side branch after test

Figure 4.25 shows the results from the ARC test done on uncycled and cycled at 5°C anode materials from the XALT cell. Two 30 Ah cylindrical full cells tested by Lian et al. [77] are added to the figure to provide context to the values. The cells were cycled with 1C charge and discharge. The 5°C cell was tested at 72% SoH, and the 45°C cell at 77% SoH. Two individual tests were done on the uncycled anode material from the XALT cell, where only one of the tests gave very weak exothermic readings. This is seen as the small orange data points in the figure. This is very different from the cycled anode material, where the figure shows an onset of thermal reactions at about 80°C and thermal runaway at 135°C.

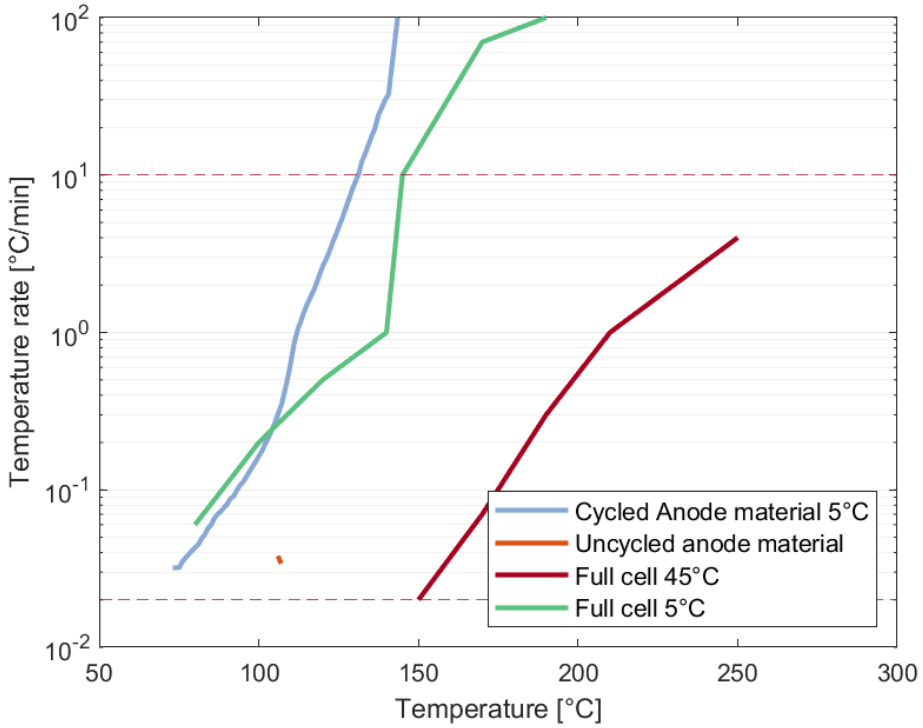


**Figure 4.25:** ARC test results with historic data from full cells by Lian et al.[77]

As suggested by Li et al. [56], thermal runaway occurs at a much lower temperature for the cell that has been cycled during conditions that promote lithium plating. The strong exothermic reaction is likely to be a reaction between electrolyte and plated lithium. The full reference cell at 5°C follows the same trend, with a low onset and thermal runaway temperatures. It is, however, higher than for only anode material. This difference can be due to this being two different cells. It can also be accounted for by heat being transferred to the electrolyte, separator, and cathode, slowing down the reaction and leading to a somewhat higher thermal runaway temperature. Whereas for the pure anode material, the heat can only be transferred between the anode and electrolyte.

If the cells cycled at 5°C were to be used for second life, temperature control would be vital. It needs ventilation at a much lower temperature than those cycled at higher temperatures. It is unsafe at elevated temperatures, which occurs more during second life due to the increased resistance. Comparing the reference cells at 5°C and 45°C, Figure 4.25 shows that cells cycled at 45°C are more suitable for second life with regards to thermal runaway and exothermic reactions.

## 4.7 Visual Changes

Figure 4.26 shows images of the anode and cathode of the cell cycled at 5°C. Visually, the anode in Figure 4.26a has changed color compared to an uncycled anode, which is completely black. Around the border, the cell is still black, which can indicate a geometric overhang[63]. A geometric overhang was also found visually by Grimsmann et al.[78]. This can visually explain the resistance decrease found in figures 4.5, 4.8, and 4.9. The graphite on the anode has become brittle and comes loose from the copper current collector. This was also found in the SEM image Figure 4.29. For the cathode in Figure 4.26b, the sheet is visually equal to the uncycled cathode.

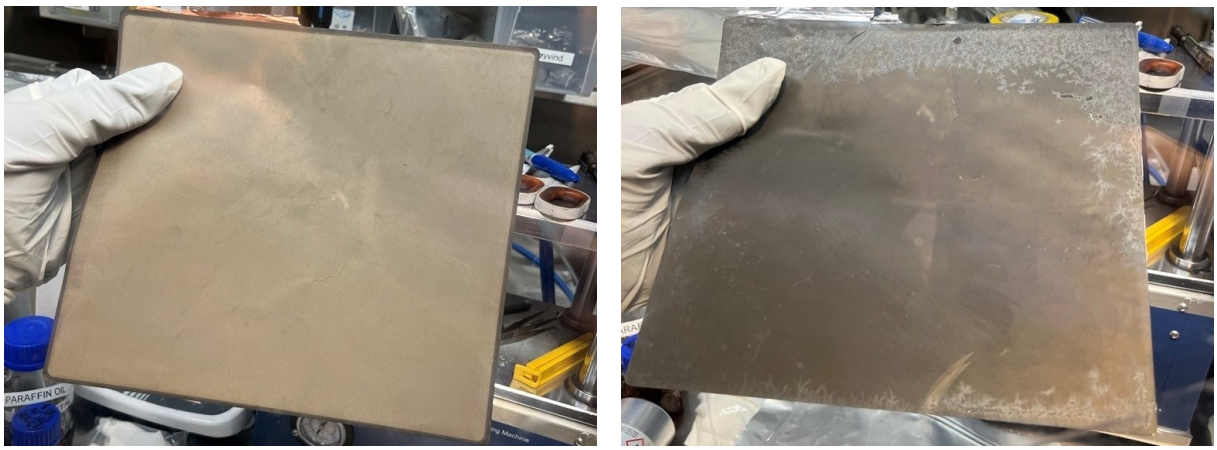


**(a)** **(b)**

**Figure 4.26:** Images of cell cycled at 5°C at 65% SoH, a) anode b) cathode

## 4.8 SEM

Figures 4.27a and 4.27b show SEM images of the cathode in an uncycled cell at two magnifications. When using SEM to look at the uncycled cell, no visual differences were found comparing the cell left to dry off the electrolyte and the one that had not.

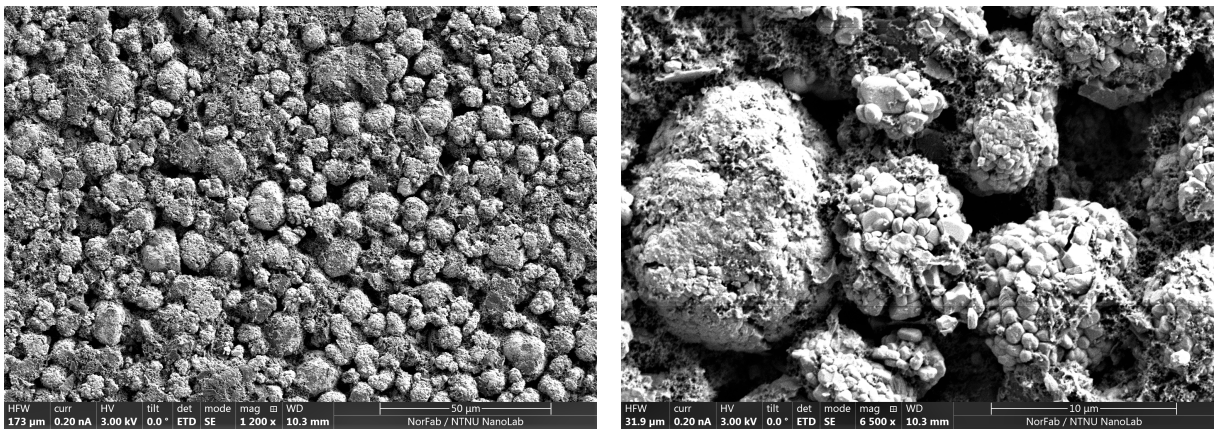


**(a)** **(b)**

**Figure 4.27:** Images of uncycled cathode material using SEM at two different magnifications

Figures 4.28a and 4.28b show uncycled anode material. The surface is relatively uniform, with the expected graphite sheets. EDX scan of the surface showed only carbon, with minor parts cobber. This is the expected materials to find on the anode surface.

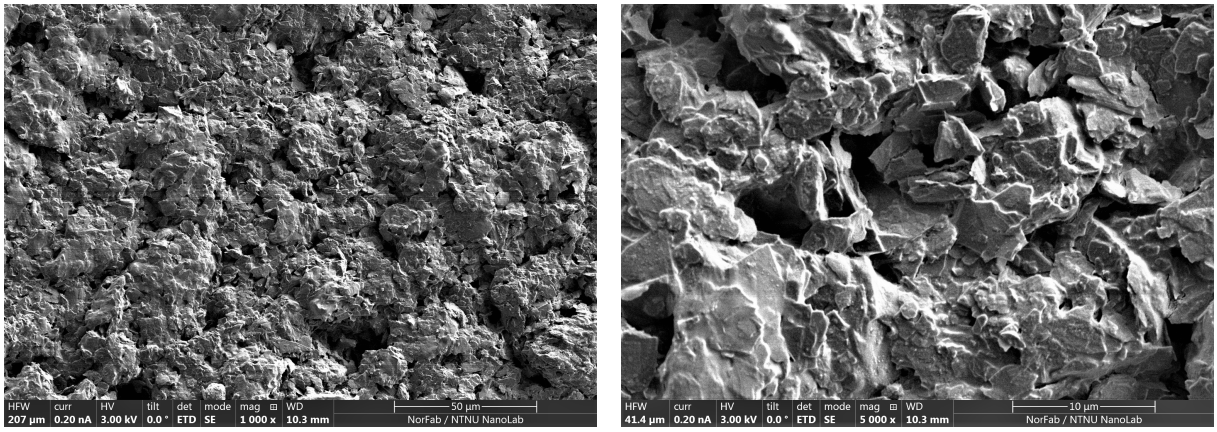


**(a)** **(b)**

**Figure 4.28:** Images of uncycled anode material using SEM at two different magnifications

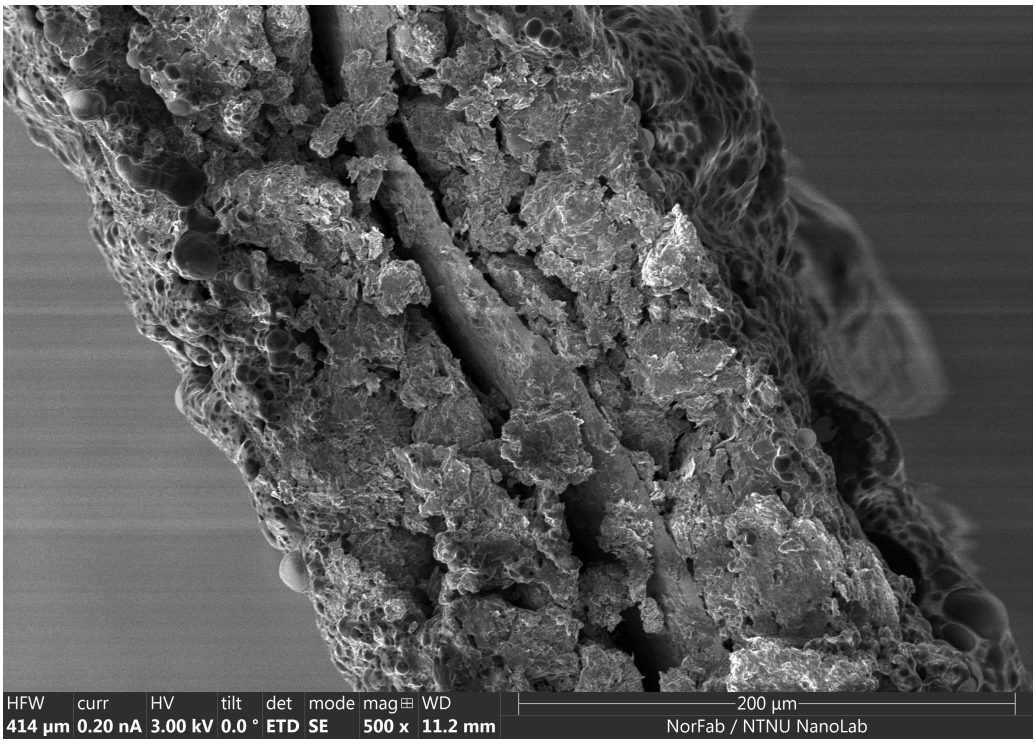


**Figure 4.29:** Cross-section SEM image of anode cycled at 5°C

SEM images of cycled anode material are shown in figures 4.29, 4.30 and 4.31. Figure 4.29 shows a cross-section image, where the current collector is in the center and layers on the outside on both sides are graphite. Outside the graphite is a bubbly substance.

The SEM images of the aged anode at 5°C are very different from the reference images for the uncycled anode. There are some areas of the mossy material mentioned by Li et al. [56] that is circled in blue in figures 4.30 and 4.31, and large areas with bubble-like shapes. The mossy materials are an indication of lithium on the surface. An EDX scan of the aged anode shows mostly carbon and oxygen, with minor parts of S, Si, Na, and all three cathode materials Co, Ni, and Mn, which can indicate some transition metal dissolution. EDX cannot detect lithium, and this is not an indication or lack thereof of the presence of lithium. The minor parts of other materials can be due to contamination of the samples during preparation or transport. The glove box is not a particle-free environment, and many different materials are investigated and used in the box. It can therefore be caused by this.

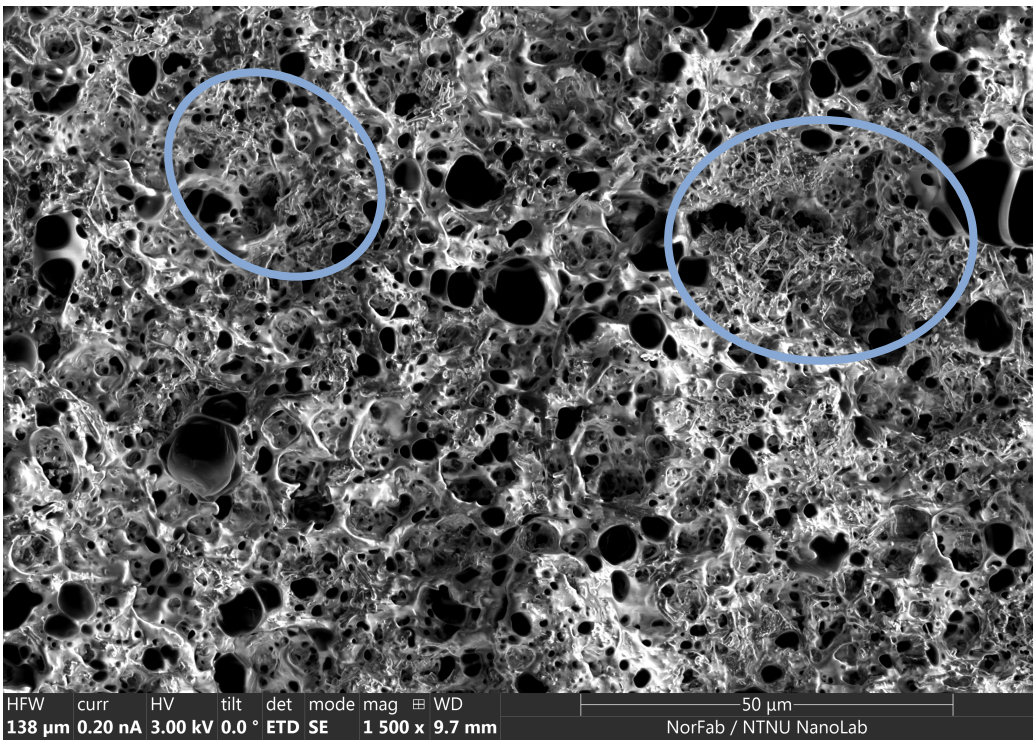


**Figure 4.30:** Anode cycled at 5°C with lithium plating in the circles

Bubbles on the anode surface are not found in any literature regarding lithium plating and SEM. The samples were not soaked in DMC, as is standard practice to remove electrolyte remains on the sample. The bubbles can therefore be a product of lithium and electrolyte reacting with air. Another explanation for the uncommon surface can be a reaction between the anode and water in the air. Even though the samples were prepared in a glove box with argon and transported in sealed pouches, there were some changes in the color of the samples when transferring the samples from the pouch to the SEM. It can, nevertheless, be narrowed down to be a reaction between lithium and materials in the air or already on the anode, as the samples have not been exposed to any other substances. At 5°C Ding et al. [79] have shown that some of the EC in the electrolyte could be in solid form. This could lead to the shape of the lithium plating being different than expected, and when the EC melts, leaving behind lithium deposits in bubble shapes. More images of the aged anode are found in Appendix C.

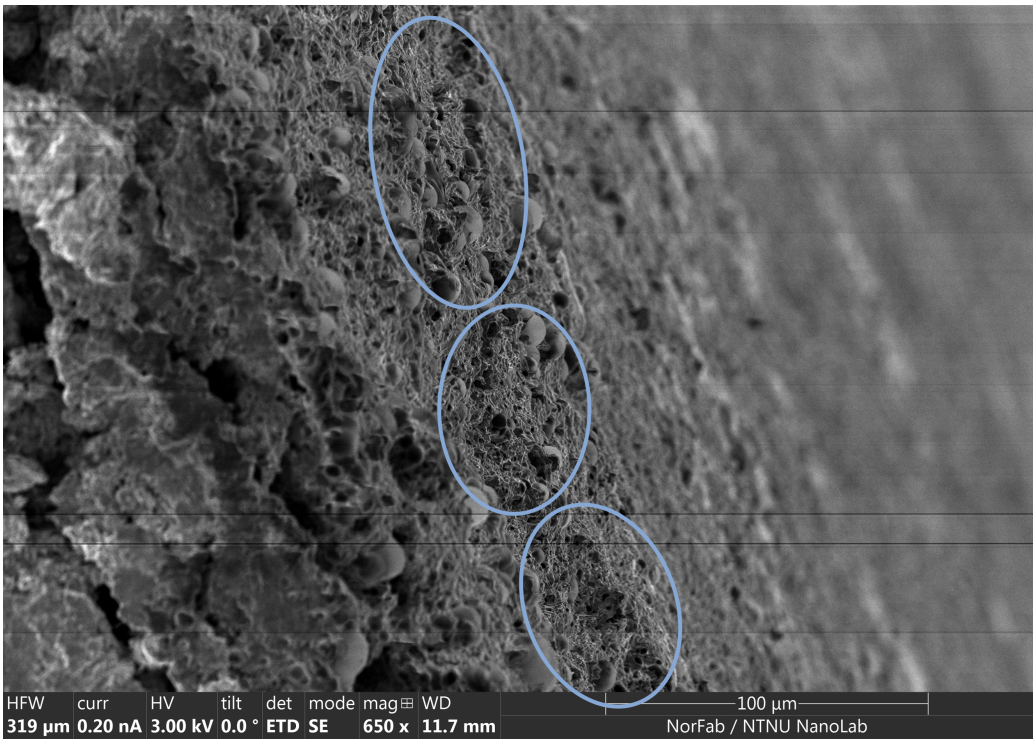


**Figure 4.31:** Cross-section image of anode cycled at 5°C with lithium plating in the circles

# Conclusion

Second life for XALT cells is possible with the right conditions. This can be decided based on in-situ analysis methods, including resistance measurements, SoH, and $dQdV$ curves.

Based on the high rate of degradation of the cell at 5°C and the low onset temperature during the ARC test, it is assumed that this cell will perform badly for second life. The ARC test also indicates that safety is not as good for this cell as for those cycled at higher temperatures. This cell has an extra strong reaction when heat is supplied and is more dangerous than cells cycled at higher temperatures. If this cell was to be used, it would require active cooling. $dQdV$ curves make it possible to separate these cells from others. Characterizing cells before starting second life makes sit possible to remove cells unsuitable for such applications.

The resistance of the cells cycled at 45°C increases more than for cells cycled at lower temperatures. This is most likely due to the increased SEI layer growth at high temperatures. It is, however, safer with high temperatures than low temperatures because a thicker SEI layer leads to increased thermal stability. The cells degrade faster than cells cycled at 25°C, which could be seen in the capacity vs. cycles plots. In regards to second life, the capacity decreases fastest for cells cycled at 45°C for first life. So far, the reduced C-rate and voltage window has decreased the capacity decrease gradient. It is necessary with more and longer periods of second life cycling to make any further conclusions about the second life abilities of 45°C cells.

For cells cycled at 25°C the capacity decrease is low, and the aging is most likely due to a slow growth of the SEI layer. The cells have the largest amount of cycles and a slow increase in resistance. Room temperature seems to be the best condition for XALT cells to achieve long cycle life. Data from IFE shows that vertical cycling leads to a larger capacity decrease than cycling at high temperatures. This should therefore be avoided for XALT cells. However, the horizontal second life performance of first life vertical cells is very similar to cells cycled horizontally for both first- and second life.

For second life long usage time at an appropriate C-rate and good safety is important. The experiments conducted in this thesis indicate that cells cycled at 5°C should be avoided, and cells cycled at 25°C have the longest cycle life for both first- and second life. Based on these results, it is clear that temperature affects first- and second life capabilities. In regards to in-situ analysis methods, $dQdV$ curves work best in differentiating the cycling temperature of the cells.

# Further Work

This master's thesis is limited with regard to time. Aeging studies take time, and especially the second life cycling is somewhat limited. Further work should include extended cycling to create a better foundation to assess aging. In addition, the number of cells used is not that high. With a larger data basis, the results are more validated with regard to statistical averages and analysis.

All cells that are currently cycled during second life are cycled at the same temperature and C-rate. Further work could include testing more conditions and C-rates. This would most likely give the best results using cells cycled at 25°C for first life. In addition, test on cells cycled at 45°C for first life at a lower C-rate during second life to see if it is worth using these cells for second life.

Only uncycled cells and cells at 5°C were opened during the work with this thesis. Opening cells cycled at other cycling conditions could lead to a broader understanding of the internal processes in the cells, both visually and using SEM.

The anode half-cell did not work at high C-rates, and further work should include working with getting these to work. That way degradation maps can be created using Alawa[64], which would give a better understanding of the $dQdV$ curves.

Lastly, further work should include investigating if the trends seen for XALT cells can be found for other chemistries, both by analyzing literature and conducting experiments on other cell types. This consists of both different NMC compositions and other cells.

# Bibliography


[1] Lene T.B. Erichsen. *Ageing performance of second-life batteries*. Tech. rep. Dec. 2022. NTNU.

[2] United Nations. *Take Action for the Sustainable Development Goals*. URL: https://www.un.org/sustainabledevelopment/sustainable-development-goals/ (visited on 20/01/2023).

[3] Jose Alarco, Peter Talbot and The Conversation. *The history and development of batteries*. URL: https://phys.org/news/2015-04-history-batteries.html (visited on 23/01/2023).

[4] SSB. *To av tre nye personbiler er elbiler*. nb. URL: https://www.ssb.no/transport-og-reiseliv/landtransport/statistikk/bilparken/artikler/to-av-tre-nye-personbiler-er-elbiler (visited on 20/02/2023).

[5] Jason Porzio and Corinne D. Scown. 'Life-Cycle Assessment Considerations for Batteries and Battery Materials'. In: *Advanced Energy Materials* 11.33 (2021), p. 2100771. ISSN: 1614-6840. DOI: 10.1002/aenm.202100771.

[6] Omar Velázquez-Martínez et al. 'A Critical Review of Lithium-Ion Battery Recycling Processes from a Circular Economy Perspective'. en. In: *Batteries* 5.4 (Dec. 2019), p. 68. ISSN: 2313-0105. DOI: 10.3390/batteries5040068.

[7] Juner Zhu et al. 'End-of-life or second-life options for retired electric vehicle batteries'. en. In: *Cell Reports Physical Science* 2.8 (Aug. 2021), p. 100537. ISSN: 26663864. DOI: 10.1016/j.xcrp.2021.100537.

[8] CIC energiGUNE. URL: https://cicenergigune.com/en/blog/gigafactories-europe-commitment-economic-recovery-battery-factories (visited on 01/02/2023).

[9] Cun Wang et al. 'State estimation and aging mechanism of 2nd life lithium-ion batteries: Non-destructive and postmortem combined analysis'. In: *Electrochimica Acta* 443 (2023), p. 141996. ISSN: 0013-4686. DOI: https://doi.org/10.1016/j.electacta.2023.141996.

[10] *Electrochemistry - Cells and Batteries*. URL: https://chem.libretexts.org/Bookshelves/Introductory_Chemistry/Chemistry_for_Changing_Times_(Hill_and_McCreary)/08%5C%3A_Oxidation_and_Reduction/8.03%5C%3A_Electrochemistry-_Cells_and_Batteries (visited on 23/01/2023).

[11] *Standard Electrode Potentials*. URL: https://chem.libretexts.org/@go/page/48909 (visited on 04/02/2023).

[12] Moran et. al. *Principles of engineering thermodynamics*. eng. Edition: 8th ed., SI version. Wiley, 2015. ISBN: 978-1-118-96088-2.

[13] W. Wang et al. 'Chapter 1 - Electrochemical cells for medium- and large-scale energy storage: fundamentals'. en. In: *Advances in Batteries for Medium and Large-Scale Energy Storage*. Ed. by Chris Menictas, Maria Skyllas-Kazacos and Tuti Mariana Lim. Woodhead Publishing Series in Energy. Woodhead Publishing, Jan. 2015, pp. 3–28. ISBN: 978-1-78242-013-2. DOI: 10.1016/B978-1-78242-013-2.00001-7.

[14] *Electrode Potentials and their Measurement*. URL: https://chem.libretexts.org/@go/page/48908 (visited on 04/02/2023).

[15] Hans-Georg Schweiger et al. 'Comparison of Several Methods for Determining the Internal Resistance of Lithium Ion Cells'. In: *Sensors* 10.6 (2010), pp. 5604–5625. ISSN: 1424-8220. DOI: 10.3390/s100605604.

[16] UL Research institutes. *What Are Lithium-Ion Batteries?* URL: https://ul.org/research/electrochemical-safety/getting-started-electrochemical-safety/what-are-lithium-ion (visited on 15/11/2022).

[17] Li-Po He et al. 'Recovery of cathode materials and Al from spent lithium-ion batteries by ultrasonic cleaning'. en. In: *Waste Management* 46 (Dec. 2015), pp. 523–528. ISSN: 0956-053X. DOI: 10.1016/j.wasman.2015.08.035.

[18] P. U. Nzereogu et al. 'Anode materials for lithium-ion batteries: A review'. In: *Applied Surface Science Advances* 9 (June 2022), p. 100233. ISSN: 2666-5239. DOI: 10.1016/j.apsadv.2022.100233.

[19] Michio Inagaki et al. 'Chapter 12 - Carbon Materials in Lithium-ion Rechargeable Batteries'. In: *Advanced Materials Science and Engineering of Carbon*. Butterworth-Heinemann, Jan. 2014, pp. 267–287. ISBN: 978-0-12-407789-8. DOI: 10.1016/B978-0-12-407789-8.00012-0.

[20] Edward Buiel and J. R Dahn. 'Li-insertion in hard carbon anode materials for Li-ion batteries'. en. In: *Electrochimica Acta* 45.1 (Sept. 1999), pp. 121–130. ISSN: 0013-4686. DOI: 10.1016/S0013-4686(99)00198-X.

[21] Ghassan Zubi et al. 'The lithium-ion battery: State of the art and future perspectives'. In: *Renewable and Sustainable Energy Reviews* 89 (June 2018), pp. 292–308. ISSN: 1364-0321. DOI: 10.1016/j.rser.2018.03.002.

[22] John Warner. *Lithium-ion battery chemistries : a primer*. Elsevier, 2019. ISBN: 0-12-814778-4.

[23] M. Matson and A.W. Orbaek. *Inorganic Chemistry For Dummies*. Wiley, 2013. ISBN: 978-1-118-21794-8. URL: https://books.google.no/books?id=EbNPAQAAQBAJ.

[24] Naoki Nitta et al. 'Li-ion battery materials: present and future'. In: *Materials Today* 18.5 (June 2015), pp. 252–264. ISSN: 1369-7021. DOI: 10.1016/j.mattod.2014.10.040.

[25] Alexandra K. Stephan. 'A Pathway to Understand NMC Cathodes'. In: *Joule* 4.8 (Aug. 2020), pp. 1632–1633. ISSN: 2542-4351. DOI: 10.1016/j.joule.2020.08.004.

[26] Hong Sun and Kejie Zhao. 'Electronic Structure and Comparative Properties of LiNixMnyCozO2 Cathode Materials'. In: *The Journal of Physical Chemistry C* 121.11 (Mar. 2017), pp. 6002–6010. ISSN: 1932-7447. DOI: 10.1021/acs.jpcc.7b00810.

[27] Satishkumar B. Chikkannanavar, Dawn M. Bernardi and Lingyun Liu. 'A review of blended cathode materials for use in Li-ion batteries'. In: *Journal of Power Sources* 248 (Feb. 2014), pp. 91–100. ISSN: 0378-7753. DOI: 10.1016/j.jpowsour.2013.09.052.

[28] Pengcheng Zhu et al. 'A review of current collectors for lithium-ion batteries'. In: *Journal of Power Sources* 485 (Feb. 2021), p. 229321. ISSN: 0378-7753. DOI: 10.1016/j.jpowsour.2020.229321.

[29] Seong Jin An et al. 'The state of understanding of the lithium-ion-battery graphite solid electrolyte interphase (SEI) and its relationship to formation cycling'. In: *Carbon* 105 (Aug. 2016), pp. 52–76. ISSN: 0008-6223. DOI: 10.1016/j.carbon.2016.04.008.

[30] M.R. Wright. *An Introduction to Aqueous Electrolyte Solutions*. Wiley, 2007. ISBN: 978-0-470-84293-5.

[31] Sheng Shui Zhang. 'A review on electrolyte additives for lithium-ion batteries'. In: *Journal of Power Sources*. International Power Sources Symposium 162.2 (Nov. 2006), pp. 1379–1394. ISSN: 0378-7753. DOI: 10.1016/j.jpowsour.2006.07.074.

[32] Doron Aurbach et al. 'Design of electrolyte solutions for Li and Li-ion batteries: a review'. In: *Electrochimica Acta*. Polymer Batteries and Fuel Cells:Selection of Papers from First International Conference 50.2 (Nov. 2004), pp. 247–254. ISSN: 0013-4686. DOI: 10.1016/j.electacta.2004.01.090.

[33] Alexandre Chagnes and Jolanta Swiatowska. 'Electrolyte and Solid-Electrolyte Interphase Layer in Lithium-Ion Batteries'. In: *Lithium Ion Batteries*. Ed. by Ilias Belharouak. Section: 6. Rijeka: IntechOpen, 2012. DOI: 10.5772/31112.

[34] Cynthia A. Lundgren et al. 'Lithium-Ion Batteries and Materials'. In: *Springer Handbook of Electrochemical Energy*. Ed. by Cornelia Breitkopf and Karen Swider-Lyons. Springer, 2017, pp. 449–494. ISBN: 978-3-662-46657-5. DOI: 10.1007/978-3-662-46657-5_15.

[35] Daehyun Kim et al. 'Second-Order Discrete-Time Sliding Mode Observer for State of Charge Determination Based on a Dynamic Resistance Li-Ion Battery Model'. In: *Energies* 6 (Oct. 2013), pp. 5538–5551. DOI: 10.3390/en6105538.

[36] Mathias Petzl and Michael A. Danzer. 'Advancements in OCV Measurement and Analysis for Lithium-Ion Batteries'. In: *IEEE Transactions on Energy Conversion* 28.3 (2013), pp. 675–681. DOI: 10.1109/TEC.2013.2259490.

[37] E. Lemaire-Potteau, M. Perrin and S. Genies. 'BATTERIES — Charging Methods'. In: *Encyclopedia of Electrochemical Power Sources*. Ed. by Jürgen Garche. Elsevier, 2009, pp. 413–423. ISBN: 978-0-444-52745-5. DOI: https://doi.org/10.1016/B978-044452745-5.00885-6.

[38] Silje Nornes Bryntesen et al. 'Opportunities for the state-of-the-art production of lib electrodes—a review'. In: *Energies* 14.5 (2021), p. 1406. DOI: https://doi.org/10.3390/en14051406.

[39] Ali Davoodabadi et al. 'On electrolyte wetting through lithium-ion battery separators'. In: *Extreme Mechanics Letters* 40 (2020), p. 100960. DOI: https://doi.org/10.1016/j.eml.2020.100960.

[40] Seong Jin An et al. 'Fast formation cycling for lithium ion batteries'. In: *Journal of Power Sources* 342 (2017), pp. 846–852. DOI: https://doi.org/10.1016/j.jpowsour.2017.01.011.

[41] Julius Schmitt et al. 'Impedance change and capacity fade of lithium nickel manganese cobalt oxide-based batteries during calendar aging'. In: *Journal of Power Sources* 353 (2017), pp. 183–194. ISSN: 0378-7753. DOI: https://doi.org/10.1016/j.jpowsour.2017.03.090.

[42] Peter Keil et al. 'Calendar Aging of Lithium-Ion Batteries'. en. In: *Journal of The Electrochemical Society* 163.9 (July 2016). Publisher: IOP Publishing, A1872. ISSN: 1945-7111. DOI: 10.1149/2.0411609jes.

[43] Christoph R. Birkl et al. 'Degradation diagnostics for lithium ion cells'. In: *Journal of Power Sources* 341 (2017), pp. 373–386. ISSN: 0378-7753. DOI: https://doi.org/10.1016/j.jpowsour.2016.12.011.

[44] Gregory L Plett. *Battery modeling*. eng. ISBN: 9781630810238 Volume: vol. 1. Artech House, 2015.

[45] Matthieu Dubarry, Nan Qin and Paul Brooker. 'Calendar aging of commercial Li-ion cells of different chemistries – A review'. In: *Current Opinion in Electrochemistry* 9 (2018), pp. 106–113. ISSN: 2451-9103. DOI: https://doi.org/10.1016/j.coelec.2018.05.023.

[46] K. Jalkanen et al. 'Cycle aging of commercial NMC/graphite pouch cells at different temperatures'. In: *Applied Energy* 154 (2015), pp. 160–172. ISSN: 0306-2619. DOI: https://doi.org/10.1016/j.apenergy.2015.04.110.

[47] Xianke Lin et al. 'Lithium Plating Mechanism, Detection, and Mitigation in Lithium-Ion Batteries'. In: *Progress in Energy and Combustion Science* 87 (2021), p. 100953. ISSN: 0360-1285. DOI: https://doi.org/10.1016/j.pecs.2021.100953.

[48] R. Spotnitz. 'Simulation of capacity fade in lithium-ion batteries'. In: *Journal of Power Sources* 113.1 (2003), pp. 72–80. ISSN: 0378-7753. DOI: https://doi.org/10.1016/S0378-7753(02)00490-1.

[49] Balazs Gyenes et al. 'Understanding Anomalous Behavior in Coulombic Efficiency Measurements on Li-Ion Batteries'. In: *Journal of The Electrochemical Society* 162.3 (Dec. 2014), A278. DOI: 10.1149/2.0191503jes.

[50] Kristen A. Severson et al. 'Data-driven prediction of battery cycle life before capacity degradation'. In: *Nature Energy* 4.5 (May 2019), pp. 383–391. ISSN: 2058-7546. DOI: 10.1038/s41560-019-0356-8.

[51] Jia Guo et al. 'Understanding the mechanism of capacity increase during early cycling of commercial NMC/graphite lithium-ion batteries'. In: *Journal of Energy Chemistry* 74 (2022), pp. 34–44. ISSN: 2095-4956. DOI: https://doi.org/10.1016/j.jechem.2022.07.005.

[52] M. Broussely et al. 'Aging mechanism in Li ion cells and calendar life predictions'. In: *Journal of Power Sources* 97-98 (2001), pp. 13–21. ISSN: 0378-7753. DOI: https://doi.org/10.1016/S0378-7753(01)00722-4.

[53] Sung Park, A. Savvides and M.B. Srivastava. 'Battery capacity measurement and analysis using lithium coin cell battery'. In: *ISLPED'01: Proceedings of the 2001 International Symposium on Low Power Electronics and Design*. 2001, pp. 382–387. DOI: 10.1109/LPE.2001.945436.

[54] Jun-Fan Ding et al. 'A review on the failure and regulation of solid electrolyte interphase in lithium batteries'. In: *Journal of Energy Chemistry* 59 (2021), pp. 306–319. ISSN: 2095-4956. DOI: https://doi.org/10.1016/j.jechem.2020.11.016.

[55] Xuning Feng et al. 'Influence of aging paths on the thermal runaway features of lithium-ion batteries in accelerating rate calorimetry tests'. In: *Int. J. Electrochem. Sci* 14.1 (2019), pp. 44–58.

[56] Yalun Li et al. 'Thermal runaway triggered by plated lithium on the anode after fast charging'. In: *ACS applied materials & interfaces* 11.50 (2019), pp. 46839–46850. DOI: https://doi.org/10.1021/acsami.9b16589.

[57] Sungjemmenla et al. 'Understanding the Cathode–Electrolyte Interphase in Lithium-Ion Batteries'. In: *Energy Technology* 9 (2022), p. 2200421. ISSN: 2194-4296. DOI: 10.1002/ente.202200421.

[58] Zewen Zhang et al. 'Cathode-Electrolyte Interphase in Lithium Batteries Revealed by Cryogenic Electron Microscopy'. In: *Matter* 4.1 (Jan. 2021), pp. 302–312. ISSN: 2590-2385. DOI: 10.1016/j.matt.2020.10.021.

[59] Chenxi Zu, Huigen Yu and Hong Li. 'Enabling the thermal stability of solid electrolyte interphase in Li-ion battery'. In: *InfoMat* 3.6 (2021), pp. 648–661. ISSN: 2567-3165. DOI: 10.1002/inf2.12190.

[60] Chun Zhan et al. 'Dissolution, migration, and deposition of transition metal ions in Li-ion batteries exemplified by Mn-based cathodes – a critical review'. In: *Energy Environ. Sci.* 11.2 (2018), pp. 243–257. DOI: 10.1039/C7EE03122J.

[61] Lena Spitthoff, Paul R. Shearing and Odne Stokke Burheim. 'Temperature, Ageing and Thermal Management of Lithium-Ion Batteries'. In: *Energies* 14.5 (2021). ISSN: 1996-1073. DOI: 10.3390/en14051248.

[62] Shuai Ma et al. 'Temperature effect and thermal impact in lithium-ion batteries: A review'. In: *Progress in Natural Science: Materials International* 28.6 (Dec. 2018), pp. 653–666. ISSN: 1002-0071. DOI: 10.1016/j.pnsc.2018.11.002.

[63] Leo Wildfeuer et al. 'Experimental Characterization of Li-Ion Battery Resistance at the Cell, Module and Pack Level'. In: *2019 Fourteenth International Conference on Ecological Vehicles and Renewable Energies (EVER)*. May 2019, pp. 1–12. DOI: 10.1109/EVER.2019.8813578.

[64] Matthieu Dubarry and David Anseán. 'Best practices for incremental capacity analysis'. In: *Frontiers in Energy Research* 10 (2022). ISSN: 2296-598X. DOI: 10.3389/fenrg.2022.1023555.

[65] Susanne Hansen Troøyen and Torleif Lian. *Thermal stability of NMC442 cathode material studied by accelerating rate calorimetry*. 978-82-464-3289-2. Norwegian Defence Research Establishment.

[66] MN Richard and JR Dahn. 'Accelerating rate calorimetry study on the thermal stability of lithium intercalated graphite in electrolyte. I. Experimental'. In: *Journal of The Electrochemical Society* 146.6 (1999), p. 2068.

[67] Wei Cai et al. 'Experimental simulation of internal short circuit in Li-ion and Li-ion-polymer cells'. In: *Journal of Power Sources* 196.18 (Sept. 2011), pp. 7779–7783. ISSN: 0378-7753. DOI: 10.1016/j.jpowsour.2011.04.024.

[68] Hossein Maleki and Jason N. Howard. 'Internal short circuit in Li-ion cells'. In: *Journal of Power Sources* 191.2 (June 2009), pp. 568–574. ISSN: 0378-7753. DOI: 10.1016/j.jpowsour.2009.02.070.

[69] Preben Vie. *Conversation with a representative from IFE.*

[70] Barai, A., Uddin, K., Widanage, W.D. et al. 'A study of the influence of measurement timescale on internal resistance characterisation methodologies for lithium-ion cells.' In: *Sci Rep 8,21* (). DOI: https://doi.org/10.1038/s41598-017-18424-5.

[71] Lena Spitthoff et al. 'Incremental Capacity Analysis (Dq/Dv) as a Tool for Analysing the Effect of Ambient Temperature and Mechanical Clamping on Degradation'. In: *Available at SSRN 4329605* (2023).

[72] Matthieu Dubarry, Cyril Truchot and Bor Yann Liaw. 'Synthesize battery degradation modes via a diagnostic and prognostic model'. In: *Journal of Power Sources* 219 (2012), pp. 204–216. ISSN: 0378-7753. DOI: https://doi.org/10.1016/j.jpowsour.2012.07.016.

[73] Antonis Nanakoudis. *EDX Analysis with SEM: How Does it Work?* URL: https://www.thermofisher.com/blog/materials/edx-analysis-with-sem-how-does-it-work/ (visited on 06/06/2023).

[74] Ju Young Kim et al. 'Effect of the dielectric constant of a liquid electrolyte on lithium metal anodes'. In: *Electrochimica Acta* 300 (2019), pp. 299–305. ISSN: 0013-4686. DOI: https://doi.org/10.1016/j.electacta.2019.01.113.

[75] Marco-Tulio F Rodrigues. 'Coulombic efficiency and capacity retention are not universal descriptors of cell aging'. In: *Journal of The Electrochemical Society* 169.11 (2022), p. 110514.

[76] Christopher Orendorff, Joshua Lamb and Leigh Anna Marie Steele. 'SNL Abuse Testing Manual.' In: (July 2017). DOI: 10.2172/1369524.

[77] Torleif Lian et al. 'Changes in thermal stability of cyclic aged commercial lithium-ion cells'. In: *ECS Transactions* 89.1 (2019), p. 73.

[78] F. Grimsmann et al. 'Hysteresis and current dependence of the graphite anode color in a lithium-ion cell and analysis of lithium plating at the cell edge'. In: *Journal of Energy Storage* 15 (2018), pp. 17–22. ISSN: 2352-152X. DOI: https://doi.org/10.1016/j.est.2017.10.015. URL: https://www.sciencedirect.com/science/article/pii/S2352152X17302268.

[79] Michael S Ding, Kang Xu and T Richard Jow. 'Liquid-solid phase diagrams of binary carbonates for lithium batteries'. In: *Journal of the Electrochemical Society* 147.5 (2000), p. 1688.

# Appendix A

# HPPC Test

Figure A.1 shows the schedule used for the HPPC test done during the characterization of the cells.

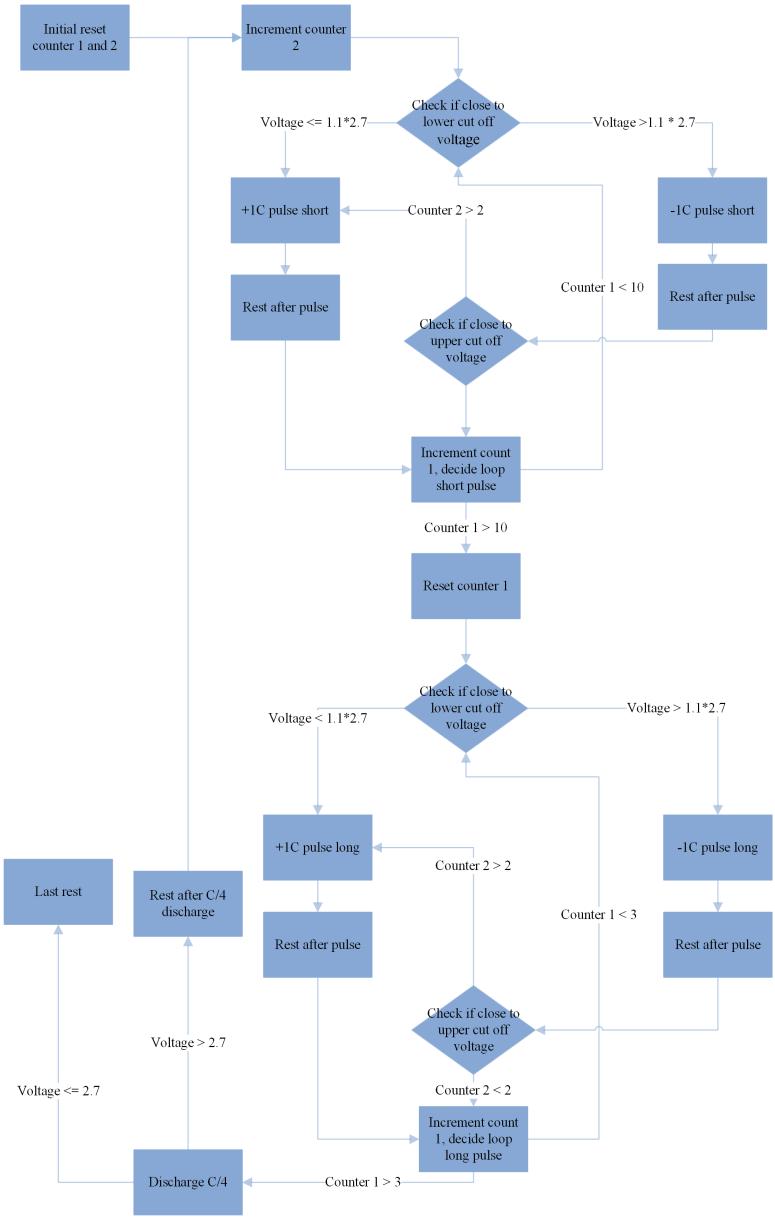


**Figure A.1:** HPPC test schedule

# Appendix B

# Degradation Maps

Degradation maps from Spithoff et al. [71].

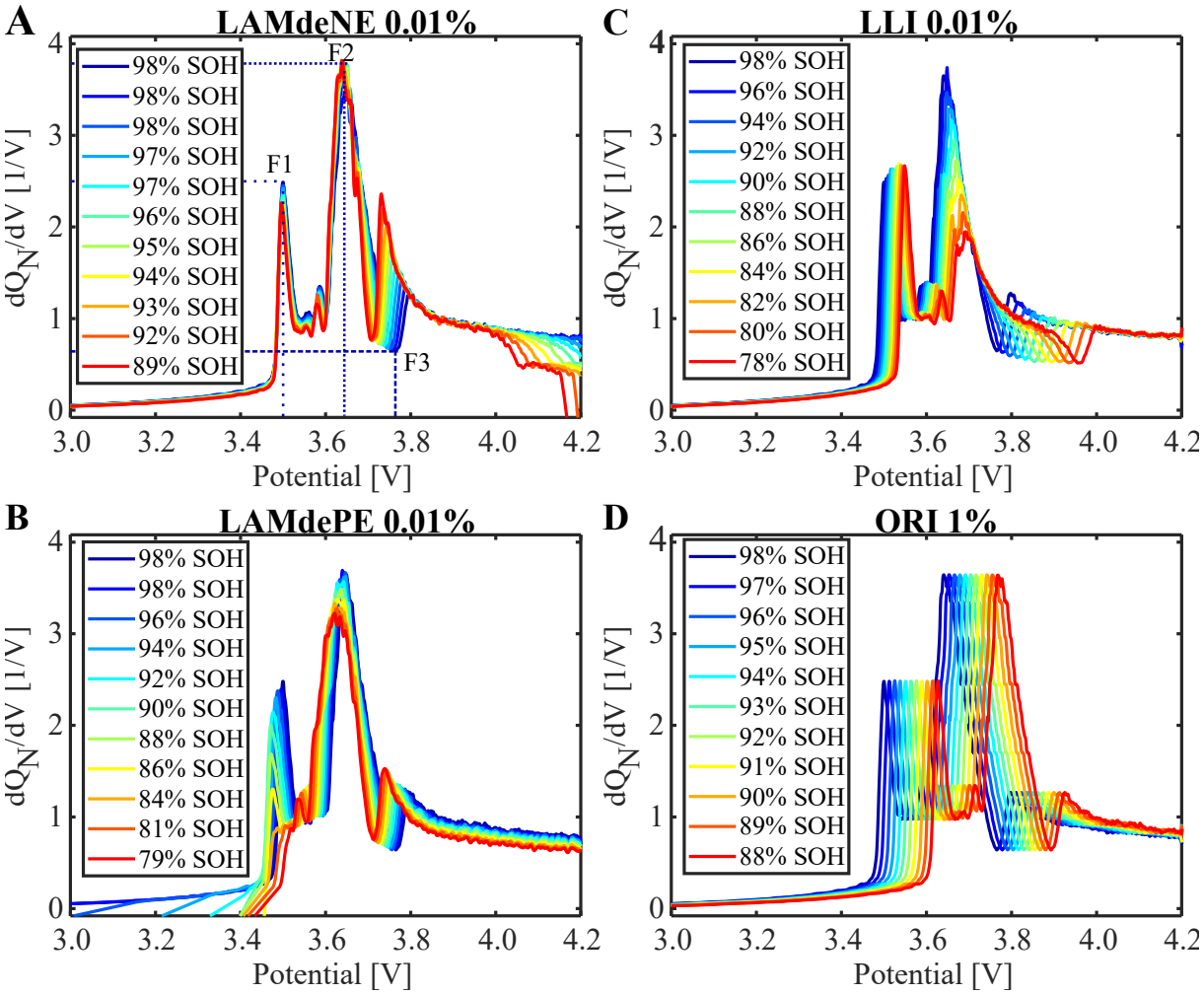


**Figure B.1:** Degradation maps from Spithoff et al. [71]

# Appendix C

# SEM Images

SEM images of anode on cell cycled at 5°C at 65% SoH at different magnifications.

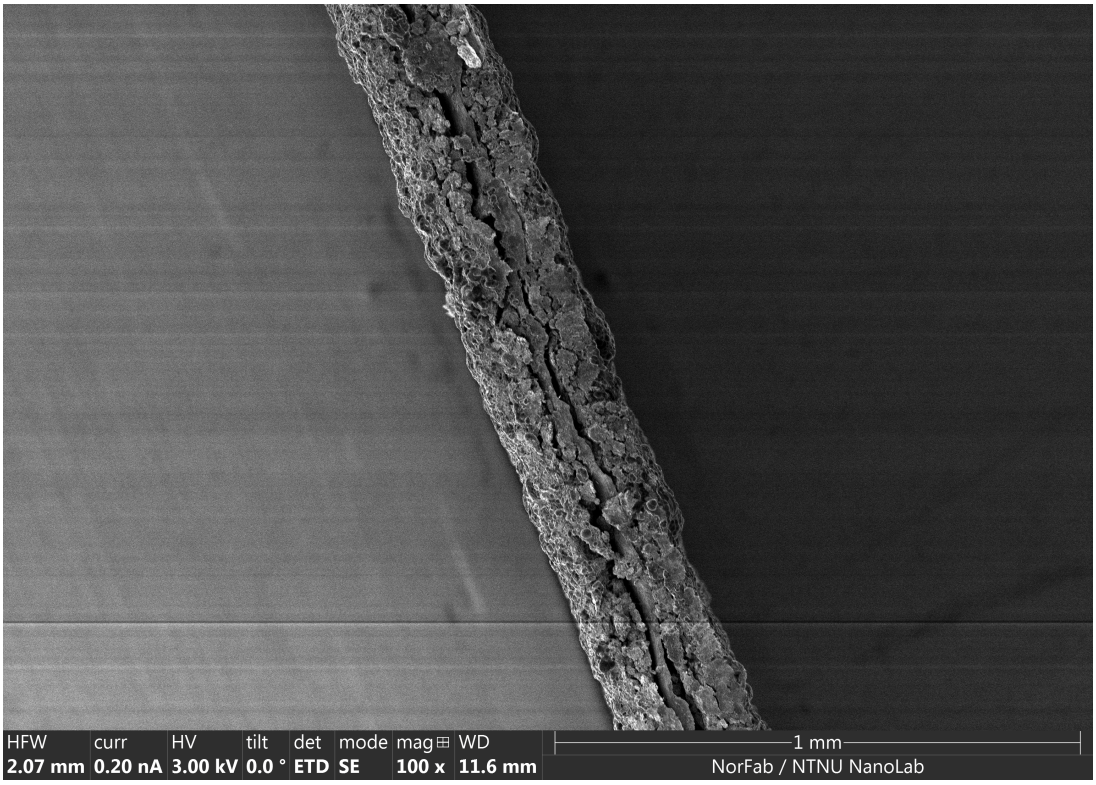


**Figure C.1:** SEM image of cross-section of anode cycled at 5°C at 65% SoH at 100 magnification

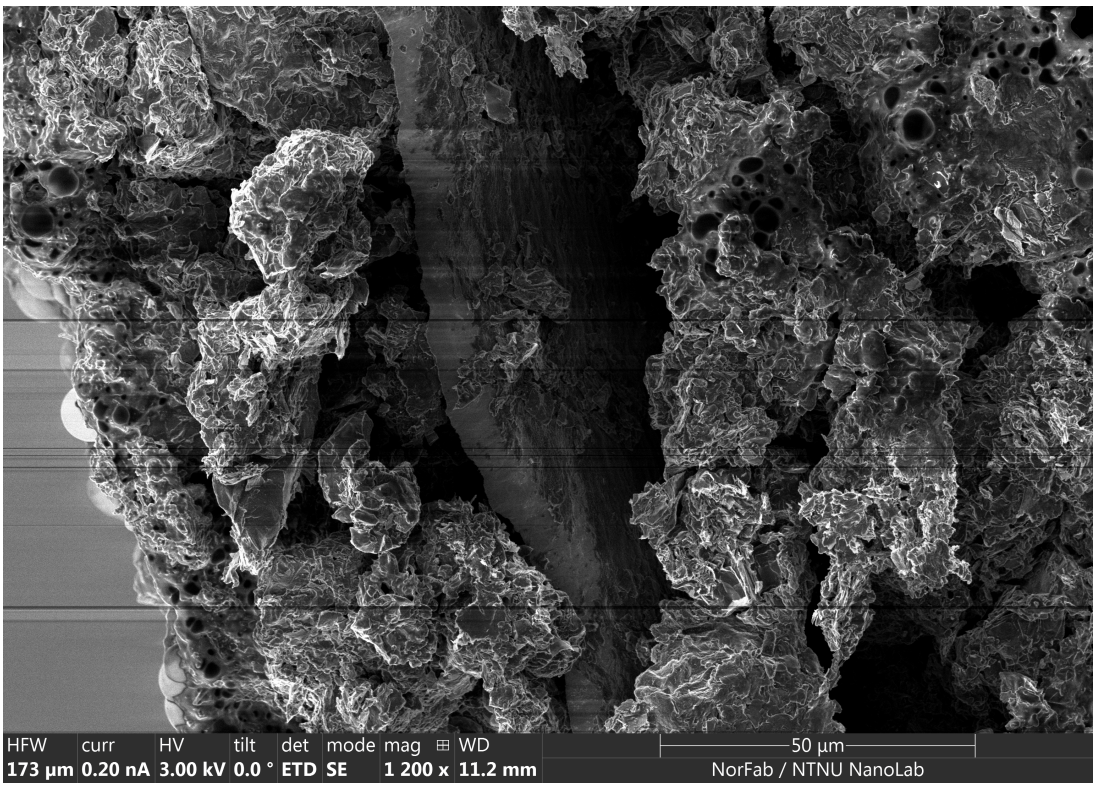


**Figure C.2:** SEM image of a cross-section of anode cycled at 5°C at 65% SoH at 1200 magnification, with current collector in the center

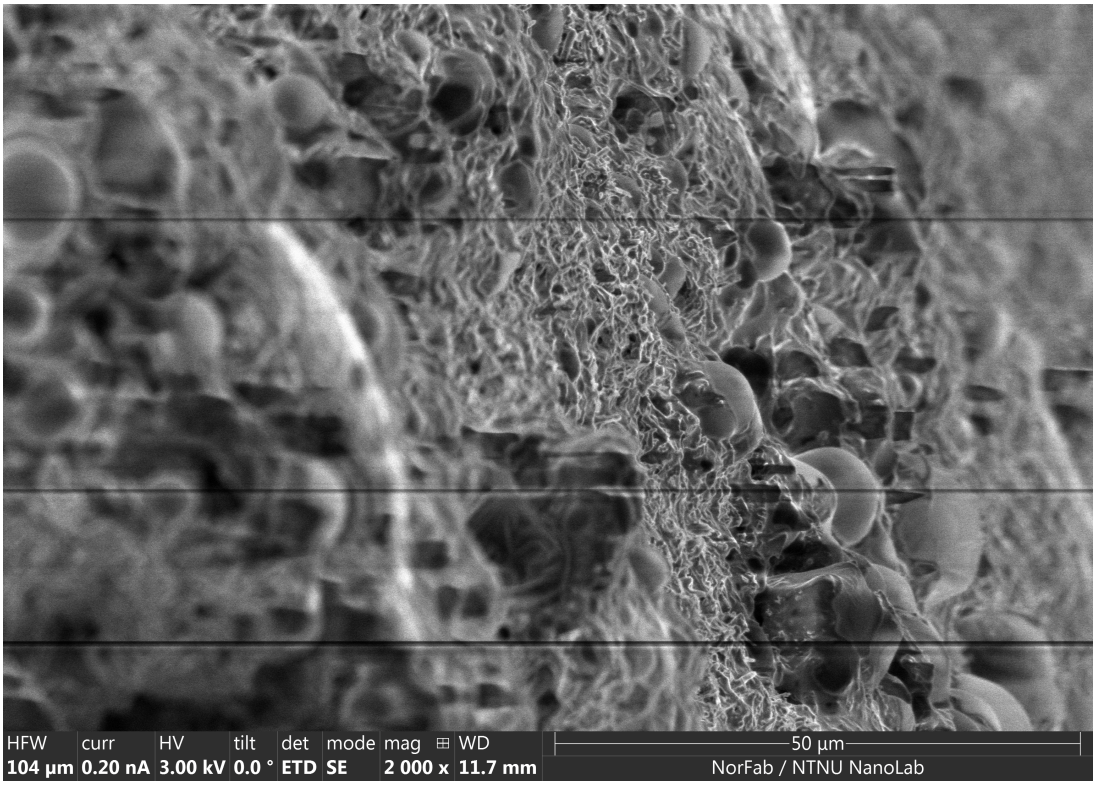


**Figure C.3:** SEM image of a cross-section of anode cycled at 5°C at 65% SoH at 2000 magnification

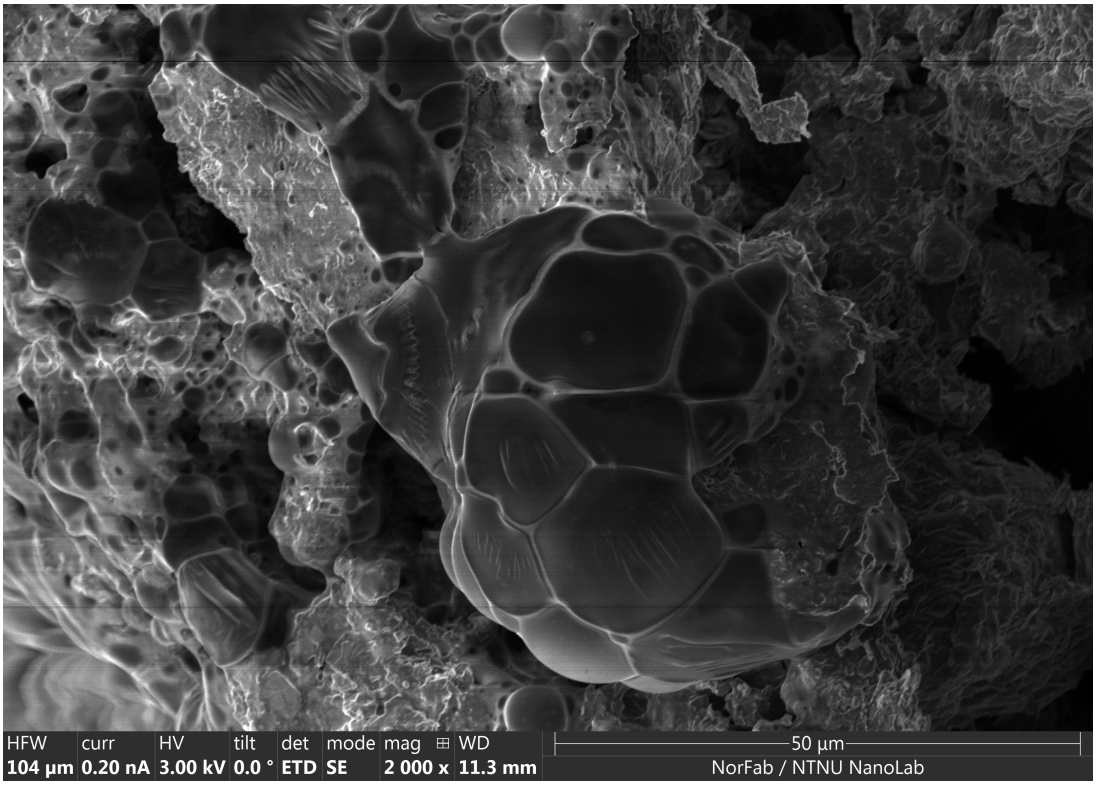


**Figure C.4:** SEM image of a bubble on the anode surface of a cell cycled at 5°C at 65% SoH

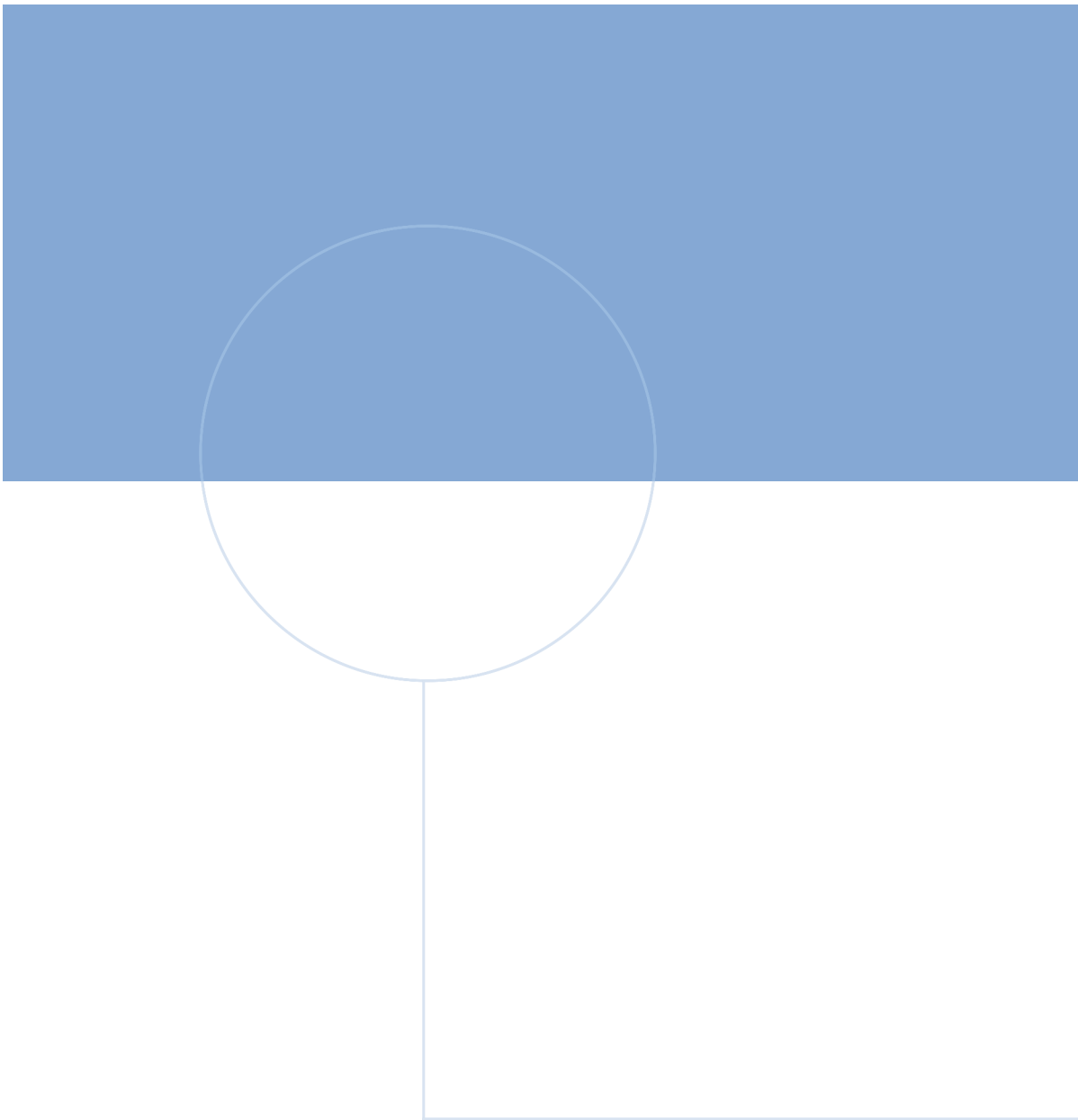

NTNU

Norwegian University of
Science and Technology